The inositol pyrophosphates are essential for the development of mammals

Sining He

Advised by Charles Brearley and Feng Rao

A thesis presented for the degree of Doctor of Philosophy at the University of East Anglia

School of Biological Sciences

March 2022

ABSTRACT

Inositol polyphosphates, generated from a second messenger IP_3 by a series of kinases, are a family of endogenous metabolites conserved across evolution. Inositol polyphosphates participate in diverse physiological activities, including insulin secretion, ubiquitination, apoptosis, cancer development. However, limited by techniques in imaging and measuring inositol phosphates in living cells, the spatial and temporal mechanism of these small molecules and their kinases remains poorly understood.

The kinases of IP_6 (IP6Ks), including three mammalian homologs (IP6K1-3), are responsible for the production of inositol pyrophosphate (5-IP_7, IP_7) from the substrate IP6. IP6K1 and IP6K2 are widely spread in all tissues, while IP6K3 only exists in muscle and brain. Deletion of IP6K1 or IP6K2 reduces the accumulation of IP_7 to some extent. Mice with IP6K1 deletion are male sterile, while IP6K2 deletion in mice does not show apparent phenotypes. However, little is known about the functions and mechanisms of IP_7 in mammalian development. My research is to study the functions and mechanisms of IP_7 in mammals by concurrently deleting IP6K1 and IP6K2 to deplete IP_7 in mice, at least in many tissues of mice.

Results in this thesis demonstrate that concurrent IP6K1 and IP6K2 deletion in mice (Double knockout, DKO) leads to neonatal lethality associated with respiratory failure. Embryonic DKO lung has smaller size, reduced air space and

thicker alveolar walls, which are associated with the immaturity of type I and II lung epithelial cells and reduced expression of surfactant proteins. RNA-seq analysis reveal strong upregulation of innate immune response genes in DKO fetal lungs, which also display activation of the NF-kappa B and IRF3 pathways and increased levels of myeloid cells. Consistent with the findings, immune activation in fetal lung could be due to altered development of the hematopoietic system, which showed myeloid-biased differentiation in fetal livers. Finally, H2AX phosphorylation is upregulated in DKO livers and lungs, suggesting defective DNA damage repair.

Taken together, this study demonstrates that inositol pyrophosphates are essential for mouse viability, whose depletion leads to multiple developmental alterations in hematopoietic and pulmonary systems that may together cause respiratory failures.

Abbreviations

5-IP7/IP7: Inositol pyrophosphates

AGM: Aorta-gonad-mesonephros region

AP2: Apetala 2

AT1/2 cells: Alveolar type I/II cells

ATM: The ataxia-telangiectasia mutated kinase

BasoE: Basophilic erythroblast

BCA assay: Bicinchoninic acid assay

BCL11A: B-cell lymphoma/leukemia 11A

BER: Base excision repair

BFU-E: Burst-forming unit erythroid

Bmp: Basic metabolic panel

BPD: Bronchopulmonary dysplasia

BSA: Bovine serum albumin

CFU-E: Colony-forming unit erythroid

cGAMP: cyclic GMP–AMP

cGAS: Cyclic GMP-AMP Synthase

CHK2: Checkpoint kinase 2

CK2: Casein kinase II

CKO: Conditional knockout

CLP: Common lymphoid progenitors

CMP: Common myeloid progenitors

CO2: Carbon dioxide

COUP-TF: COUP transcription factor

CRISPR Cas9: Clustered regularly interspaced short palindromic repeats associated protein 9

CRLs: Cullin-Ring E3 Ligases

DAG: 1,2-diacylglycerol

DAPI: 4,6-diamidino-2-phenylindole

DEPC: Diethyl pyrocarbonate

DKO: Double knockout

DMEM: Dulbecco's Modified Eagle Medium

DNA-PKcs: DNA-dependent protein kinase, catalytic subunit

DRED: Direct repeat erythroid-definitive

DSBR: DNA double-strand breaks repair

DSBs: Double strand DNA breaks

E0.5: Embryonic day 0.5

EDTA-K2: Dipotassium ethylenediaminetetraacetic acid

EPO: Erythropoietin

EPOR: Erythropoietin receptor

ER: Endoplasmic reticulum

Fgf: Fibroblast growth factor

GATA1: GATA Binding Protein 1

GMP: Granulocyte macrophage progenitor

GPCR: G protein-coupled receptor

GRP1: General receptor for phosphoinositides-1

H&E staining: Hematoxylin and eosin staining

HPLC: High performance liquid chromatography

HR: Homologous recombination

HSCs: Hematopoietic stem cells

IKK: the kinases of IκB

IL1b: Interleukin 1 beta

IP6Ks: The kinases of IP6

IPMK: Inositol phosphate multikinase

IPs: Inositol phosphates

IR: Ionizing radiation

IRF3: Interferon regulatory factor 3

IκBα: Nuclear factor of kappa light polypeptide gene enhancer in B-cells inhibitor, alpha

KAP1: KRAB-associated protein-1

KLF1: Kruppel Like Factor 1

KO: Knockout

LCR: The locus control region

LDB1: LIM Domain Binding 1

LMO2: LIM Domain Only 2

lncRNA: long non-coding RNA

LPS: Lipopolysaccharides

MBD2: Methyl-CpG Binding Domain Protein 2

MEF: Mouse Embryonic Fibroblasts

MEP: Megakaryocyte erythroid progenitor

miRNA: Micro RNA

MYB: MYB Proto-Oncogene, Transcription Factor

NaF: Sodium fluoride

NEMO: NF-kappa-B essential modulator

NER: nucleotide excision repair

NF-E4: Nuclear Factor, Erythroid 4

NF-kappa B: Nuclear factor kappa-light-chain-enhancer of activated B cells

NHEJ: Nonhomologous end-joining

NK cells: Natural killer cells

NKX2.1: NK2 Homeobox 1

NSR1: Nuclear localization sequence-binding protein

OrthoE: Orthochromatic erythroblast

P21: Postnatal day 21

PA: Perchloric acid

PBS: Phosphate-buffered saline

PFA: Paraformaldehyde

PH domain: Pleckstrin homology domain

PI3K: Phosphoinositide 3-kinase

PIKE: PI3-kinase enhancer

PIP2: phosphatidylinositol 4,5-bisphosphate

PLC: Phospholipase C

PolyE: Polychromatic erythroblast

PPIP5Ks: Diphosphoinositol Pentakisphosphate Kinases

ProE: Pro-erythroblast

qPCR: Quantitative polymerase chain reaction

SCD: Sickle cell disease

SDS-PAGE: SDS-polyacrylamide gel electrophoresis

Shh pathway: Sonic hedgehog pathway

SIN1: Stress-activated protein kinase-interaction protein 1

SPA/ SPB/ SPC/SPD: Surfactant Protein A/B/C/D

SSBs: DNA single-strand breaks

STING: Stimulator of interferon genes

Syt: Synaptotagmin

TBK1: TANK-binding kinase 1

TIAM: T-lymphoma invasion and metastasis-inducing protein

TR2: Testicular receptor 2.

TR4: Testicular receptor 4

TTF1: Thyroid transcription factor 1, also known as NKX2.1

TTT complex: Tel2, Tit1 and Tti2 complex

TUNEL assay: Terminal deoxynucleotidyl transferase (TdT) dUTP Nick-End Labeling

α-SMA: Smooth muscle actin

List of figures

List of tables

Attached Video

The left is wild-type infant and the right is DKO infant. The wild-type infant is reddish and opens its mouth more frequently while the DKO infant is in dark and is less active.

Publications

Lin, H., Zhang, X., Liu, L., Fu, Q., Zang, C., Ding, Y., Su, Y., Xu, Z., **He, S.**, Yang, X., Wei, X., Mao, H., Cui, Y., Wei, Y., Zhou, C., Du, L., Huang, N., Zheng, N., Wang, T., & Rao, F. (2020). Basis for metabolite-dependent Cullin-RING ligase deneddylation by the COP9 signalosome. Proceedings of the National Academy of Sciences of the United States of America, 117(8), 4117–4124.

Zhang, X., Shi, S., Su, Y., Yang, X., **He, S.**, Yang, X., Wu, J., Zhang, J., & Rao, F. (2020). Suramin and NF449 are IP5K inhibitors that disrupt inositol hexakisphosphate–mediated regulation of cullin–RING ligase and sensitize cancer cells to MLN4924/pevonedistat. Journal of Biological Chemistry, 295(30), 10281–10292.

Acknowledgements

I met a lot of new things in England during the first year of my PhD study. Professor Brearley and Professor Hemmings gave me a lot of supports. I enjoyed the research with genuine interest and self-motivation. I always worked overtime, so I had more chances to appreciate the Rule of Law. Thank you, Andrew Gates. I also want to thank Megen, Jake, Neil, Sirinda and Yinghong. They also helped me a lot at the UEA.

Over the last three years, I studied the functions and mechanisms of inositol polyphosphates at the SUSTECH. Professor Rao provides a lot of resources and ideas for me in the research. I learn a lot from him. Focus on the research and spend more time. Curiosity and self-motivation push me to reveal the functions and mechanisms of inositol pyrophosphates in the development of mice embryos. I have to learn a lot of knowledge and techniques of embryos, lungs and hematopoietic stem cells. I also thank those who provide me with assistance in SUSTECH, especially the animal centre staffs, Miss Guo, Miss Lin, Miss Sun, and Miss Zhao. Colleagues who always work until midnight encourage me to give priority to the experiments. I always remember Ben Ma, Yang Su, Huifang Wang, Zhenhua Zhu, Na Li, Yuebo Zhao, Xiayun Wei, Cheng Zhou. Then help me a lot. My cooperators also help me a lot. I show my respects to Chang Li, Weitao Cao, Yi Wen, Sheng Yu, professor Liu and professor Yin. Because of their contribution, I put my project forward at a faster speed. I also want to thank Ying Wang, Xibin Lu, Mengru Zhuang, Yuanchu She, Xiaoshi Li. I learn many techniques from them.

I always show my most tremendous respect to my parents, Mrs Ho and Mr Ho. They always support my decisions with only one requirement, my happiness. They are more concerned about the satisfaction of their children than their own life. They love their children in a self-sacrificed way. I have had an independent life from high school. I have left home to study for over 15 years. I cherish any love from them, but I seldom let them know. I am concerned about their health and their moods. Miss Chang opens a window about life and love for me. I am going to pick it up as a long-term project.

Curiosity has been the only factor of my research over the last 4 years. I have a good time at UEA and SUSTECH, where I become more independent in the study. In the future, curiosity will continue to push me to pursue achievements in scientific researches.

Table of Contents

Chapter 1 Introduction

1.1 Introduction

Ins(1,4,5)P_3, IP_3, was identified as an important secondary messenger in the 1980s (Michell et al., 1981). Together with 1,2-diacylglycerol (DAG), IP_3 is produced from phosphatidylinositol 4,5-bisphosphate (PIP2) by PLC isozyme PLC-beta upon activation of G protein-coupled receptor (GPCR) (Berridge & Irvine, 1984). IP_3, consisting of an inositol ring and three phosphate groups, is a negatively charged organic molecule and binds to the positively charged amino acids such as arginine and lysine of IP3 receptor on the endoplasmic reticulum calcium channel and activates the release of calcium to the cytoplasm (Bosanac et al., 2004). After this secondary messenger realizes its functions, a series of inositol phosphate kinases catalyze the phosphorylation of IP_3 to generate several higher inositol phosphates. Inositol phosphate multikinase (IPMK) converts IP_3 to Ins(1,4,5,6)P_4, the substrate of the same kinase. IP_4 is then phosphorylated at 3 position generating Ins(1,3,4,5,6)P_5. While there remains some speculation whether IP_3 is the metabolic precursor of IP_6 in all eukaryotes, the physiological production of IP_6 resides solely with IP5K. IP_6 is itself the substrate for producing more highly phosphorylated molecules, the inositol pyrophosphates, including IP_7 and IP_8. Vip1/PPIP5K catalyzes the conversion of IP_6 to 1-IP_7 while Ksc1/IP6K synthesizes 5-IP_7. Vip1/PPIP5K also phosphorylates 5-IP_7 and generates 1,5-IP_8 whereas Ksc1/IP6K transforms phosphorylated 1-IP_7 into 1,5-IP_8. Therefore, the synthesis

of IP_8 from IP_6 includes two steps, pyrophosphorylation on carbon 1 and on carbon 5 (Monserrate & York, 2010) (Figure 1-1).

These inositol phosphates are not simple metabolic intermediates. They and their kinases that interconvert them also participate in cellular processes like apoptosis, transcriptional regulation, insulin secretion, and in pathophysiological contexts to cancer development. IP_4 (specifically, Ins(1,4,5,6)P_4) and IP_5 (Ins(1,3,4,5,6)P_5) take part in recruiting chromatin-remodelling complex and regulate gene transcription. IP_6 plays an important role in mRNA export, genomic stability, HIV package and Cullin-Ring E3 Ligases (CRLs) regulation (Monserrate & York, 2010) (Dick et al., 2018) (Scherer et al., 2016). IP_7, through regulating proteins interaction and pyrophosphorylation, is significant to insulin secretion, endocytosis and so on (Saiardi *et al.*, 2002) (Park et al., 2017). $InsP_8$ is the intracellular Pi signalling molecule serving as the ligand of SPX1 for controlling Pi homeostasis in plants (Dong et al., 2019). Shears *et al*. have also established that IP_8 is involved in osmotic regulation and tumour cells proliferation (Nagpal et al., 2021)

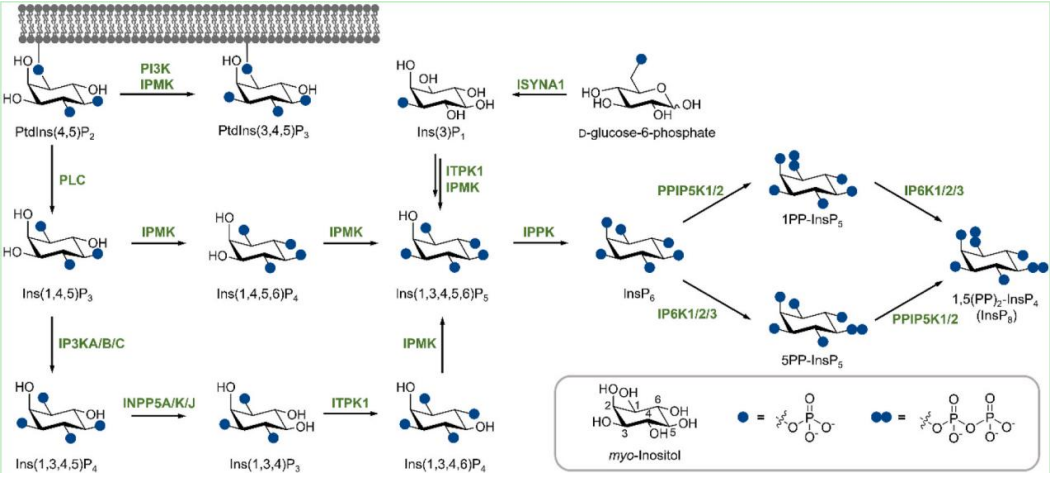

Figure 1-1 The synthesis of inositol pyrophosphates. $Ins(1,4,5)P_3$, from PIP_2, is further phosphorylated into $Ins(1,4,5,6)P_4$, $Ins(1,3,4,5,6)P_5$ and $InsP_6$ by IPMK and IP5K separately. IP6Ks and PPIP5K further pyrophosphorylate IP_6 into 5-IP_7 and 1-IP_7, both of which can be further catalysed to 1,5-IP_8 by PPIP5K or IP6Ks. In addition, a branch of producing $Ins(1,3,4,5,6)P_5$ from $Ins(1,4,5)P_3$ is through $Ins(1,3,4,5)P_4$, $Ins(1,3,4)P_3$, $Ins(1,3,4,6)P_4$ and $Ins(1,3,4,5,6)P_5$ (Kröber et al., 2021).

Up to now, it is still unclear how most of the inositol phosphates and pyrophosphates realize their functions. The primary barrier to research on inositol phosphates is limited approaches to detect inositol phosphates, especially detecting their cellular localization and measuring the concentration of inositol polyphosphates in living cells. The current method for measuring the cellular concentration of these inositol phosphates involves radioactive labelling with metabolic precursors. In vitro, high performance liquid chromatography (HPLC) and gel electrophoresis are standard tools to measure the concentration of inositol polyphosphates (Losito et al., 2009).

David Furkert *et al.* used triplexed affinity reagents linked to IP_6 and IP_7 to pull down interactive proteins. Combining with the mass spectrometry, they found many proteins interacting with IP_6 and IP_7 (Furkert et al., 2020). This research will

provide many crucial clues about the functions and mechanisms of inositol phosphates and pyrophosphates in cellular pathways. To confirm the interaction between these interactive candidates and IP_7 will be beneficial to understanding the functions and mechanisms of inositol pyrophosphates and polyphosphates.

Gain and loss of functions are essential strategies to study the functions of proteins. In fact, the method of gain and loss of functions can also be applied to study the roles of inositol pyrophosphates because we can manipulate their kinases to increase or reduce the synthesis of inositol pyrophosphates. The redundancy of IP6Ks limited the research on the functions and mechanisms of inositol pyrophosphates. There are three IP6 kinases in mammals, including IP6K1, IP6K2 and IP6K3. IP6K3 is mainly expressed in brain and muscle tissues, while IP6K1 and IP6K2 are widely expressed in the whole body. Therefore, deletion of IP6K1 or IP6K2 can reduce the accumulation of IP_7 but cannot lead to complete loss of IP_7. In fact, reducing the accumulation of IP_7 also have effects on the development of mammals. For example, IP6K1 deletion leads to male sterility. The IP6K1 KO mice are more petite than WT mice in regular diet (Bhandari et al., 2008). IP6K2 can regulate cellular energy dynamics through interacting with creatine kinase-B (Nagpal et al., 2021). Therefore, complete depletion of IP_7 is vital to the research on the functions and mechanisms of IP_7. Wilson et al. depleted IP_7 completely by deleting IP6K1 and IP6K2 in HCT116 with CRISPR Cas9 technology and revealed the importance of IP_7 in regulating cellular phosphate homeostasis (M. S. Wilson

et al., 2019). However, IP6K1 and IP6K2 are on the same chromosome in mammals, on chromosome 9 in mice and chromosome 13 in humans. Thus, there is little chance to obtain double deletions of IP6K1 and IP6K2 mice from crossing IP6K1 KO mice and IP6K2 KO mice. Therefore, it is necessary to develop the mice of double deletions of IP6K1 and IP6K2 or even triple omissions of IP6Ks to reveal the functions and mechanisms of IP_7 in the development of mammals.

1.2 Inositol pyrophosphates in mammals

1.2.1 Synthesis of the inositol pyrophosphates in living cells

The synthesis of inositol pyrophosphates starts from GPCR stimulation ligands. Upon the activation of GPCR, PtdIns(4,5)P_2 on the cytoplasm is cleaved by phospholipase C into IP_3 and DAG (Berridge & Irvine, 1984). IP_3 and DAG are important secondary messengers which transfer the extracellular signals into the cytosol. IP_3 binds to the IP_3 receptor on the endoplasmic reticulum (ER) calcium channel and activates the calcium released from ER into the cytosols (Bosanac et al., 2004). IP_3 in the cells can be further converted into inositol polyphosphates and inositol pyrophosphates by related kinases. IPMK can add phosphate group at positions 3 and 6 to the inositol ring of IP_3 and generate IP_4 and IP_5. IP5K phosphorylates IP_5 at position 2 of producing IP_6. IP_6 can be further pyrophosphorylated into inositol pyrophosphate, including 1-IP_7, 5-IP_7 and 1,5-IP_8. PPIP5K1/2 pyrophosphorylates IP6 at position 1 and produce 1-IP_7, while IP6K1/2/3 pyrophosphorylates IP_6 at position 5 and generate 5-IP7. In addition, IP_7 can be further pyrophosphorylated into IP_8 by PPIP5K1/2 or IP6K1/2/3.

PPIP5K1/2 pyrophosphorylates 5-IP_7 into 1,5-IP_8 while IP6K1/2/3 pyrophosphorylates 1-IP_7 into 1,5-IP_8. Therefore, the generation of IP_8 from IP_6 depends on the combined functions of PPIP5K1/2 and IP6K1/2/3 (Park et al., 2017). The concentration of inositol pyrophosphates is most commonly measured with a standard technique of radio labelling cells with [3H] *myo*-inositol, extraction of inositol phosphates and their separation with HPLC.

In mammalian cells, the concentrations of IP_6 and 5-IP_7 are 10–100 and 0.5–5μM respectively. Therefore, the concentration of 5-IP_7 is only 1-5% of IP_6 in the living cells. In addition, although there are two kinds of IP_7, including 1-IP_7 and 5-IP_7, 1-IP_7 comprises only 2-10% of total IP_7 while 5-IP_7 occupies more than 90% of total IP_7 in the living cells. The concentration of IP_8 is only 10-20% of the concentration of IP_7 so that it is not easy to be detected (Park et al., 2017). In this project, I study the functions of inositol pyrophosphates by deleting IP6K1 and IP6K2. Therefore, I focus on the roles and mechanisms of 5-IP_7, hereafter IP_7.

1.2.2 Mechanism of the inositol pyrophosphates in regulating cellular processes

The functions and mechanisms of action of inositol pyrophosphates are the most critical projects in this field. Previous studies on mechanisms of inositol pyrophosphates in regulating cellular processes are mainly on interacting with proteins and pyrophosphorylating proteins (Figure 1-2).

Inositol pyrophosphates can bind to proteins with specific domains. IP_7 binds to proteins with pleckstrin homology (PH) domain and C2 domain. For example, IP_7

competes with PtdIns(3,4,5)P_3, PIP_3, to binds to Akt which has a PH domain. In general, PIP_3 recruits Akt to the membrane where Akt is phosphorylated and activated. However, the interaction between IP_7 and Akt affects the phosphorylation of Akt. Therefore, Akt has higher activity in the IP6K1 KO mice (Chakraborty et al., 2010; Xu et al., 2013). IP_7 also interacts with proteins with PH-domain like SIN1 (stress-activated protein kinase-interaction protein 1), GRP1 (general receptor for phosphoinositides-1), PIKE (PI3-kinase enhancer) and TIAM (T-lymphoma invasion and metastasis-inducing protein) (Park et al., 2017). IP_7 has a 45-fold higher affinity than IP_6 to Ca^{2+} sensor protein synaptotagmin-1 (Syt1) which has a C2-domain. Syt1 is required for neurotransmitter release because 5-IP_7 suppresses synaptic vesicle fusion during exocytosis through direct interaction with Syt1 (Lee et al., 2017). IP_7 binds to CK2 and enhances the TTT complex phosphorylation by CK2. The IP_7 binding to CK2 is essential to the stability of DNA-PKcs and ATM and its downstream apoptosis (Rao et al., 2014). IP7 also binds to the RhoGAP domain of PI3K p85 alpha and Na+/K+-ATPase-alpha 1. This binding leads to the degradation of Na+/K+-ATPase-alpha 1 through recruiting AP2 which mediates endocytosis (Chin et al., 2020). Our lab has recently demonstrated a role for IP7 in transmitting GPCR stimuli (Zhang et al., 2021). Thus, IP6K1 is phosphorylated and activated by PKC and PKD upon acetylcholine stimulation of muscarinic GPCR receptor. The IP7 then generated could work together with Ca2+ as coincident messengers in insulin exocytosis.

Protein pyrophosphorylation is a common protein modification, which regulates cellular pathways, including cell growth, metabolism and survival (Chakraborty, 2017). With radiolabeled IP_7, Saiardi et al. revealed that proteins like NSR1, YGR and SRP40 could be pyrophosphorylated by IP_7 (Saiardi *et al.*, 2004). Inositol pyrophosphates can transfer beta phosphates to the pre-phosphorylated proteins substrates without enzymes. Current researches show that CK2 phosphorylation provides substrates for the pyrophosphorylation by IP_7 (Park et al., 2017). However, there is no antibody for pyrophosphorylation. The evidence of protein pyrophosphorylation by IP_7 is from radio labelling (Azevedo et al., 2009; Bhandari, Saiardi, et al., 2007).

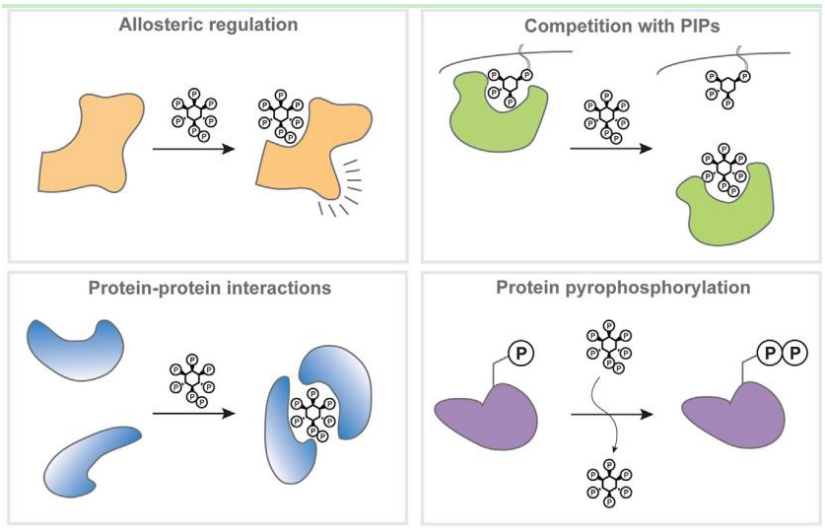

Figure 1-2 Mechanism of inositol pyrophosphates in regulating proteins (Furkert et al., 2020). The mechanisms of inositol pyrophosphates in cellular pathways include allosteric regulation, competition with PIPs, protein-protein interactions and protein pyrophosphorylation.

1.3 Mice embryonic development

Mice development begins from fertilization of the egg and ends at the birth of

infants. This process always lasts 19.5 days from the occurrence of a vaginal plug, which is marked at E0.5. The development of mice embryos can be separated into four stages, including cleavage and blastulation (0-5 d), implantation, gastrulation, and early organogenesis (5-10 d), organogenesis (10-14 d), fetal growth and development (14-19 d).

During the stages of cleavage and blastulation, the embryos are developed from fertilization to implantation. Fertilization begins from the combination of sperm and oocyte. Then the zygote is cleaved into 2 cells, 4 cells and 8 cells. The first differentiation events are morula compaction and blastocyst formation. The blastocyst has two cell lineages: the trophectoderm and inner cell mass. The embryonic stem cells are developed from inner cell mass at this stage. Embryo implantation in the uterus at E5 is an essential step during the development of embryos.

The second stage of embryonic development is a crucial stage for the formation of mesoderm and definitive endoderm. Important activities during this stage include the embryo turning, the appearance of forelimb and hindlimb buds as well as the appearance of lung buds. At the beginning of this stage, the embryos are very simple. During the amplification and differentiation in this stage, the embryos become more complex with many organs appearing.

The third stage of embryo development is organogenesis from E10 to E14. At this stage, more organs appear and develop. At the end of this stage, the embryos have

enucleated red blood cells.

At the last stage of embryo development, the organs become more mature. At the end of this stage, the embryos can adapt to the outside environment (Richard Behringer *et al*., 2003 Manipulating the Mouse Embryo: A Laboratory Manual, Fourth Edition).

1.4 Mice embryonic lethality

Genetically engineered mice are powerful tools of functional genomics studies. As such, mice can be used in the studies of gain or loss of gene function. With the development and application of a new gene-editing method, CRISPR-Cas9, it has become easier to produce genetical engineered mice. Nevertheless, embryonic lethality can be a problem in assigning gene function, as it is a prevalent phenotype in genetically modified mice indicated by an abnormal Mendelian ratio of genotypes among the offspring born from heterozygous crosses. In addition, the homozygous mutant offspring always have a smaller litter size than the wild-type mice. If gene modification leads to embryonic lethality, there will not be any homozygous mutant mice among the offspring born from heterozygous crosses. At the same time, the ratio of heterozygous mice to wild-type mice is about 2:1.

In circumstances in which homozygous mutations cause lethality, it is useful to determine developmental stage at which lethality occurs. E12.5 is a good starting point for analysis. At this stage, it is also easy to recognize the pregnant mice. To systematically dissect, examine, and genotype every embryo and implantation site,

we can establish the stage of lethality of homozygous mutant embryos. If no homozygous mutated embryos are detected and all implantation sites contain normal embryos, it is likely that the genetically mutated embryos died before implantation and did not translocate to the uterus. If no homozygous mutants are found but with some implantation sites remaining, the mutants will have died after implantation but before E10. However, if there are homozygous mutants at E12.5, it is informative to postpone the dissecting time to find out the precise dead time of homozygous mutants.

If homozygous mutants die before implantation, assessment of the morphology of the blastocyst is useful. For the homozygous mutants that have died just after implantation, we should see only trophoblast giant cell at implantation sites at E4.5-E5.5.

Successful implantation depends on the effective communication between the embryos and the pregnant mice, which requires the development of extraembryonic tissues, the trophoblast, primitive endoderm, and their derivatives. At E8.5-E9.5, establishing the connection between the placenta and fetal circulation is a crucial step for embryonic development. The link will supply the fetus with oxygen and nutrients. The defect in the placenta is a common cause of embryonic lethality. Defects in the development of blood, heart, or vessels can cause cardiovascular insufficiency, another primary cause of embryonic defects. A pale body, the small size of fetal liver or lack of blood indicates hematopoietic defects. Morphogenetic

defects in the heart or abnormalities in vasculogenesis or angiogenesis can severely affect embryonic development (Papaioannou & Behringer, 2012).

As there is a significant difference between the outside environment and the uterus, embryos have to face many challenges at birth or after birth. Neonatal lethality is from many reasons, including surviving parturition, respiratory failures, abnormal feeding and homeostasis defaults. The precise timing of neonatal lethality can provide vital clues to determine the causes of lethality (Turgeon, Meloche and Recherche, 2009). In addition, the molecular markers in specific tissues also provide essential indicators of the developmental status of the mutants. The expression of these molecular markers can be detected through Western Blot, RNA sequencing, qPCR, immunofluorescent staining or immunohistochemistry (Ward et al., 2012).

1.5 Fetal lung development

The lungs and the trachea are developed from the anterior foregut endoderm. The lungs developments begin from E9 with the expression of Nkx2.1 in the endoderm and lung buds appear at E9.5. The development of lungs in mice can be classified into 5 stages, including embryonic stages (E9.5-E12.5), pseudoglandular stage (E12.5-E16.5), canalicular stage (E16.5-E17.5), saccular stage (E18.5-P5) and alveolarization stage (P0-P14). During the first stage, the trachea separates from the oesophagus completely. Branching morphogenesis begins from the

psedoglandular stage and produces a lot of airways and terminal branches. After that, with the differentiation and maturation of pulmonary epithelium cells, pulmonary alveoli are developed from E16.5 to prepare for breathing after birth. However, alveoli are fully mature up to P14. The lung mesenchyme becomes thinner during the canalicular and saccular stages (Figure 1-3). It is also essential to developing fetal lungs because the lungs mesoderm promotes the branching and maturation of lungs (Herriges & Morrisey, 2014).

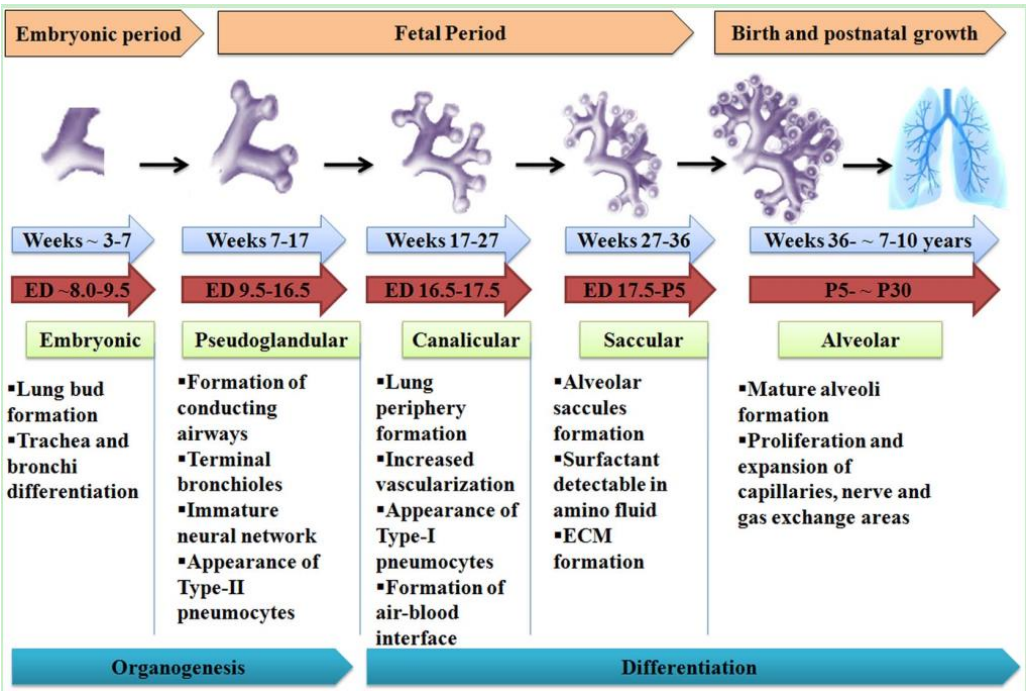

Figure 1-3 The development of fetal lung in the mice and human. During the embryonic stage, it sees lung bud formation, trachea and bronchi differentiation. At the pseudoglandular stage, it develops conducting airway and terminal bronchioles. Then, lung periphery and air-blood interface are formatted at canalicular stages. During the saccular stage, alveolar saccules are developed and surfactant proteins are secreted to amino fluid. The last stage is for the maturation of alveoli (Hussain et al., 2017).

From the lungs buds and trachea to a tree-like network, lungs experience many changes during gestational stages. There are three branching modes to make the

lungs complex, including domain branching, orthogonal bifurcation and planar bifurcation (Herriges & Morrisey, 2014; Metzger et al., 2008).

The development of lungs, via specification, branching and patterning, is regulated by many molecular pathways at different stages. The pathways of Wnt, Bmp and Fgf play essential roles in the development of the lungs. The expression of NKX2.1 is vital to the formation of the trachea and lungs buds on the anterior foregut endoderm. The Wnt and Bmp signalling pathways are necessary for the expression of NKX2.1 in the stage of lung specification. During the branching stage, inactivation of the Fgf pathway results in lung branching defects. In addition, Bmp4 and sonic hedgehog (shh) pathways also function on the branching morphogenesis of lungs. Other factors, including transcription factors, epigenetic regulators, miRNA and lncRNA, also regulate the differentiation and maturation of pulmonary epithelial cells through upregulating or downregulating gene expression in the fetal lungs (Herriges & Morrisey, 2014) (Barkauskas et al., 2017).

1.6 Bronchopulmonary dysplasia in newborn infants

Bronchopulmonary dysplasia (BPD), a result of pulmonary prematurity with defects in air exchange, is a common lung disease in newborn infants. The arrested airway morphogenesis, induced by the functional defects during the canalicular and the saccular stages, always results in the decrease of alveoli and defects of air exchange. Inflammation in the lungs can induce BPD, while the pulmonary injury will lead to inflammation response and finally develop into the BPD (Blackwell *et*

al., 2011; Balany and Bhandari, 2015; Jobe, 2016; Shahzad *et al.*, 2016; Kalikkot, Cuevas and Shivanna, 2017).

Preterm inflammation, due to mechanical ventilation and hyperoxia, is a common cause of BPD (Balany & Bhandari, 2015; Shahzad et al., 2016). Lipopolysaccharide, LPS, produced by *Escherichia coli* can inhibit airway morphogenesis, which shows similarity to BPD in the lungs with activation of macrophages. Moreover, block of the NF-kB pathway or depletion of NF-kB in macrophages can rescue airway branching in the cultured lung with LPS treatment (Blackwell *et al.*, 2011). Here, IL1 beta, released by macrophages, is an essential factor in inducing inflammation that disrupts airway morphogenesis, while inhibition of IL1 beta can protect lung airway morphogenesis from LPS infection (Hogmalm *et al.*, 2016). Further evidence for a role for IL 1 beta in fetal pulmonary function arises from the observation that overexpression of IL1 beta in the pulmonary alveolus affects the maturation and differentiation of pulmonary epithelial cells and leads to BPD at birth (Hogmalm *et al.*, 2014).

1.7 NF-κB pathway

The family of nuclear factor-κB (NF-κB) includes NF-κB1 (p50), NF-κB2 (p52), RelA (p65), RelB and c-Rel. These transcriptional factors play a vital role in activating inflammation and innate immune response through promotion of the expression of pro-inflammatory genes, including interferons and cytokines. The precursors of NF-κB1 and NF-κB2 are P105 and P100. The proteins are activated

on processing into mature P50 and P52. However, the mature processed NF-κB proteins are maintained in an inactive state in the cytoplasm by interacting with the inhibitor of κB (I κB).

The activation of NF-κB, by removal from influence of IκB, is vital to the activation of the immune response. In general, the activated NF-κBs translocate into the nucleus and service as transcriptional factors. Upon upstream signals, such as cytokines, growth factors, and stress, the kinases of IκB (IKK) are activated by phosphorylation. The IKK complex consists of a regulator subunit (NEMO) and two catalytic subunits, IKK alpha and IKK beta. The activated IKK can phosphorylate IκB, and this phosphorylation results in the release of NF-κBs from IκB. Phosphorylated IκB is then ubiquitinated and degraded by E3 and proteasome separately. Finally, free NF-κBs are activated and translocate into the nucleus and promote pro-inflammation gene expression. In addition, the activation of NF-κBs does not always lead to the degradation of IκB. For example, the phosphorylation of NF-κB2 precursor P100 by IKKα activates its processing into P52. The P52 then binds to RelB and services as a transcriptional factor (Liu *et al.*, 2017, Peng *et al.*, 2020)(Figure 1-4).

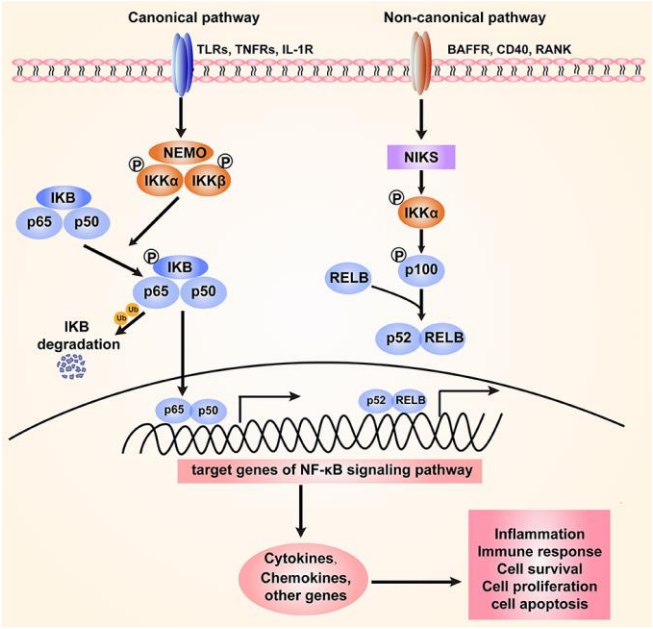

Figure 1-4 The activation of NF-κB. In the canonical pathway, IKK alpha and IKK beta are phosphorylated upon upstream signals, such as cytokines, growth factors, and stress. Then, the activated IKK phosphorylated IκB, which releases from NF-κBs. Finally, free NF-κBs are activated and translocate into the nucleus and promote pro-inflammation gene expression. In the noncanonical pathway, phosphorylated IKKα activates the NF-κB2 precursor P100, which is then processed into P52. The P52 then binds to RelB and services as a transcriptional factor (Peng et al., 2020).

1.8 DNA damage response

DNA damage leads to genome disability. DNA damage results from endogenous and exogenous factors, including reactive oxygen species, UV light, and genotoxic chemicals. DNA damage activates the DNA damage response pathway to repair DNA breaks. If the DNA break can be repaired well, the cell function is restored. If the DNA repair does not work accurately, it will lead to mutation in the genome and can be inherited to daughter cells through the cell cycle. The development of cancer cells is from the accumulation of mutation. On the other hand, inaccurate DNA repair can also lead to blockage of transcription in cells will finally result in

cell death.

Double strand DNA breaks (DSBs) are the most hurtful types of DNA damage because they do not have an intact template for DNA repair. DSBs leads to chromosome aberration and translocation and are related to many diseases and developmental defects. DSBs always results from ionizing radiation (IR) and genotoxic chemicals. There are two methods to repair DSBs, homologous recombination (HR) and nonhomologous end-joining (NHEJ). In the HR pathway, DNA repair uses a sister chromatid as a homologous template to repair the DSBs during the cell cycle phage. However, if there is no homologous template, cells rely on NHEJ to repair DSBs. However, in the NHEJ pathway, the cell ligates the broken end directly and brings deletions or insertions to the site of DSBs. The response to the DSBs is called DNA double-strand breaks repair (DSBR).

Except for DSBR, there are other pathways to repair DNA single-strand breaks (SSBs). Base excision repair (BER) and nucleotide excision repair (NER) are the major mechanisms to repair SSBs. BER is responsible for the base with slight chemical alterations. In the NER, it removes the single-strand DNA segment while the intact single-strand DNA services as a template to synthesize DNA by DNA polymerase(Giglia-mari et al., 2011).

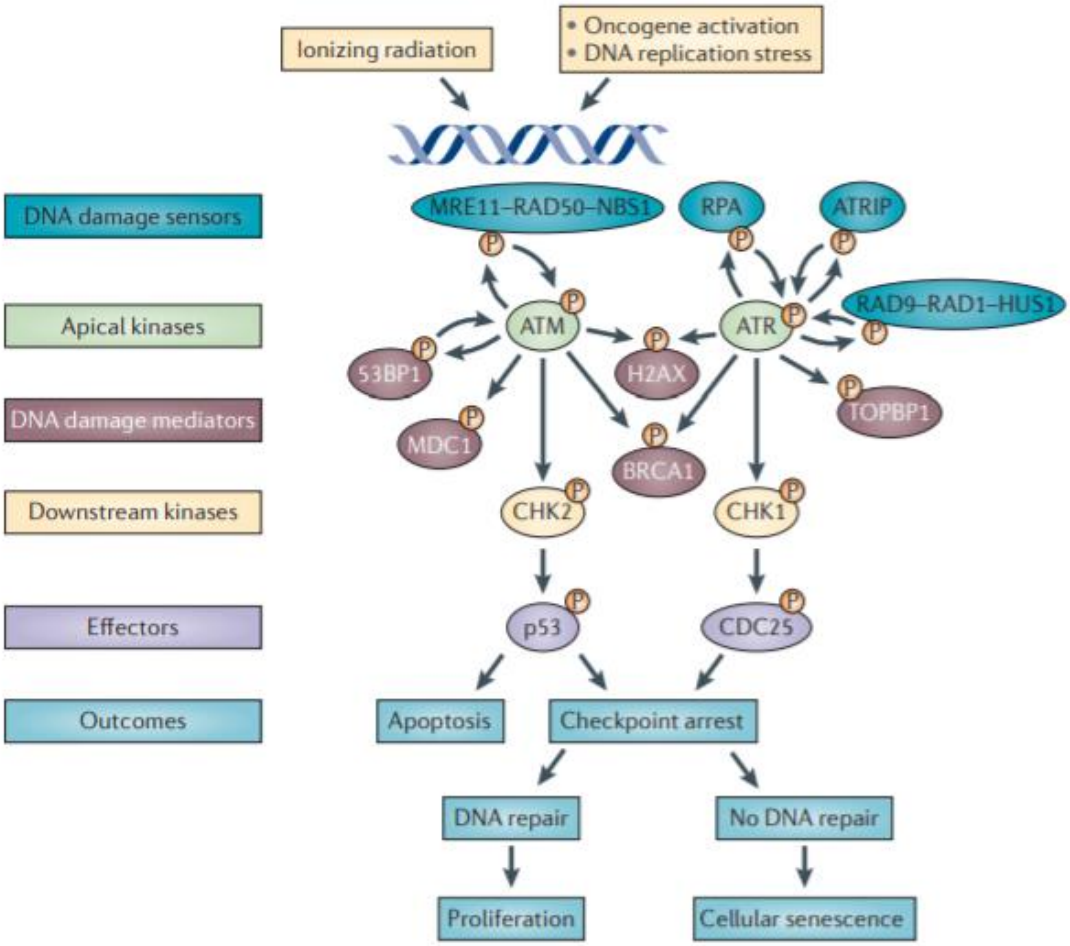

Figure 1-5 DNA damage response. The DNA sensor MRN recognizes DSBs while SSBs are detected by RPA and the RAD9-RAD1-HUS1 complex. The apical kinases ATM and ATR then phosphorylates H2AX. Phosphorylated H2AX is important to recruit MDC1 which is important to amplifying the DNA response signalling. ATM and ATR also phosphorylate CHK2 and CHK2 separately, both of which are important kinases of the effector of apoptosis and checkpoint arrest. (Sulli & Micco, 2012)

However, DNA repair defects can activate DNA damage checkpoint which leads to cell cycle arrest or cell death. DNA damage results in the activation of ATM and ATR, which response to DSBs and SSBs separately. ATM then phosphorylates H2AX, CHK2, MDC1 and BRCA1 to amplify DNA response signalling. On the other hand, ATR phosphorylates H2AX, BRCA1, TOPBP1 and CHK1. All of the

substrates of ATM and ATR are mainly the NA damage mediators and downstream kinases. These important players are essential to DNA repair, cell cycle arrest, chromatin remodelling and apoptosis. Activated H2AX is vital to the recruitment of DNA repair elements while P53 is an important cell cycle checkpoint and leads to cell cycle arrest. Cell cycle arrest is an important mechanism to prevent unrepaired DNA from being duplicated. In addition, activation of P53 and CHK2 leads to cell cycle arrest and induces apoptosis (Figure 1-5)(Giglia-mari, Zotter and Vermeulen, 2011, Sulli and Micco, 2012).

1.9 Hematopoietic erythropoiesis

Erythroid lineage cells are developed from mesoderm. The first appearance of erythroid lineage cells is at the yolk sac where it is close to the endoderm cells and form blood islands. At E7.5, primitive erythrocytes appear at yolk sac blood islands. However, only part of erythroid lineage cells differentiates into primitive erythrocytes while some erythroid lineage cells differentiate into hematopoietic stem cells (HSCs), which can differentiate into red blood cells and other immune cells. At E9, definitive progenitors generated at the yolk sac and placenta move to the fetal liver and differentiate into definitive red blood cells. Then, HSCs translocate into embryos from the yolk sac and firstly localize in the aorta-gonad-mesonephros region (AGM), where it generates hematopoietic progenitors and migrate to fetal livers. The fetal liver is the vital site for HSCs expansion and

differentiation during the middle and late gestational stages. Around birth, hematopoietic stem cells begin to migrate to the bone marrow where HSCs produces definitive red blood cells and other immune cells after birth. Adhesion receptors and chemoattractant receptors on the surface of hematopoietic stem cells is very crucial to their trafficking (Mazo, Massberg and von Andrian, 2011, Dzierzak and Philipsen, 2013)).

The differentiation of HSCs to erythrocytes follows the path from pluripotent stem cells to committed progenitors, from differentiating cells to differentiated cells. Firstly, HSCs differentiate into common myeloid progenitors (CMP) and common lymphoid progenitors (CLP). The common lymphoid progenitors then differentiate into T and B lymphocytes or natural killer cells. On the other hand, the differentiation of CMP divides into two paths, megakaryocyte erythroid progenitor (MEP) and granulocyte macrophage progenitor (GMP). GMP then differentiates to differentiating cells such as monocytes and finally differentiates to mature immune cells, including mast cells, basophils, neutrophils, eosinophils, macrophages and dendritic cells. MEP generates megakaryocytes which finally differentiate into red blood cells and platelets. In detail, the differentiation of erythroid lineage cells can be separated into more stages, HSC, CMP, MEP, BFU-E (burst-forming unit erythroid), CFU-E (colony-forming unit erythroid), ProE (pro-erythroblast), BasoE (basophilic erythroblast), PolyE (polychromatic erythroblast), OrthoE (orthochromatic erythroblast), reticulocyte and erythrocyte (Dzierzak & Philipsen,

2013).

BFU-E and CFU-E, the most immature erythroid progenitors, are defined by their ability to form mature erythroid cells colonies. In mice, it takes 7 days for BFU-E to form mature colonies of erythroid cells but only takes 2 days for CFU-E to form mature erythroid cells colonies. However, a CFU-E derived colony includes over a thousand mature erythroid cells while a BFU-E derived colony has only dozens of cells (Palis, 2014). During the process of erythropoiesis, the progenitor cells gradually lose the ability for self-renewal and differentiate to erythroid precursors and finally to mature red blood cells. In the maturation of erythroid precursors, which is from ProE to OrthoE, these erythroid precursor cells experience a series of changes, including accumulation of hemoglobin, nucleus condensation, reduced RNA content and cell size, as well as limited ability of cell divisions (Palis, 2014). After enucleation from OrthoE, the reticulocyte loses its nucleus and becomes mature red blood cells, which are essential to oxygen transportation. In definitive erythropoiesis, only after enucleation in the fetal livers or adult bone marrow, the reticulocytes enter the bloodstream. However, primitive erythropoiesis occurs from the yolk sac at E7.5, releases ProE into the bloodstream. The maturation of primitive erythroid cells occurs in the bloodstream and also develop into mature enucleated red blood cells at the late gestational stage (Figure 1-66)(Palis, 2014).

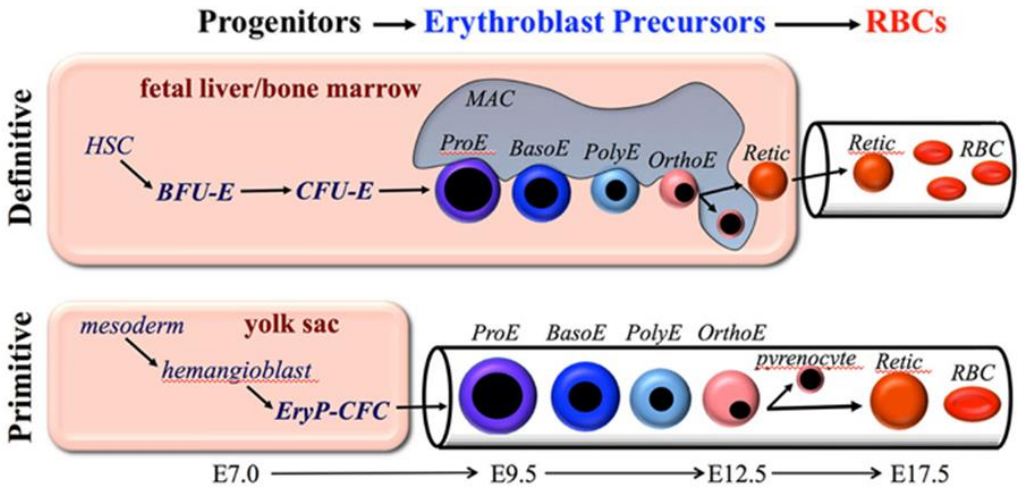

Figure 1-6 The process of erythropoiesis. During the process of erythropoiesis, the progenitor cells gradually lose the ability for self-renewal and differentiate to erythroid precursors and finally to mature red blood cells. The erythroblast precursors can be separated into ProE, BasoE, PolyE and OrthoE in according to their morphological characteristics. After enucleation from OrthoE, the cells will further develop into mature red blood. In definitive erythropoiesis, only after enucleation in the fetal livers or adult bone marrow, the reticulocytes enter the bloodstream. However, primitive erythropoiesis occurs from the yolk sac at E7.5, releases ProE into the bloodstream. The maturation of primitive erythroid cells occurs in the bloodstream and also develop into mature enucleated red blood cells at the late gestational stag (Palis, 2014).

The processes of erythropoiesis are regulated by many factors, including extracellular signals, transcription factors, epigenetic regulators and miRNA (Hattangadi et al., 2011). For example, erythropoietin (EPO) which is released from the kidney and binds to erythropoietin receptor (EPOR), is the most crucial signal for amplification and differentiation of erythroid cells. The stimulation of EPO and EPOR can regulate several pathways, including PI3K, MAPK, STAT5 and PKC pathways, which are also essential players in erythropoiesis (Jafari et al., 2019). GATA1, Klf1, LMO2 and LDB1 are essential transcription factors to induce the expression of genes necessary for erythroid cells (Hattangadi et al., 2011). In addition, the epigenetic modifications, including histone methylation and

acetylation, which are essential to the activation and repression of gene expression, have a gradual change in the process of erythropoiesis (Hattangadi et al., 2011). miRNAs also regulate genes essential to erythropoiesis because miRNAs can lead to mRNA degradation or translation inhibition. miR-451 is necessary for erythropoiesis. miR-150 is vital to the differentiation of MEP cells to megakaryocytic lineage cells. Other miRNAs, such as miR-144, miR-233 and miR-191 are also essential regulators of erythropoiesis (Jafari *et al.*, 2019, Hattangadi *et al.*, 2011).

1.10 Hemoglobin switching

Hemoglobin is a tetramer polypeptide with two heterodimers. In humans, the adult hemoglobin consists of two α and two β chains. Actually, the adult hemoglobin is different from embryonic globin and fetal globin because the hemoglobin experiences switching during gestational stages. Firstly, the embryonic globin (ζ_2 ε_2) is composed of two ζ and two ε chains. In the first hemoglobin switching, α and γ chains take the place of ζ and two ε chains separately and become fetal hemoglobin ($\alpha_2\gamma_2$). This switching happens during the gestational stage. During the second hemoglobin switching, the adult hemoglobin with two α and two β chains gradually become the major hemoglobin while there is a few fetal globins in the mature red blood cells (Wilber et al., 2011). In mice, hemoglobin also including 4 peptide units. The hemoglobin also experiences switching twice, from βh1 to εy, from εy to β major and β minor globin while the ζ also switches to α chain. βh1

globin is expressed as early as E7.5 at the yolk sac and is replaced by εy globin from E10.5 to E15.5. Then, the adult β globin, including β major and β minor globin, become the predominant chain in the late gestational stage and last for the whole lifespan (Figure 1-7) (Kingsley et al., 2006; Sankaran et al., 2010a; Sankaran & Orkin, 2013; Wilber et al., 2011). Hemoglobin is essential to the functions of red blood cells and disorder of hemoglobin would lead to severe disease. For example, β-thalassemia and sickle cell disease (SCD) are because of the disorder of β hemoglobin. β-thalassemia is from insufficient production of β hemoglobin, which leads to precipitation of α hemoglobin in erythroid precursors. Sickle cell disease is from the accumulation of mutated β hemoglobin in erythrocytes and finally block small bloodstream (Sankaran & Orkin, 2013).

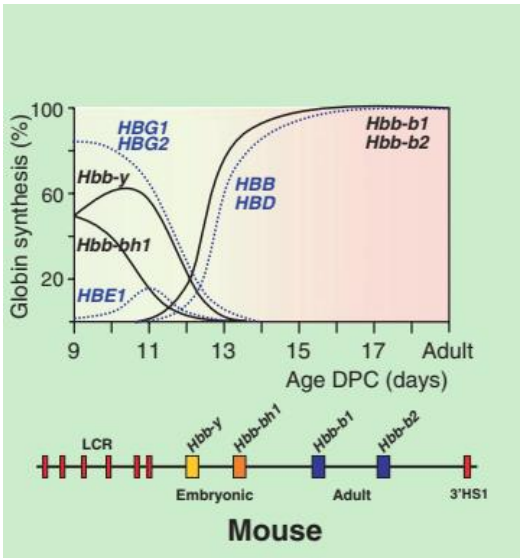

Figure 1-7 β globin switching the mice. The β globin also experiences switching twice, from βh1(Hbb-bh1) to εy(Hbb-y), from εy to β major and β minor (Hbb-b1, Hbb-b2). βh1 globin is expressed as early as E7.5 at the yolk sac and is replaced by εy globin from E10.5 to E15.5. Then, the adult β globin, including β major and β minor globin, become the predominant chain in the late gestational stage and last for the whole lifespan (Sankaran et al., 2010).

Hemoglobin switching is a transcriptional activity. The locus control region (LCR), an upstream enhancer, is essential for the expression of β hemoglobin. In addition, many transcription factors play a vital role in the hemoglobin switching. BCL11A is crucial for the fetal to adult hemoglobin switching because it represses the expression of γ globin (Sankaran, Xu and Orkin, 2010). Sox6 also inhibits fetal globin by silencing the expression of εy globin (Yi et al., 2006). KLF1 is also essential to the switching from fetal to adult globin because it regulates the expression of BCL11A and γ globin (Zhou et al., 2010). Other transcription factors, such as NF-E4, COUP-TF, DRED/TR2/TR4, MBD2, also regulate hemoglobin switching (Sankaran et al., 2010a; Sankaran & Orkin, 2013; Wilber et al., 2011). In addition, histone modification also regulates the expression of β hemoglobin (Kingsley et al., 2006).

1.11 Tracking the differentiation of hematopoietic stem cells

To track the differentiation of hematopoietic stem cells is a practical tool of hematopoietic research. During the maturation and differentiation of hematopoietic stem cells, genes expressed in the differentiating and differentiated cells are different. This provides us with a strategy for the differentiation of hematopoietic stem cells. For example, single-cell RNA sequencing and mass spectrometry technology can be used to track HSCs differentiation through measuring the expression of mRNA and protein accumulation. Polylox barcoding combined with sequencing is also used to track the differentiation of hematopoietic stem cells

(Dharampuriya *et al.*, 2017; Lee-Six and Kent, 2020). Currently, flow cytometry is the most popular technology for tracking the differentiation of hematopoietic stem cells. With technical advances in more useful antibodies, dyes and flow cytometry, this method will continue to contribute to the research on hematopoietic research. With a different expression of cell surface markers in diverse cell populations, hematopoietic stem cells, hematopoietic progenitor cells (including MMP, CLP, CMP MEP and GMP), differentiating and differentiated cells can be classified and purified with flow cytometry (Dharampuriya et al., 2017; Mayle et al., 2013). For example, combined antibodies of KLS (c-Kit$^+$ (K), Lin$^-$ (L), and Sca-1$^+$(S)) are always used to enrich hematopoietic stem and progenitor cells while marker phenotypes of Lin$^-$ Il7rα^- c-Kit$^+$ Sca-1$^-$ CD34$^+$ CD16/32$^-$, Lin$^-$ Il7rα^- c-Kit$^+$ Sca-1$^-$ CD34$^-$ CD16/32$^-$ and Lin$^-$ Il7rα^- c-Kit$^+$ Sca-1$^-$ CD34$^+$ CD16/32$^+$ are used to classify and enrich CMP, MEP and GMP populations separately (Mayle *et al.*, 2013; Grinenko *et al.*, 2018)(Figure 1-8). In addition, the surface markers of erythroid cells are changing in the maturation of erythroid cells. The expression of Kit reduces in the differentiation of erythropoiesis while Ter119 has an increased expression in the maturation. However, CD71 increases and then decreases in this process. As these markers have a changing expression pattern during the maturation of erythroid cells, we can use these surface markers to track the maturation and differentiation of erythroid cells at different stages. CD71 and Ter119 are always used to identify and analyse mouse erythroid progenitors

(Koulnis *et al.*, 2011; Dzierzak and Philipsen, 2013).

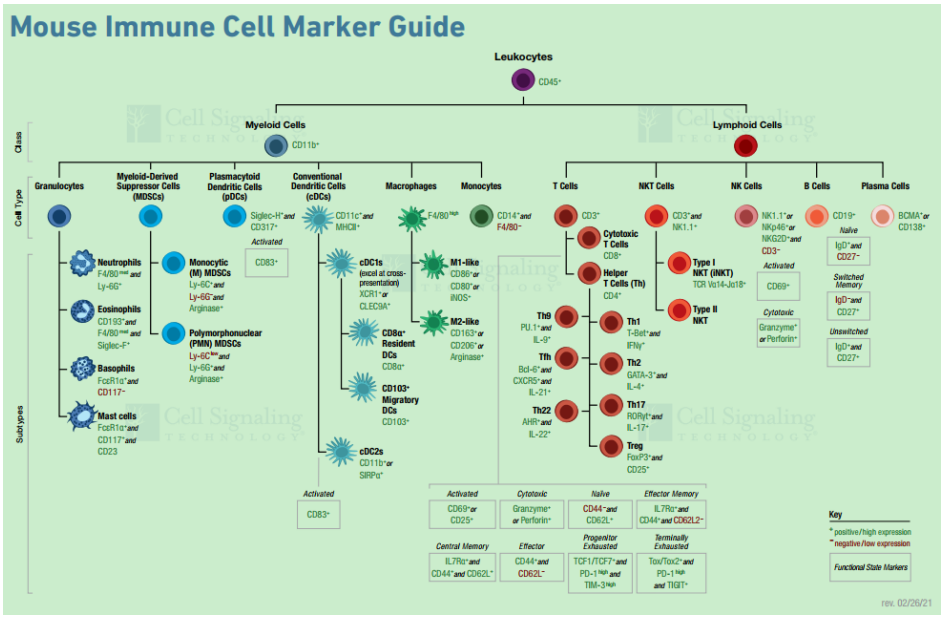

Figure 1-8 Mouse immune cell marker guide of Cell Signalling Technology. All the immune cells express CD45 while myeloid cells express CD11b, which can be used to distinguish lymphoid cells and myeloid cells. According to the expression of surface receptors, the subtypes of myeloid cells and lymphoid cells can be further tracked with specific antibodies (*Mouse Immune Cell Marker Guide*, 2021).

Chapter 2 Materials and methods

2.1 Animal care

All mice in this project were raised at the Animal Center of South University of Science and Technology, China (Sustech), which provides an approved environment for specific-pathogen-free mice. All the mice used in experiments in this project follow the regulations of the Laboratory Animal Welfare and Ethics Committee of Sustech.

2.2 Development of IP6K1 conditional knockout mice

The conditional knockout mice (C57/B) of IP6K1$^{WT/loxp}$ are from Snyder's lab. The strategy to establish the mice is inserting the loxp elements in intron 5 and exon 6 separately so as to target the exon 6 of IP6K1 under the control of the Cre enzyme. The sequence of loxp element is ATAACTTCGTATAGCATACATTATACGAAGTTAT, a 34 bp DNA spacer (Bhandari, Juluri, et al., 2008)

2.3 Development of double conditional knockout mice (CKO) of IP6K1 and IP6K2

The development of double CKO mice is on the base of the heterozygous mice of IP6K1$^{WT/loxp}$. Exon 2 of IP6K2 is targeted for cleavage by Cre recombinase. Another recombinase element flox, which was also recognized by the Cre enzyme, was inserted in intron 1 and intron 2 of IP6K2 separately. The sequence of flox element is:

GCATCGCATTGTCTGAGTAGGTGGCTAGCAGTACTATAACTTCGTATAG GATACTTTATACGAAGTTATGGACTAACAGAAGAACCCGTTGTG, a 93 bp DNA fragment. The development of double CKO mice was performed at GemPharmatech, Nanjing, China.

2.4 Generation of heterozygous double knockout mice IP6K1$^{+/-}$IP6K2 $^{+/-}$

To produce the heterozygous mice of double knockout of IP6K1 and IP6K2, the heterozygous double conditional knockout mice IP6K1$^{WT/loxp}$IP6K2 $^{WT/flox}$ were crossed with CMV-Cre mice (BIOCYTOGEN, Beijing, China) which could express Cre enzyme in the whole body. Mice around two months were mated. Female mice of IP6K1$^{wt/loxp}$IP6K2 $^{wt/flox}$ crossed with male mice of CMV-Cre. Reciprocally, male mice of IP6K1$^{wt/loxp}$IP6K2 $^{wt/flox}$ were crossed with female mice of CMV-Cre. The heterozygous double knockout mice of IP6K1and IP6K2 among the offspring were confirmed by PCR as well as Sanger sequencing.

2.5 Production of heterozygous female mice of IP6K1$^{+/-}$IP6K2 $^{+/-}$

As we need a large number of female heterozygous DKO mice to maintain embryonic research, we have to produce a large number of female heterozygous DKO mice in advance. The male heterozygous double knockout mice of IP6K1$^{+/-}$ IP6K2 $^{+/-}$ were mated with a population of wild-type female mice, readily available from the animal centre. Through this method, I produced a large number of heterozygous DKO mice for embryonic research. In fact, the crossing of heterozygous double knockout mice is not an excellent approach to produce

numerous heterozygous DKO mice.

2.6 DNA isolation from mice tissues and genotyping

Mice tails or tissues were heated at 100 degrees in 200 µl 40mM NaOH and for 40 minutes, then cooled n to room temperature. 200 µl 25mM Tris-HCl (pH5.5) was added to the lysate and mixed well. 2 µl of the resulting solution was mixed with 10 µl pre-stained taq mixture (CWbio), 7 µl H2O, 2 µM primer forward and reverse, and PCR conducted as follows:

For IP6K1/IP6K3 genotyping

1. 95 degrees, 2 minutes,
2. 95 degrees 30 seconds,
3. 56 degrees 30 seconds (56 degrees for IP6K1, 54 degrees for IP6K3),
4. 72 degrees 30 seconds,
5. 33 cycles from step 2 to step 4,
6. 72 degrees 5 minutes,
7. Stop at 4 degrees.

For IP6K2 genotyping

1. 95 degrees, 2 minutes,
2. 95 degrees 30 seconds,
3. 65 degrees 30 seconds, with 0.5 degree decrease every cycle,
4. 72 degrees 30 seconds,
5. 20 cycles from step 2 to step 4,

6. 95 degrees 30 seconds,
7. 55 degrees 30 seconds,
8. 72 degrees 30 seconds,
9. 19 cycles from step 6 to step 8,
10. 72 degrees 5 minutes,
11. Stop at 4 degrees.

For VAV Cre/CMV Cre/NKX2.1 Cre genotyping

1. 95 degrees, 2 minutes,
2. 95 degrees 30 seconds,
3. 62 degrees 30 seconds, (62 degrees for VAV Cre, 58 degrees for CMV Cre and NKX2.1 Cre)
4. 72 degrees 30 seconds,
5. 33 cycles from step 2 to step 4,
6. 72 degrees 5 minutes,
7. Stop at 4 degrees.

The PCR samples were separated on 2% agarose gel.

Genotyping primers were as follows:

K1 F	GAGGTGAGTCTGCTCCTGTG
K1KO F	GGTGCTGAGCTTGGTTTTGC
K1 R	AAGGTTGGCAGGATTACCTTC

K2 F	GTCCTCCAGGAAACCAGAAGCCC
K2 R	TGTCCCAGGGGAATCTATGTTG
K2KO R	CCTGACTCTAGGGACTGGGGAA
Cre F	GCCTGCATTACCGGTCGATGC
Cre R	CAGGGTGTTATAAGCAATCCC
VAV Cre F	GGTGTTGTAGTTGTCCCCACT
VAV Cre R	CAGGTTTTGGTGCACAGTCA
K3WT F	GATGTCCGGATGATTGACTT
K3WT R	GGGGAAATCTAGACTACCCTAG
K3KO F	GAAGATCCGTCCCTGAATGCT
K3KO R	ATTTTCCCAGGCCCATTGCT

2.7 Dissection of pregnant mice to obtain homozygous DKO mice embryos at specific stages

According to the experience, one female heterozygous DKO mouse and one male heterozygous DKO mouse were put in a cage at 4-5 p.m. When a copulatory plug was checked in the following day, embryos of the stage was marked as E0.5. Then the female mice were separated from male mice while the male mice could be used

for mating a week later. From E11.5, it is easy to confirm whether the female mice were pregnant. Pregnant mice at the different stages were dissected after humane dispatch with CO_2 to obtain embryos.

2.8 Isolate tissues from mice embryos

Embryos from E13.5 were isolated from the pregnant mice with the assistant of disserting microscopy. The liver of the embryos was separated carefully. It is a large red organ. The lung is a white organ with two lobes of tissues. The lung is attached to the heart and was carefully separated from the heart. All tissues isolated from the embryos were frozen with liquid nitrogen and stored at -80 degrees for RNA and proteins analysis or were fixed in 4% paraformaldehyde (PFA) for immunohistochemical or immunofluorescent research.

2.9 Analysis of maturation of erythroid progenitor cells with fetal liver

The livers were isolated from E13.5 embryos and washed with PBS twice before being transferred into 2 mL cold staining buffer (PBS with 5mM glucose and 0.2% BSA). The livers were dissociated into single cells by pipetting mechanically in the buffer. There are about 10^7 cells in a normal fetal liver of an E13.5 embryo.10^6 cells were transferred to a new tube and washed with cold staining buffer twice. The antibody of APC-CD71 (working concentration is 0.25 μg/ml) and PE-Ter119 (working concentration is 0.125 μg/ml) were added to each tube and incubated on ice for one hour in a dark environment. The cells were washed with 3mL cold staining buffer and resuspended with 400 μL cold staining buffer with DAPI (final

concentration 0.5 μ g/ml).

Each tube was analysed by a FACS analyser (BD). The dead cells were excluded with the DAPI signal. The differentiation and maturation of hematopoietic stem cells are classified by the signals of Ter119 and CD71

2.10 Tracking differentiation of hematopoietic stem cells in fetal livers

Fetal livers at E15.5 were harvested in PBS and dissociated into single cells by pipetting. The cells were washed with cell staining buffer containing 0.3% BSA twice. The cells were then incubated with related antibodies at 4 degrees for 30 minutes in a dark environment. After staining, the cells were washed with 2 mL cell staining buffer twice and finally resuspended with 200μL cell staining buffer containing 0.3% BSA. The stained cells were then analysed by FACS sorter (BD).

2.11 Analyse the immune cells with fetal lungs

Fetal lungs at E18.5 were harvested in PBS and dissociated into single cells by grinding lungs tissues with a syringe end on the 70μm cell filter, under which a 50mL tube is used to collect the cell suspension. The cells were washed with cell staining buffer containing 0.3% BSA twice. The cells were then incubated with related antibodies at 4 degrees for 30 minutes in a dark environment. After staining, the cells were washed with 2 mL cell staining buffer twice and finally resuspended with 200μl cell staining buffer containing 3% BSA each. The stained cells were then analysed by the FACS sorter.

2.12 Blood cells analysis

200 μL of blood were harvested from the venous sinus of mature mice (over two months). The blood is collected to the EDTA-K2 tube to prevent coagulation. In addition, the tube should be subtly shaken to make sure no coagulation in the wall after blood collection. Whole blood samples after collection were analyzed by a hematology analyser (DF50CRP, Dymind) sooner.

2.13 Isolate proteins from the tissues of mice embryonic tissues for Western Blot

40 μL of strong RIPA buffer is added to every 1 mg of tissues. A metal ball is used to lysate the tissues mechanically with a tissue lyser (60HZ for 60s, incubated on ice for 10 minutes, 60HZ for 60s). After that, the lysis solution is stilled on ice for 10 minutes before being centrifuged at 12000rpm for 10 minutes at 4 degrees. The supernatant is transferred into a new tube. After measuring the proteins concentration by the BCA method, equivalent amounts of proteins samples were harvested and added with proteins loading buffer. The sample solutions were then heated at 100 degrees for 10 minutes and stored at -20 degrees for further analysis.

2.14 Separate proteins by SDS-polyacrylamide gel electrophoresis (SDS-PAGE)

SDS-PAGE gels were produced according to the molecular weight of targeted proteins. In this project, for separating the proteins under 30kD, I use 12% or 15% acrylamide in the separating gel while I use 8% acrylamide in the separating gel

for separating proteins over 50kD. The concentration of acrylamide in the stacking gels is 4%. 1 μg of protein sample is loaded into the stacking gel wells along with 5μL Pierce pre-stained protein molecular weight marker (ThermoFisher Scientific) as a ladder. Gels were run at a constant 80V electric until the blue front band reaches the separating gel and narrows down to a thin line. Then, the gels were run at a constant 120V electric until the blue front band runs off the gel. The running buffer contains 25 mM Tris, 192 mM glycine and 0.1% SDS.

2.15 Protein transfer and imaging

Proteins samples separated by the SDS-PAGE gel were transferred to the PDVF membrane in the transfer buffer (25 mM Tris, 192 mM glycine) containing 20% methanol. After being transferred to the PDVF membrane, the membrane is blocked by 5% skim milk (BD Difco) in the TBST (20 mM Tris, 150 mM NaCl, 0.1% Tween 20, pH 7.4-7.6) for one hour at room temperature. The membrane is incubated with the primary antibody on a shaking incubator at 4 degrees overnight. The membrane is then washed with TBST 3 times, 5 minutes each, before being incubated with a secondary antibody at room temperature for one hour. Then the membrane is rewashed with TBST for 3 times, 10 minutes each. Proteins were visualized by adding Pierce ECL Western Blotting Substrate (ThermoFisher Scientific) before being applied to the imaging system (Champchem i610 plus). Images were captured automatically by the software of the imaging system.

2.16 Antibodies and reagents

Antibodies	Supplier	Item NO.	Usage
IRF3	ABclonal	A11118	WB
P-IRF3 (S396)	Cell Signaling Technology	29047S	WB
NF-kappa B	Cell Signaling Technology	8242T	WB
P-NF-kappa B (S536)	Cell Signaling Technology	3033T	WB
P-H2AX (S139)	Cell Signaling Technology	9718S	WB, IF
P-P53(S15)	Cell Signaling Technology	9284S	WB
P-CHK2(T68)	Cell Signaling Technology	2661S	WB
P-KAP1(S824)	Bethyl	A300-767A	WB
IKK-beta	Cell Signaling Technology	8943T	WB
P-IKK alpha/beta (S176/180)	Cell Signaling Technology	2697T	WB
P-IKB	Cell Signaling Technology	2859T	WB
IKB	Cell Signaling Technology	4814T	WB
Beta Actin	Proteintech	66009-1-Ig	WB
P-AKT (T308)	Cell Signaling Technology	13038T	WB
P-AKT (S473)	Cell Signaling Technology	9271S	WB
PARP	Cell Signaling Technology	9532S	WB
GAPDH	Abmart	M20006F	WB

AMPK alpha	Cell Signaling Technology	5831T	WB
P-AMPK (T172)	Cell Signaling Technology	2535S	WB
IP6K2	Sigma	SAB4502132-100UG	WB
IP6K1	GeneTex	GTX103949	WB
CD71-APC	Biolegend	113819	FACS
CD90.2	BioLegend	140306	FACS
CD45	BioLegend	103138	FACS, IF
CD8a	BioLegend	100723	FACS
CD11c	BioLegend	117328	FACS
NK1.1	BioLegend	108707	FACS
CD19	BioLegend	115552	FACS
IL-7Ra	BioLegend	135014	FACS
TCRb	BioLegend	109218	FACS
Ly-6G	BioLegend	108456	FACS
I-A/I-E	BioLegend	107620	FACS
F4/80	BioLegend	123146	FACS
CD86	BioLegend	105014	FACS
FCER1a	BioLegend	134310	FACS
TCRb	BioLegend	109246	FACS
CD34	BioLegend	152208	FACS
CD11b	BioLegend	101217	FACS
Ly-6A/E	BioLegend	108124	FACS
CD19	BioLegend	152406	FACS
CD16/32	BioLegend	101318	FACS
CD4	BioLegend	100568	FACS
CD11c	BioLegend	117352	FACS

CD8a	BioLegend	100766	FACS
CD45R/B220	BioLegend	103260	FACS
CD4	BioLegend	100531	FACS
CD4	BioLegend	100559	FACS
CD4	BioLegend	100548	FACS
CD4	BioLegend	100529	FACS
CD4	BioLegend	100540	FACS
CD4	BioLegend	100512	FACS
CD4	BioLegend	100566	FACS
CD4	BioLegend	100528	FACS
CD4	BioLegend	100530	FACS
CD127	BioLegend	135019	FACS
TER119	BioLegend	116207	FACS
CD19	BioLegend	115529	FACS
CD49b	BioLegend	103503	FACS
CD16/32	BioLegend	101302	FACS
Zombie	BioLegend	423105	FACS
CD117	BioLegend	105808	FACS
CD4	BD Biosciences	740208	FACS
CD11b	BD Biosciences	612800	FACS
Siglec-F	BD Biosciences	740388	FACS
Ly-6G	BD Biosciences	563978	FACS
TCRb	BD Biosciences	612821	FACS
FceR1 alpha	Thermo Fisher	47-5898-82	FACS
Pro-SPC	Santa Cruz	SC133143	IF
Isolectin B4	Sigma	L2895-.2MG	IF
Ki67 (FITC)	Biorbyt	orb14083	IF
T1A	R&D Systems	AF3244	IF

Myeloperoxidase	R&D Systems	AF3667	IF
MUC5B	Novus	NBP1-92151	IF
MUC5AC	thermo	MA5-12178	IF
Acetylated Tubulin	Sigma	T7451-100UL	IF
α SMA-Cy3	Sigma	C6198	IF
CC10	Santa Cruz	sc-365992	IF
CD31	Abcam	ab7388	IF
Anti-rabbit IgG (H+L), F(ab')2 Fragment (Alexa Fluor® 488 Conjugate)	Cell Signaling Technology	4412S	Secondary antibody for IF
Anti-rabbit IgG (H+L), F(ab')2 Fragment (Alexa Fluor® 555 Conjugate)	Cell Signaling Technology	4413S	Secondary antibody for IF
Goat anti-Mouse IgG (H+L) Cross-Adsorbed Secondary Antibody, Alexa Fluor 488	Life technologies	A-11001	Secondary antibody for IF
Goat anti-Mouse IgG (H+L) Cross-Adsorbed Secondary Antibody, Alexa Fluor 568	Life technologies	A-11004	Secondary antibody for IF
Goat anti-Mouse IgG (H+L) Cross-Adsorbed Secondary Antibody, Alexa Fluor 594	Life technologies	A-11005	Secondary antibody for IF
Donkey anti-Goat IgG (H+L) Cross-	Life technologies	A-11055	Secondary

Adsorbed Secondary Antibody, Alexa Fluor 488		antibody for IF

Regents	**Supplier**	**Item NO.**
Tunel assay kit	Beyotime	C1091
Senescence β-Galactosidase Staining Kit	Beyotime	C0602
2'3'-cGAMP ELISA Kit	Cayman	501700
Reactive Oxygen Species Assay Kit	Beyotime	S0033S
2xTaq MasterMix（Dye）	CWbio	CW0682L
RevertAid First Strand cDNA Synthesis Kit	Thermo Fisher SCIENTIFIC	K1622
SYBR green realtime PCR master mix	TOYOBO	QPK-201
TRIzol™ Reagent	Invitrogen™	15596018
Hematoxylin and Eosin Stain Kit	Leagene Biotechnology	DH0006
RIPA Lysis Buffer (Strong)	Beyotime	P0013B
NP-40 Lysis Buffer	Beyotime	P0013F
PBS	Thermo Fisher SCIENTIFIC	
DMEM	Thermo Fisher SCIENTIFIC	

2.17 RNA isolation

RNA was isolated according to the manufacturer's protocol, after ensuring that all reagents and tubes are RNAse-free. Briefly, 1mL Trizol (Life) was added to each tissue sample. After being physical disruption by vortexting, the lysis solution was centrifuged at 12,000rpm at 4 degrees C for 10 minutes. 500 μL supernatant was transferred to a new tube, and 100 μL chloroform added to each sample. After shaking for half a minute, the solution was stilled for 5 minutes before being centrifuged at 12,000 rpm for 10 minutes at 4 degrees C. The upper supernatant (150μL) was transferred to a new tube with addition of an equal volume of isopropanol. After incubation at room temperature for 15 minutes, the solution was centrifuged at 12,000rpm at 4 degrees C for 10 minutes. The supernatant was discarded, and the pellet was washed with 75% ethanol twice. The pellet was air-dried, and 50μL of DEPC water was used to dissolve the RNA. RNA was used for reverse transcription immediately or stored at -80 degrees C.

2.18 Reverse transcription and quantitative PCR

1μg of RNA is used for cDNA synthesis with the cDNA synthesis kit (Thermo Fisher) following the protocol. In brief, the mixture of RNA and primer were heated at 65 degrees for 5 minutes, then cooled on ice for 2 minutes, mixed with dNTP, reaction buffer, RNase inhibitor and reverse transcription enzyme before being incubated at 25 degrees for 8 minutes and 42 degrees for 1 hour. The reaction is terminated at 70 degrees for 5 minutes. The reverse transcription reaction

production is stored at 4 degrees in a short time or -20 degrees in a long time. Synthesized cDNA is used to measure the expression of specific genes through qPCR. A mixture of 5μL Syber green (Takara), 0.5μL of primer (terminal concentration is 1 μM), 4.5μL cDNA (after the products of RT-PCR were diluted to 20 volumes with ddH2O) is applied to the standard process of qPCR.

The primers of qPCR in this study were as follows:

SPA F	GAGGAGCTTCAGACTGCACTC
SPA R	AGACTTTATCCCCCACTGACAG
SPB F	GGCTGTGTCCCAGGTGTGCC
SPB R	AGGCTCCACAGCAGGGAGGG
SPC F	TAGCCCCGAGTGAGCGAGCA
SPC R	GTGGGTGTGGAGGGCTTGGC
SPD F	GCCTGGTCGTGATGGACGGG
SPD R	AGGGCCCTGCAACCCTGAGA
T1A F	CAGGAGACGGCATGGTGCCC
T1A R	AGGCTTCGTCCCACGCTCTCT
TTF1 F	CATGGGCAAGGGTCAGGGGC
TTF1 R	GCCTGGCCCTGTCTGTACGC
CC10 F	GCGGGCACCCAGCTGAAGAG
CC10 R	GAGCCGAGGAGACACAGGGCA

GAPDH F	GTCGTGGAGTCTACTGGTGTC
GAPDH R	GAGCCCTTCCACAATGCCAAA
IP6K2 F	ACACTATAACCCTTGGAGCATGA
IP6K2 R	TCATAGCGGGAAGTCAGGT
IP6K1 F	GCTGGGGGTCAGGGTCTGTG
IP6K1 R	GGAAGCCCTCGATGGAGAGT
IP6K3 F	CCGTCACATGAAGAAGTGCG
IP6K3 R	CCTGAATCCCTCCACCGAGA
EPO F	ACAAAGCCATCAGTGGTCTACG
EPO R	TCTGGAGGCGACATCAATTCC
EPOR F	GGTGAGTCACGAAAGTCATGT
EPOR R	CGGCACAAAACTCGATGTGTC
BCL11A F	AACCCCAGCACTTAAGCAAA
BCL11A R	ACAGGTGAGAAGGTCGTGGT
SOX6 F	AATGCACAACAAACCTCACTCT
SOX6 R	AGGTAGACGTATTTCGGAAGGA
HBB-Y F	TGGCCTGTGGAGTAAGGTCAA
HBB-Y R	GAAGCAGAGGACAAGTTCCCA
HBA-X F	CTACCCCCAGACGAAG ACCTA

HBA-X R	CTTAACCGCATCCCCTACGG
HBB-BH1 F	TGGACAACCTCAAGGAGACC
HBB-BH1 R	ACCTCTGGGGTGAATTCCTT
HBB-BS F	ATGGCCTGAATCACTTGGAC
HBB-BS R	ACGATCATATTGCCCAGGAG
IL1B F	GAAATGCCACCTTTTGACAGTG
IL1B R	TGGATGCTCTCATCAGGACAG
ACTIN F	GGCCCAGAGCAAGAGAGGTATCC
ACTIN R	AGCCACGATTTCCCTCTCAGC
IFNB1 F	AGCTCCAAGAAAGGACGAACA
IFNB1 R	GCCCTGTAGGTGAGGTTGAT
HIF1A F	TCTCGGCGAAGCAAAGAGTC
HIF1A R	AGCCATCTAGGGCTTTCAGATAA
IFI44 F	ATGCTCCAACTGACTGCTCG
IFI44 F	ACAGCAATGCCTCTTGTCTTT
IRF7 F	GCGTACCCTGGAAGCATTTC
IRF7 R	GCACAGCGGAAGTTGGTCT
GBP3 F	CAGCTAATCCGGGCAAAATCG
GBP3 R	ATGGGCCGACCATTTAACTTC

OAS1A F	GCCTGATCCCAGAATCTATGC
OAS1A R	GAGCAACTCTAGGGCGTACTG

2.19 Tissues samples preparation for immunohistochemical and immunofluorescent studies

Fresh tissues were isolated from embryos with the assistance of disserting microscopy. Tissues were washed with cold PBS twice. Then follow the processes of fixation and dehydration.

1. 4% PFA for 2 hours,
2. PBS for 5 minutes, twice,
3. PBS overnight,
4. 50% ethanol for 40 minutes,
5. 70% ethanol for 40 minutes,
6. 80% ethanol for 40 minutes,
7. 95% ethanol for 40 minutes,
8. 95% ethanol for 40 minutes,
9. Absolute ethanol for 40 minutes,
10. Absolute ethanol for 40 minutes,
11. Xylenes for 25 minutes,
12. Xylenes for 25 minutes,

13. Paraffin for 30 minutes,
14. Paraffin for 30 minutes,
15. Paraffin for 40 minutes.
16. Then tissues were embedded into wax blocks.

2.20 Hematoxylin and eosin (H&E) staining

The process of H&E staining follows the protocol of the company. Briefly,

1. Dewax the paraffin section with xylene for 5 minutes, twice;
2. Dehydrate with absolute ethanol for 5 min twice,
3. 95% ethanol for 5 minutes,
4. 90% ethanol for 5 minutes,
5. 80% ethanol for 5 minutes,
6. ddH_2O for 3 minutes.
7. Stain with hematoxylin for 5 minutes,
8. Then flouting water for 20 minutes.
9. Differentiate with 1% HCl in ethanol for 2 seconds,
10. ddH_2O for 30 seconds.
11. Blue with 0.2% NH_4OH for 20 seconds,
12. ddH_2O for 30 seconds.
13. Stain with eosin for 3 minutes
14. ddH_2O for 1 second.
15. Dehydrate with ethanol, 80% for 10 seconds,

16. 90% for 10 seconds,
17. 95% for 1 minute twice,
18. 100% ethanol 2 minutes twice.
19. Xylenes for 2 minutes, three times
20. Cover-slip the slide with neutral resin.

2.21 TUNEL assay

The process follows the protocol of the kit as follows.

1. Immerse the slide in xylenes for 5 minutes, twice.
2. Rehydration. Immerse the slide in 100% ethanol for 5 minutes,
3. 90% ethanol for 2 minutes,
4. 70% ethanol for 2 minutes,
5. ddH_2O for 2 minutes.
6. Incubate with 20µg/ml proteinase K for 15 minutes at RT.
7. Rinse slide with PBS briefly three times.
8. Immerse the slide with 3% H_2O_2 in PBS for 20 minutes at RT.
9. Rinse the slide with PBS three times.
10. Labelling. Incubate the slide with the TDT enzyme mixture (5µl TdT enzyme and 45µl Biotin-dUTP) at 37 degrees C in the dark.
11. Add Streptavidin-HRP working buffer (1µl Streptavidin-HRP and 49µl dilution buffer) to the slide for 30 minutes at RT.
12. Rinse the slide with PBS three times.

13. Add DAB solution for 5-30 minutes according to the results of development.
14. Stop development by rinsing the slide in PBS.
15. Stain the nucleus with hematoxylin for 1 minute and rinse in PBS three times.
16. Dehydrate with 80% ethanol for 10 seconds,
17. 90% for 10 seconds,
18. 95% for 1 minute twice,
19. 100% ethanol 2 minutes, twice.
20. Xylenes for 2 minutes, three times
21. Cover-slip the slide with neutral resin.

2.22 Immunofluorescent staining with paraffin slides

1. Dewax the paraffin section with xylenes for 5 minutes, twice.
2. Dehydrate with absolute ethanol for 2 minutes twice,
3. 95% ethanol for 2 minutes,
4. 90% ethanol for 2 minutes,
5. 70% ethanol for 2 minutes,
6. ddH_2O for 2 minutes, three times,
7. PBS for 2 minutes, three times.
8. Retrieve antigen with antigen retrieval buffer at 95 degrees for 30 minutes.
9. Wash with ddH_2O for 3 minutes, twice,
10. PBS 3 minutes, three times.

11. Immerse the slide into 3% H_2O_2 (diluted in ddH_2O) for 20 minutes.
12. Draw a circle around the tissue sections with a PAP pen and
13. Add 10% horse serum in the circle and incubate at RT for 30 minutes.
14. Incubate primary antibodies at 4 degrees overnight.
15. Immerse slide in PBS for 5 minutes, 3 times.
16. Incubate secondary antibodies at RT for 1 hour in the dark.
17. Immerse slide in PBS for 5 minutes, 3 times.
18. Stain the samples with DAPI dye for 10 minutes at RT.
19. Immerse slide in PBS for 5 minutes, 3 times
20. Cover-slip the slide with neutral resin.

2.23 MEF cells development and cell culture

E13.5 embryos were isolated from pregnant mice and placed in cold PBS. The head, tail, limbs and organs were removed from the stem body. The tail of each embryo was used for genotyping. The stem body was cut into pieces with scissors and transferred to a 15 mL tube. 1.5 ml 0.25% trypsin was added to each tube and incubated in a 37 degree C water bath for 30 minutes, with mixing of the tube every 5 minutes. The digestion was quenched with 10 mL MEF medium (DMEM, 10% FBS, P/S). The cell suspension was filtered with a 40 μm filter and centrifuge at 500*g* at 4 degrees C for 5 minutes. The medium was discarded and the cell pellets were resuspended with 4 mL medium. Cells were cultured in a 6 cm plate at 37

degrees C with 5% CO_2. The medium was changed each day. Cells were passaged every 3 days at 95% to 100% confluence.

2.24 IP_7 extraction from MEF cells

When the confluency of MEF cells reaches 90-100% confluence (2 15cm plates for one group), NaF was added into the medium for 30 minutes at a final concentration of 10mM. The medium was discarded and cells were washed with cold PBS twice. 1.8mL cold 1M perchloric acid with 5mM EDTA was added to the plate and the cells were scraped into 2mL tubes, centrifuge at 15000rpm for 10 minutes and the supernatant harvested to a new tube. TiO_2 (4mg) was added to each sample and the sample mixed by rotation for 15 minutes at 4 degrees C. The tube was centrifuged at 3,500g for 2 minutes at 4 degrees C. The supernatant was discarded and the TiO_2 beads washed by the addition of 1mL cold 1M perchloric acid (PA) with 5mM EDTA, with rotation at 4 degrees for 5 minutes, repeated twice. Inositol phosphates were eluted from TiO_2 with 200µl 10% ammonium hydroxide and the supernatant retained after centrifugation at 3,500g for 2 minutes. The elution step was repeated and the supernatants combined together. The supernatant was reduced to dryness in a centrifugal evaporator at low temperature and the samples stored at -80 degrees C before analysis by gel electrophoresis(M. S. C. Wilson et al., 2015; M. Wilson & Saiardi, 2018).

The gel electrophoresis to analyse the inositol pyrophosphates follows the protocol developed by Adolfo Saiardi's group (Losito et al., 2009) with some adjustments.

The concentration of polyacrylamide gel is 35%, and gels were stained with toluidine blue.

2.25 Statistical analysis

FACS, gene expression and blood cells analysis were calculated with a two-tailed t-test. The P value < 0.05 means statistically significant for all analyses

Chapter 3 Mice of Double knockout of IP6K1 and IP6K2 are lethal

3.1 Introduction

Inositol pyrophosphates are present at very low levels in cells. Nevertheless they have important regulatory roles controlling cellular pathways through four significant mechanisms: including allosteric regulation, competition with PIPs, protein-protein interactions and protein pyrophosphorylation (Furkert et al., 2020). Recent studies provide more and more evidence for the importance of inositol pyrophosphates in cellular functions (Cridland & Gillaspy, 2020). However, many of these studies could not assign function to specific inositol pyrophosphates or particular enzymes because of the redundancy of inositol hexakisphosphates kinases.

There are three members in the family of IP6Ks in mammals, including IP6K1, IP6K2 and IP6K3. Both IP6K1 and IP6K2 are expressed ubiquitously in all tissues, while IP6K3 is expressed in limited tissues, such as the brain and muscle. In Homo sapiens, IP6K1 and IP6K2 are on the chromosome 3 while IP6K3 is on the chromosome 6. In Mus musculus (mice), IP6K1 and IP6K2 are also on the same chromosome 9 while IP6K3 is on the chromosome 17. Previous studies have revealed the functions of IP6K1 or IP6K2 in mice through genetic editing technology. IP6K1 deletion leads to sterile male mice, while loss of IP6K2 does not show apparent phenotypes (Malla & Bhandari, 2017). In mammals, IP6K1 and

IP6K2 are the major enzymes producing inositol pyrophosphates (IP_7) from IP_6. IP6K1 produces 90% of IP_7, while IP6K2 produces only 10% of IP_7. These two enzymes have functional redundancy because both of these two genes are expressed ubiquitously. Therefore, the deletion of IP6K1 or IP6K2 can reduce the synthesis of IP_7 but cannot deplete all the IP_7 in the cells. However, to date no reported study tried to delete IP6K1 and IP6K2 at the same time in the whole body in order to study the phenotypes of the complete loss of IP_7 in mice. As IP6K1 and IP6K2 are on the same chromosome, there are few chances to get the double knockout mice from crossing IP6K1 KO mice with IP6K2 KO mice. In fact, IP6K1 is located in mm39 chr9:107,879,700-107,925,981 while IP6K2 is located in mm39 chr9:108,673,193-108,683,536 (UCSC Genome Browser). The distance between IP6K1 and IP6K2 in the mice genome is 747,413 base pairs. Therefore, we have to develop double knockout mice on the base of IP6K1 knockout mice or IP6K2 knockout mice. We have IP6K1 knockout mice, IP6K1 conditional knockout mice and IP6K2 knock out mice in our laboratory. For the purpose of studying the functions of inositol pyrophosphates in specific tissues in the future, we used the conditional IP6K1 knockout mice to develop the double conditional knockout mice. At the same time, we also obtained the conditional knockout mice of IP6K2 because we used heterozygous conditional knockout mice of IP6K1 to develop the double conditional knockout mice. This double conditional knockout mice of IP6K1 and IP6K2 is critical to the research on inositol pyrophosphate

because this is the first time when we can eliminate inositol pyrophosphate in mice through overcoming redundancy of the IP6 kinases. Previous studies have revealed that loss of kinetic functions of IP6K1 or IP6K2 would reduce the accumulation of inositol pyrophosphates, which was confirmed in cells and in mice (Wilson, Jessen and Saiardi, 2012). Mice with wholesale deletion of inositol pyrophosphates in many tissues will shed light on the functions of inositol pyrophosphates in diverse cellular and developmental processes.

3.2 Chapter aims

This chapter describes the generation and phenotypic characterization of mice with IP6K1 and IP6K2 double knockout.

3.3 Results

3.3.1 Obtain heterozygous double knockout mice from conditional double knockout mice

Our laboratory has already developed IP6K1 conditional knockout mice ($IP6K1^{WT/loxp}$), IP6K1 knockout mice, IP6K2 knockout mice and IP6K3 knockout mice. Among these mice, obvious phenotypes lie mainly in the IP6K1 knockout mice, which are smaller than the wild-type mice, with male IP6K1 mice displaying sterility. The three IP6Ks have structural similarity and functional redundancy. Single deletion of IPK1, IP6K2 or IP6K3 reduces the productions of IP_7 but does not lead to complete loss of IP_7 in many tissues though the level of IP_7 is always low in the living cells (Park et al., 2017). Actually, the loss of IP6K1 and IP6K2

does eliminate the production of IP_7 and IP_8 from IP_6 in human HCT116 cells (M. S. Wilson et al., 2019). This is the first demonstration of the overcome of functional redundancy of IP6Ks in the mammalian cells, here through targeting IP6K1 and IP6K2 with CRISPR Cas9 technology in the cells lacking expression of IP6K3. Loss of functions is a common approach to study the roles of a gene or a molecule. Therefore, it is essential to pursue the complete depletion of IP_7 in mice in order to reveal the functions and mechanisms of IP_7 in the development of mammals.

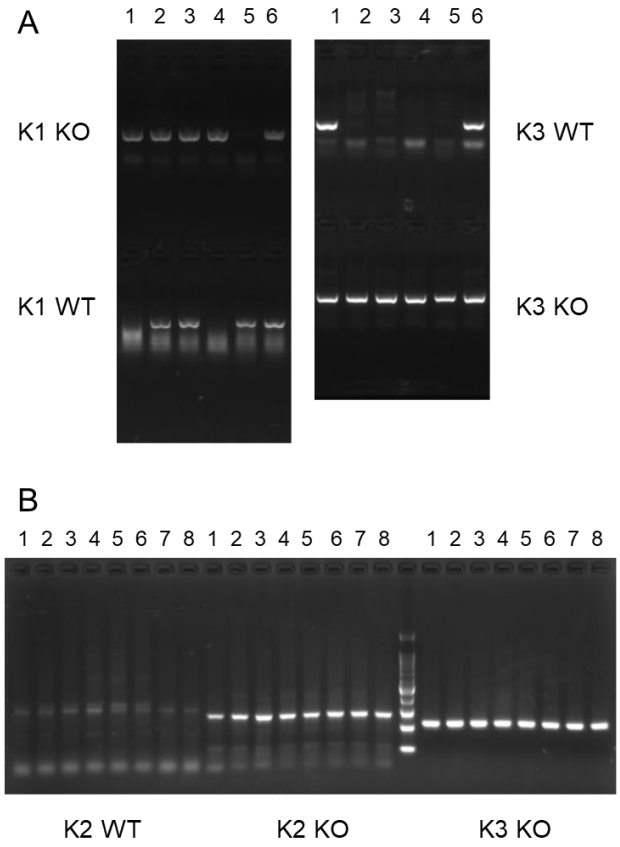

Figure 3-1 The mice of double knockout of IP6K1-IP6K3 and IP6K2-IP6K3 are viable. (A) Genotyping for the offspring of IP6K1 $^{+/-}$ IP6K3 $^{+/-}$ and IP6K1 $^{+/-}$ IP6K3 $^{+/+}$ mice. The genotype of No.4 is IP6K1 $^{-/-}$ IP6K3 $^{-/-}$. (B) Genotyping for the offspring of IP6K2 $^{-/-}$ IP6K3 $^{-/-}$. All the offspring are double knockout mice of IP6K2 and IP6K3.

IP6K1 and IP6K2 are expressed ubiquitously in mammals, while IP6K3 is

expressed in limited tissues. Our laboratory has the single knockout mice of these three kinases; we have successfully developed the double knockout mice of IP6K1-IP6K3 and IP6K2-IP6K3 through crossing because both IP6K1 and IP6K2 are on chromosome 9 in mice while IP6K3 is on chromosome 17 (Figure 3-1). However, there were no more obvious morphological phenotypes in these double knockout mice than the single knockout mice. In fact, the expression of IP6Ks in the cells are different. IP6K3 is only expression in limited tissues such as muscle, heart and brown adipose, while IP6K1 and IP6K2 are expressed ubiquitously (Figure *3-2*). These results, without measurement of inositol pyrophosphates, suggest that double deletions of IP6K1-IP6K3 or IP6K2-IP6K3 in mice cannot deplete all the inositol pyrophosphate in any tissues because of the redundancy of IP6K1 and IP6K2.

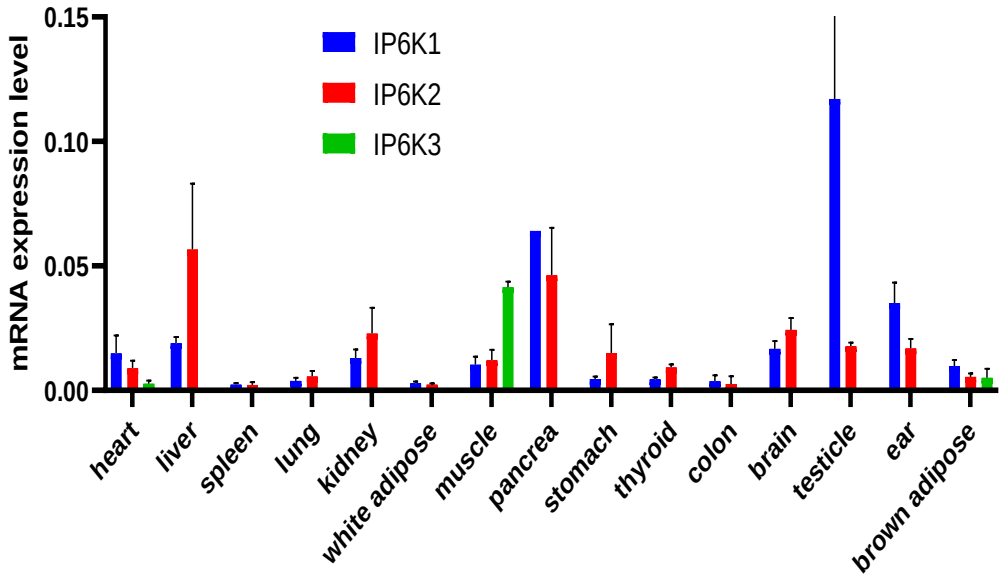

Figure 3-2 The mRNA expression of IP6K1, IP6K2 and IP6K3 are very different in mice tissues. The expression of IP6K1, IP6K2 and IP6K3 are measured in heart, liver, spleen, lung, kidney, white adipose, muscle, pancreas, stomach, thyroid, colon, brain, testicle, ear and brown adipose of adult male mice (two months), 3 mice.

Therefore, we choose to delete IP6K1 and IP6K2 for the purpose of studying the role of IP_7 in mice. Because IP6K1 and IP6K2 are located in the same chromosome with close proximity, crossing IP6K1 and IP6K2 knockout mice fail to generate alleles with double deletion of IP6K1 and IP6K2 via homologous recombination. The development of conditional double knockout mice is therefore based on the heterozygous conditional knockout mice of IP6K1 ($IP6K1^{WT/loxp}$). In order to be recognised explicitly by the Cre enzyme, a different element flox is used to target IP6K2. The rationale of the approach was: use of the loxp element to target IP6K2 and loxp element to target IP6K1, thus DNA between IP6K1 and IP6K2 on the chromosome will not be cleaved by the Cre recombinase. In order to disrupt the

functions of IP6K1 and IP6K2, exon 6 of IP6K1 and exon 2 of IP6K2 were targeted for cleavage by the Cre enzymes. From IP6K1$^{WT/loxp}$ mice, I got heterozygous mice of conditional double knockout of IP6K1-IP6K2 (IP6K1$^{WT/loxp}$ IP6K2 $^{WT/flox}$) as well as the mice of IP6K2 $^{WT/flox}$ (Figure *3-3*).

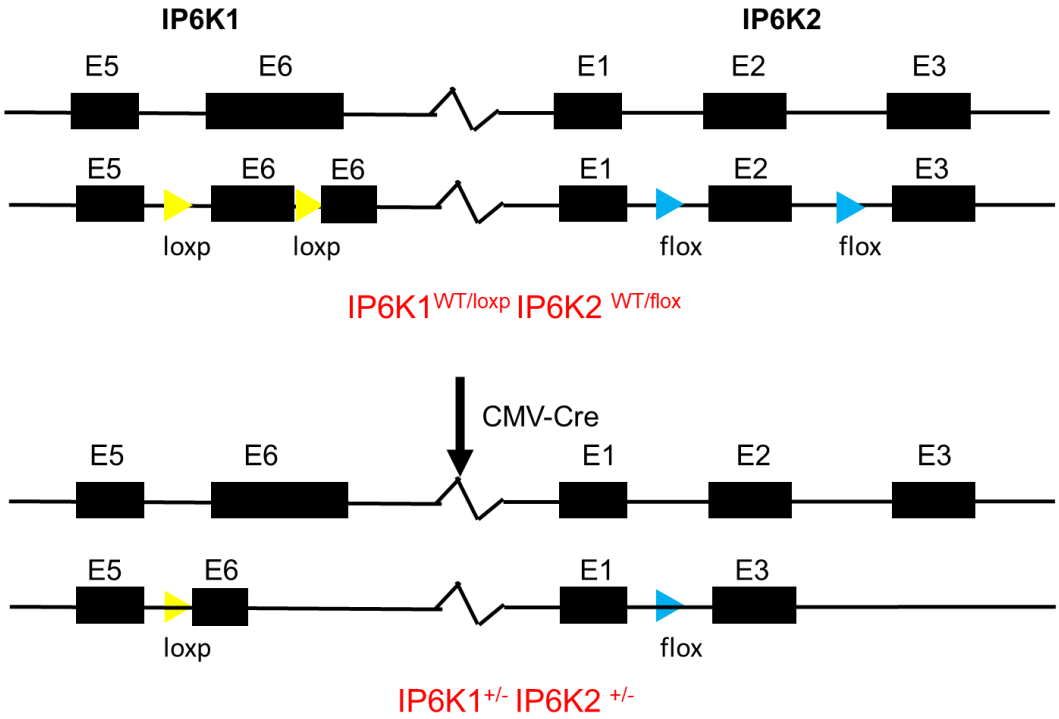

Figure 3-3 Strategy for generation of heterozygous double conditional knockout (CKO) and heterozygous double knockout (DKO) mice of IP6K1 and IP6K2. The DKO mice are produced from crossing CKO and CMV-Cre mice, which express Cre enzyme in the whole body.

The Cre-lox recombination system is commonly applied to functional research at the specific site of model organisms because researchers can easily manipulate gene expression and delete DNA with this powerful tool (Turan et al., 2011). The CMV-Cre mice, which can express the Cre enzyme in the whole body under the control of CMV promoter, were mated with IP6K1$^{WT/loxp}$ IP6K2 $^{WT/flox}$ mice. The DNA spacer between two flox elements or two loxp elements is cleaved by the Cre

enzyme. Therefore, among their offspring, exon 6 of IP6K1 and exon 2 of IP6K2 are lost on the same chromosome (Figure 3-3). The genotype of offspring was determined by PCR with primers flanking the cleaved DNA spacer (Figure 3-3, Figure 3-4, Figure 3-5). The PCR products were sent for the Sanger sequencing, and deletion of the DNA spacer deleted in IP6K1 and IP6K2 was confirmed. Finally, I obtained heterozygous mice of double knockout of IP6K1 and IP6K2 ($IP6K1^{+/-}$ $IP6K2^{+/-}$) /$(IP6K1\text{-}IP6K2)^{+/-}$ (Figure 3-3). The mice of $IP6K1^{+/-}$ $IP6K2^{+/-}$ are viable and develop without obvious apparent defects, such as the reduced weight and male sterility of the IP6K1 knockout mice.

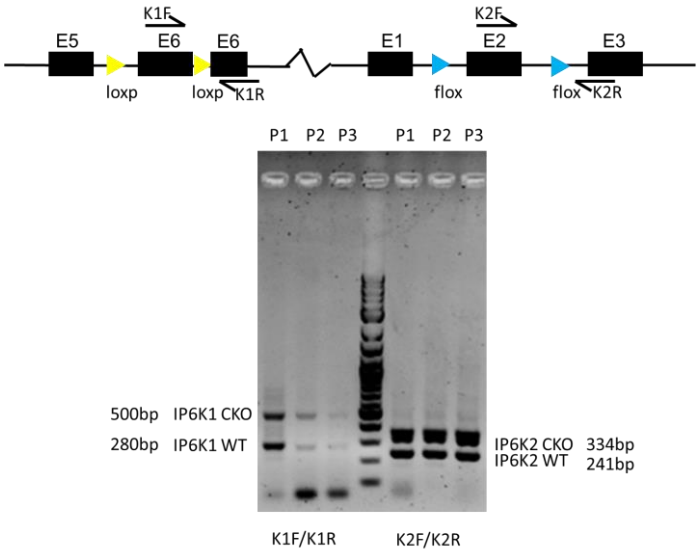

Figure 3-4 Strategy of determining the genotypes of conditional knockout mice of IP6K1 and IP6K2. P1-3 mice are the heterozygous mice of conditional knockout of IP6K1 and IP6K2. PCR bands predicted of CKO, or otherwise, of IP6K1 and IP6K2 are shown on the gel along with primers used to confirm genotype.

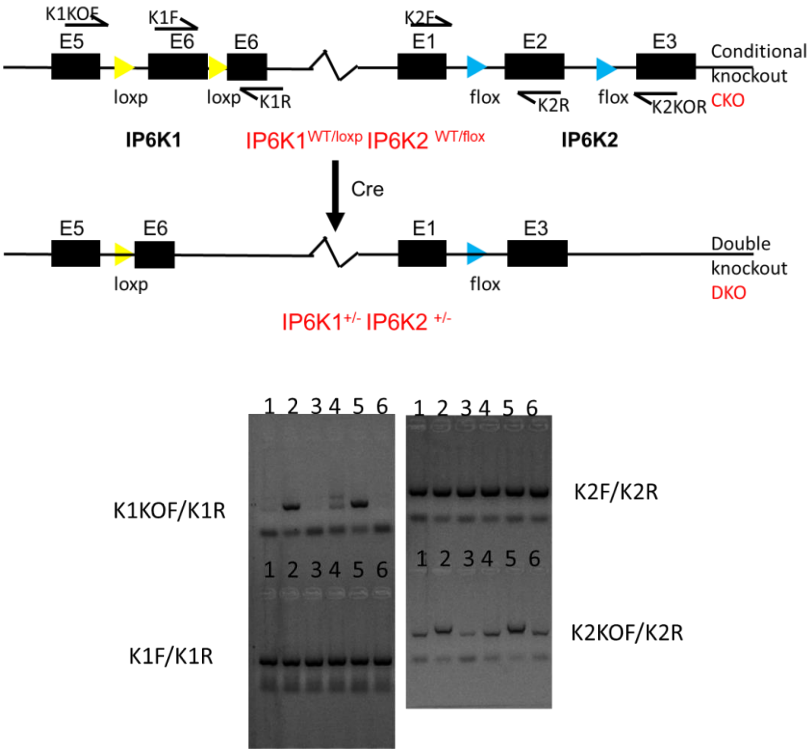

Figure 3-5 Strategy of determining the genotypes of double knockout mice of IP6K1 and IP6K2. Mice of 1-6 are individual offspring of mating of heterozygous CKO and CMV Cre mice. The genotypes of IP6K1 and IP6K2 were determined by PCR. The genes of IP6K1 and IP6K2 on the same chromosome are cleaved consistently by Cre recombinase. (K1KOF/K1R =K1KO, K1F/K1R=K1WT, K2F/K2R=K2WT, K2KOF/K2R=K2KO). Mice 2 and 5 are heterozygous DKO, while 1,3,4 and 6 are WT mice.

3.3.2 There are no homozygous knockout mice at P21.

The heterozygous knockout mice（IP6K1-IP6K2）$^{+/-}$, generated from IP6K1$^{WT/loxp}$ IP6K2 $^{WT/flox}$ and CMV-Cre mice, show no apparent morphological differences from wild-type mice. Consequently, we used heterozygous knockout mice IP6K1$^{+/-}$ IP6K2 $^{+/-}$ to generate homozygous knockout mice (IP6K1$^{-/-}$ IP6K2 $^{-/-}$). According to the Mendelian inheritance, 25% of the offspring of the self-crossing from heterozygous knockout mice are homozygous mice（IP6K1-IP6K2）$^{+/-}$. However, there were no one homozygous knockout mice (IP6K1$^{-/-}$ IP6K2 $^{-/-}$) among over 100 offspring when genotypes of these offspring were confirmed at

postnatal day 21 (P21) (Figure 3-6,

Table ***3-1***). Therefore, it is reasonable to consider that combined loss of IP6K1 and IP6K2 leads to murine lethality. Subsequent attempts were made to determine the genotypes of newborn offspring at earlier stages of development. However, at P6, no homozygous knockout mice were not recovered. Therefore, this evidence indicates that double deletions of IP6K1 and IP6K2 lead to lethality in mice during gestational stages or just after birth. As single deletion of IP6K1 or IP6K2 reduces the accumulation of inositol pyrophosphates in cells and mammals but is not lethal, it is plausible that the consequence of deleting both IP6K1 and IP6K2 is complete loss of IP_7, resulting in or contributing by other means to mice lethality. This would suggest that IP_7 is essential for murine development.

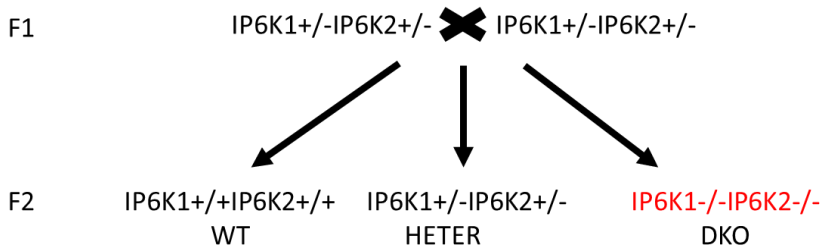

Figure 3-6 There are no homozygous DKO mice among over 100 offspring at P21 from self-crossing of heterozygous mice, while there should be 25% homozygous DKO mice among the offspring according to the Mendelian ratio. Only one allele of IP6K1 and IP6K2 could rescue mice lethality caused by ultimate loss of IP6K1 and IP6K2.

	IP6K1$^{+/+}$ IP6K2$^{+/+}$	IP6K1$^{+/-}$ IP6K2$^{+/-}$	IP6K1$^{-/-}$ IP6K2$^{-/-}$
P21	**32**	**71**	**0**

Table 3-1 Frequency of genotypes among PCR-verified progeny of crosses of heterozygous mice at P21. There is no any homozygous DKO mouse (IP6K1$^{-/-}$IP6K2$^{-/-}$) among the off-springs from self-crossing of heterozygous mice.

There were no viable IP6K1$^{-/-}$ IP6K2 $^{-/-}$ mice among the offspring from self-crossing of （IP6K1-IP6K2）$^{+/-}$, while mice individually lacking IP6K1 or IP6K2 survive though male mice of IP6K1$^{-/-}$ are sterile (Malla & Bhandari, 2017). Therefore, I sought to verify whether a single allele of IP6K1 or IP6K2 can rescue the mice lethality caused by double deletions of IP6K1 and IP6K2. This is another evidence of the importance of IP_7 in the development of mice. Heterozygous male mice of double knockout（IP6K1-IP6K2）$^{+/-}$ were used to mate with female IP6K1 knockout mice (IP6K1$^{-/-}$). Because IP6K1 knockout mice are sterile (Malla & Bhandari, 2017), male IP6K1 knockout mice cannot be used to mate with female heterozygous double knockout (IP6K1-IP6K2)$^{+/-}$. According to the genetic principle, there are only two genotypes among their offspring, IP6K1$^{WT/-}$ IP6K2$^{WT/WT}$ or IP6K1$^{-/-}$IP6K2$^{WT/-}$. If a single allele of IP6K2 cannot rescue the double deletions of IP6K1 and IP6K2, a single genotype (IP6K1$^{WT/-}$ IP6K2$^{WT/WT}$) is expected of the offspring. In fact, the mice of IP6K1$^{-/-}$IP6K2$^{WT/-}$ were viable, indicating requirement of only a single allele of IP6K2 for viability (Figure *3-7*,

Figure *3-8*).

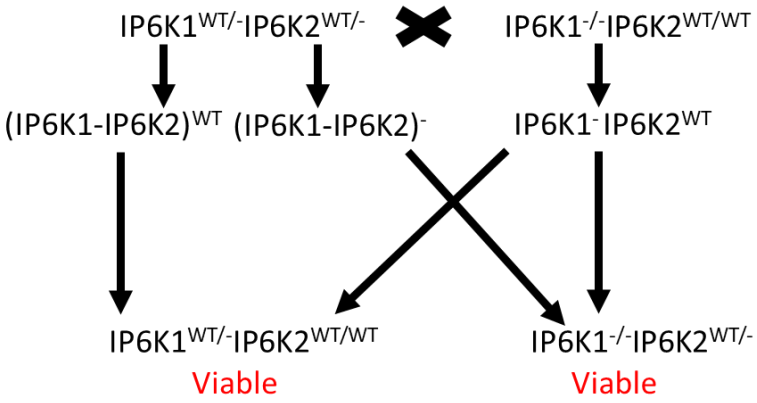

Figure 3-7 Strategy to confirm the viability of mice of IP6K1$^{-/-}$IP6K2 $^{WT/-}$. There are only two genotypes among the offspring of (IP6K1-IP6K2) $^{WT/-}$ and IP6K1 knockout mice. These two types of offspring are viable.

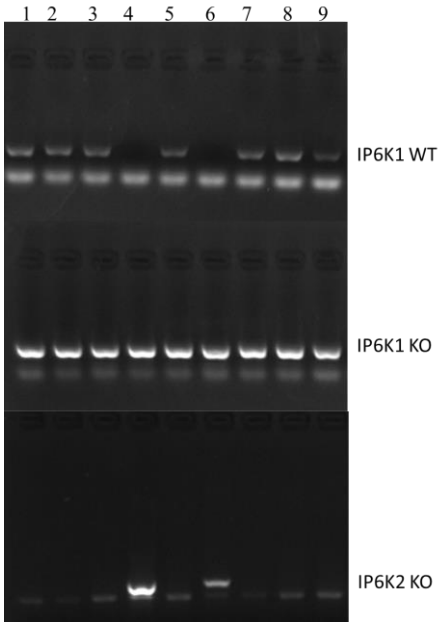

Figure 3-8 PCR verification of the genotypes of the offspring of male (IP6K1-IP6K2) $^{WT/-}$ mice and female IP6K1 knockout mice (IP6K1$^{-/-}$). Because IP6K1 and IP6K2 are on the same chromosome, IP6K1 deletion is cross-linked with IP6K2 deletions on one allele. As for the first allele, mice of 4 and 6 have the cross-linked deletions of IP6K1 and IP6K2 on one allele (IP6K1-IP6K2)$^{-}$, while mice of 1, 2, 3, 5, 7, 8 and 9 have wild-type allele (IP6K1-IP6K2)^{WT}. As for the second allele, all the mice have the IP6K1 knockout allele (IP6K1^{-}IP6K2^{WT}) because their mothers are IP6K1 knockout mice. Therefore, the genotype of No. 4 and 6 mice is IP6K1$^{-/-}$ IP6K2$^{WT/-}$ while the genotype of other mice is IP6K1$^{WT/-}$IP6K2$^{WT/WT}$. Genotypes of these mice were determined at P21 through PCR.

In order to confirm whether one allele of IP6K1 can rescue the mice of double deletions of IP6K1 and IP6K2, mice of （IP6K1-IP6K2）$^{WT/-}$ were used to mate with mice of IP6K2$^{-/-}$. There are only two genotypes among the offspring, IP6K2$^{WT/-}$ or IP6K1$^{WT/-}$IP6K2$^{-/-}$. Mice of IP6K1$^{WT/-}$IP6K2$^{-/-}$ are viable, which means that only one allele of IP6K1 can also rescue the lethality of double knockout of IP6K1 and IP6K2 (Figure *3-9*, Figure *3-10*).

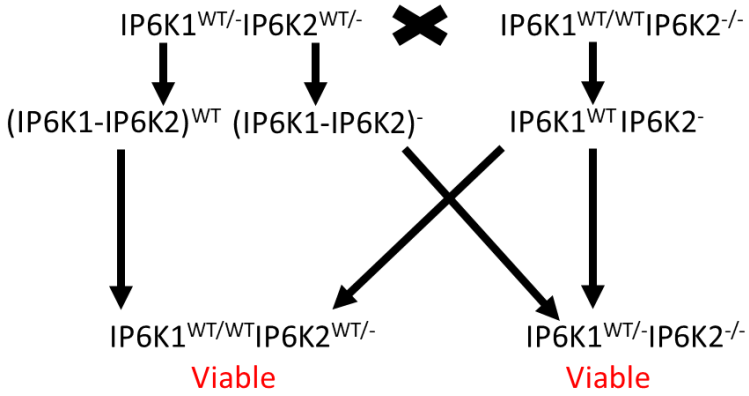

Figure 3-9 Strategy to confirm the mice of IP6K1$^{WT/-}$ IP6K2 $^{-/-}$ are viable. There are only two genotypes among the offspring of (IP6K1-IP6K2)$^{WT/-}$ and IP6K2 knockout mice. These two types of offspring are viable.

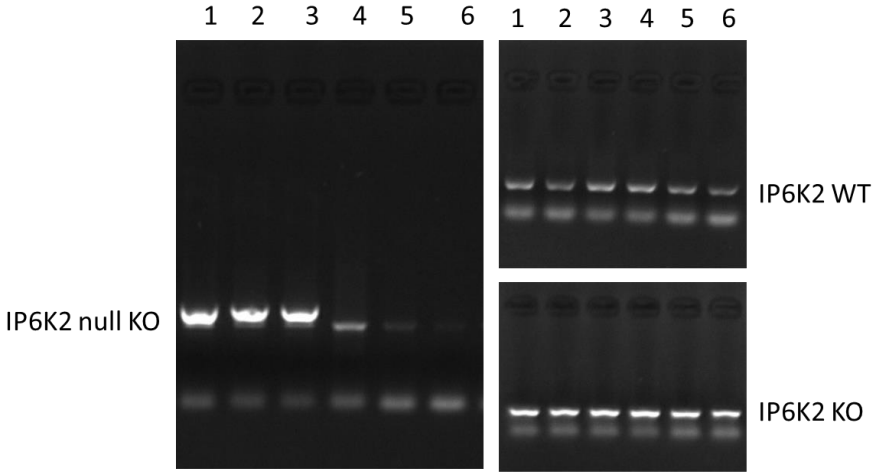

Figure 3-10 PCR verification of the genotypes of mice of IP6K1$^{WT/-}$ IP6K2 $^{-/-}$ crosses. Because IP6K1 and IP6K2 are on the same chromosome, IP6K1 deletion is cross-linked with IP6K2 deletions on one allele. Mice of 1, 2 and 3 have the cross-linked deletions of IP6K1 and IP6K2 on one allele (IP6K1-IP6K2)$^{-}$, while mice of 4, 5 and 6 have wild-type allele (IP6K1-IP6K2)^{WT}. As for the other allele, all the mice have the IP6K2 knockout allele (IP6K1^{wt}IP6K2^{-}) because their mothers are IP6K2 knockout mice. Therefore, the genotype of mice 1, 2 and 3 is IP6K1$^{WT/-}$IP6K2$^{-/-}$ while the genotype of other mice 4, 5 and 6 is IP6K1$^{WT/WT}$IP6K2$^{WT/-}$. Genotypes of these mice were determined at P21.

Double deletions of IP6K1 and IP6K2 lead to the lethality of mice while mice losing 3 alleles of these two genes (IP6K1$^{WT/-}$IP6K2$^{-/-}$, IP6K1$^{-/-}$IP6K2$^{WT/-}$) are viable. Expecting these knockouts of IP6K1 and IP6K2 to produce less IP_7 than the mice of IP6K1 or IP6K2 knockouts, these genetic experiments illustrate the importance of IP_7 in the development of mammals. Probably, one copy of IP6K1 or IP6K2 can make enough IP7 by enhancing enzyme activity while total depletion of capacity for IP_7 production is lethal.

3.3.3 Double knockout of IP6K1 and IP6K2 leads to complete loss of IP_7

Tissues such as lung and liver were used to confirm the loss of IP6K1 and IP6K2 in the homozygous embryos by measurement of protein and transcript. No IP6K1 and IP6K2 protein could be detected in the homozygous groups. In addition, the loss of IP6K1 and IP6K2 in the homozygous embryos was confirmed by qPCR (Figure *3-11*).

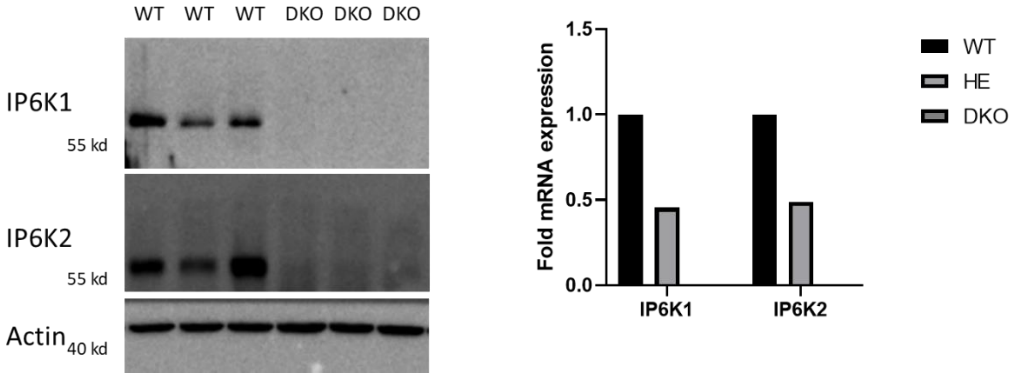

Figure 3-11 No IP6K1 or IP6K2 protein was detected in the DKO mice embryos. The results were confirmed by Western blot (n=3 WT and 3 DKO). The results of qPCR also confirmed the loss of IP6K1 and IP6K2 in the DKO group, while the levels of mRNA of IP6K1 and IP6K2 are about 50% the of the levels of wild-type groups (n=1 WT, 1 HE and 1 DKO).

IP6K1 and IP6K2 are expressed ubiquitously in the mice. They play a significant role in producing IP_7 in the cells and tissues. In order to confirm the loss of IP6K1 and IP6K2 resulted in the complete depletion of IP_7, MEF cells were developed from the embryos at E13.5. Inositol polyphosphates were extracted from MEF cells and purified with TiO_2. The eluted IPs were separated by polyacrylamide gel electrophoresis and stained with toluidine blue(M. S. C. Wilson et al., 2015; M. Wilson & Saiardi, 2018). IP_7 was not detected in the DKO MEF cells (Figure *3-12*), while IP_7 accumulation in the WT MEF cells was greater than that observed in

heterozygous MEF cells. While the loss of IP_7 is expected to reduce IP_8 levels, gel electrophoresis with toluidine blue staining is not a sensitive enough method (the sensitivity is 0. 1 nmol) to detect changes in IP_8, which ordinarily is only 10-20% of IP_7. Within the limits of the measurement approach, no difference in IP_6 levels were detected between wild type, double mutant and heterozygous MEF. Because the concentration of 5-IP_7 is only 1-5% of IP_6 in living cells (Park et al., 2017), the disruption of 5-IP_7 synthesis from IP_6 is expected to have little influence on IP_6 levels, a result confirmed in the present study.

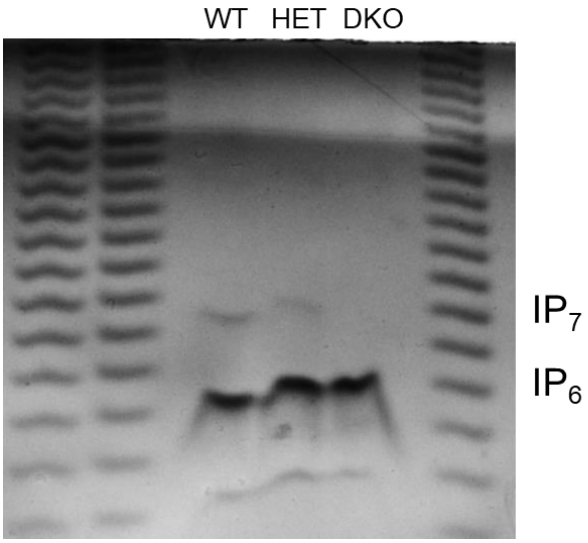

Figure 3-12 Double knockout of IP6K1 and IP6K2 eliminates the production of IP_7 in MEF cells. Cell extracts were analysed by polyacrylamide gel electrophoresis with toluidine blue staining.

3.3.4 The homozygous knockout mice embryos have anaemia

The embryos from heterozygous DKO self-crossing were dissected from E13.5. Compared with WT embryos, the DKO embryos did not show apparent phenotypes at E13.5 and E14.5. However, from E15.5, the homozygous knockout embryos

begin to show obvious anaemia. For example, homozygous knockout embryos have pale bodies, while heterozygous embryos have no differences from wild-type embryos. Both of the wild-type and heterozygous embryos are more reddish than the homozygous embryos. The homozygous embryos are also smaller than the wild-type or heterozygous embryos (Figure *3-13*).

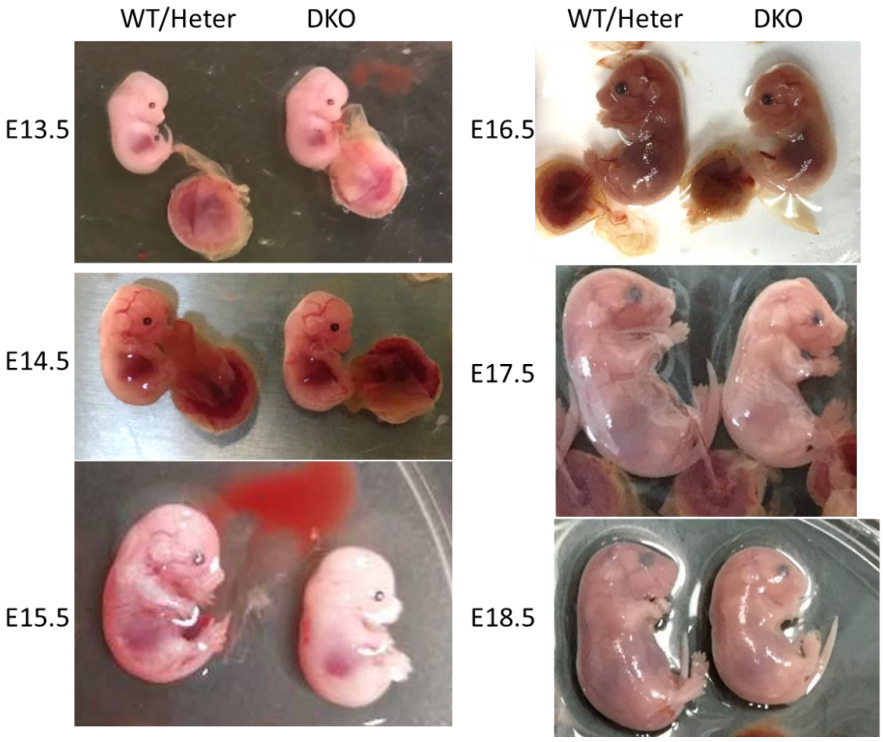

Figure 3-13 At E13.5 and E14.5, the differences between WT and DKO embryos are not noticeable. The DKO embryos show anaemia from E15.5. From E15.5 to E18.5, compared with wild-type and heterozygous embryos, the DKO embryos are pale and more petite.

Previous studies have shown that adult IP6K1 knockout mice have less weight than WT mice (Bhandari et al., 2008). The DKO embryos show this phenotype from later gestational stages. DKO embryos have a more severe phenotype than IP6K1 mice because IP6K1 knockout mice reduce the accumulation of IP_7 (Bhandari et al., 2008), while DKO embryos deplete IP_7 to undetectable levels. This reveals the importance of IP_7 in the cellular pathways during development.

3.3.5 Maturation of erythroid cells of homozygous embryos is affected

The development of hematopoietic stem cells during the gestational stages starts from the York sac where blood islands appear around E7.5. At E10.5, hematopoietic stem cells begin to occur within the embryos and first localize in the aorta gonad mesonephros (AGM) region and then migrate to the fetal liver, an important site for hematopoietic stem cells differentiation and maturation during later gestational stages. Finally, the hematopoietic stem cells colonize the bone marrow at birth (Dzierzak & Philipsen, 2013). From E15.5, the DKO fetal livers are smaller than the WT fetal livers (Figure 3-14). Because fetal livers are the primary site for expansion and maturation of hematopoietic stem cells during middle and late gestational stages, it is reasonable to consider that the development and differentiation of hematopoietic stem cells are affected upon loss of inositol pyrophosphates in mice.

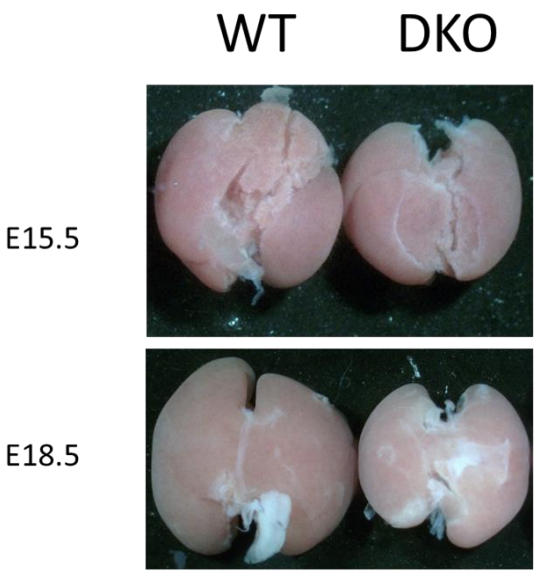

Figure 3-14 Fetal livers of DKO embryos are smaller than the liver of WT embryos. The fetal livers were isolated and compared at E15.5 and E18.5.

The fetal liver is the primary site of hematopoietic cells and their progenitors during the late gestational stage. In addition, the DKO embryos show anaemia with pale bodies, which indicates defects in the red blood cells. Therefore, the fetal livers of WT and DKO embryos were harvested to check whether the maturation and differentiation of erythroid progenitor cells are affected in the homozygous embryos. During the maturation and differentiation of hematopoietic stem cells, the differentiated hematopoietic cells develop specific antigens on their cell membranes, which are important markers of these cells. Antibodies of TER119 (mature erythroid cell marker) and CD71 can be applied to analyse the maturation of erythroid cells (Koulnis et al., 2011). During the maturation of erythroid progenitors, these lineage cells have an increased expression of Ter119 while the expression of CD71 first increases first and then decreases (Dzierzak & Philipsen, 2013). Single cells isolated from fetal livers at E13.5 were stained by Ter119-PE and CD71-APC antibodies and analysed by the FACS method. During the maturation of erythroid progenitors, the expression of Ter119 increases while the expression of CD71 increases and then decreases. Therefore, the erythroid progenitors can be classified into five groups according to their expression of Ter119 and CD71 (Koulnis et al., 2011). The five groups of erythroid progenitor cells, from S0 to S5, represent the different stages of erythropoiesis (Figure 3-15). According to the results, the DKO fetal livers have fewer cells in the S3 but more cells in S4. There are only 77.4% of S3 cells in the DKO fetal livers, while there

are more than 84.9% of S3 cells in the WT fetal livers. On the other hand, there are more S4 in the DKO fetal livers. This means the maturation and differentiation of erythroid progenitors are affected in the homozygous group (Figure 3-15).

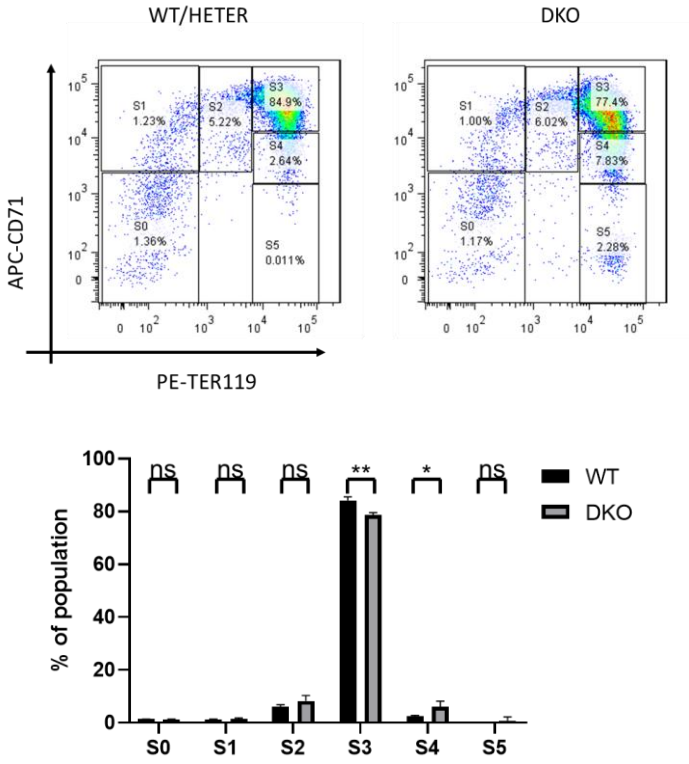

Figure 3-15 The maturation of erythroid cells is affected in the DKO embryos. Cells from fetal liver of E13.5 were dissociated, stained with APC-CD71 and PE-TER119 antibodies and analysed with a FACS analyser. Scatter plots are shown in the upper panels, with extracted data for developmental stages in the lower. Significant differences between control and DKO embryos is shown with asterisks (n = 5 WT and 3 DKO) (ns no significance, *p < 0.05, **p < 0.01, ***p < 0.001).

Fetal livers are the crucial sites for hematopoietic stem cells expansion and differentiation. The FACS analysis showed that double deletions of IP6K1 and IP6K2 affected the maturation and differentiation of erythroid progenitors. This affected erythropoiesis will affect red blood cells, which are essential transporter of oxygen and nutrient for embryos from the mother. If there are functional defects

in the oxygen or nutrients transportation to the embryos, it will have a negative effect on the development of embryos.

Because the fetal livers of DKO embryos are smaller than the fetal livers of wild-type and heterozygous embryos, it is likely that loss of inositol pyrophosphates affects the maturation and differentiation of erythroid progenitor cells evidenced through the FACS method.

3.3.6 Hemoglobin switching is affected in the erythroid cells upon loss of inositol pyrophosphates

The maturation of erythroid progenitor cells is affected in the DKO fetal livers. The affected differentiation of hematopoietic stem cells also has a negative effect on the hemoglobin switching. In order to confirm whether hemoglobin switching in the DKO fetal livers is affected, the expression of Hbb-y and Hbb-bh1 globin in fetal livers was measured by qPCR. During the maturation of hematopoietic cells, Hbb-bh1 is replaced by Hbb-y globin, which is a critical switching from embryonic globin to fetal globin (Sankaran, Xu and Orkin, 2010). However, homozygous knockout fetal livers expressed more Hbb-y globin than these of wild-type or heterozygous fetal embryos. In contrast, homozygous DKO fetal livers have reduced Hbb-bh1 globin (Figure 3-16). More Hbb-y globin and less Hbb-bh1 globin indicate a faster hemoglobin switching. This is consistent with more S4 and fewer S3 in the DKO fetal livers (Figure 3-15).

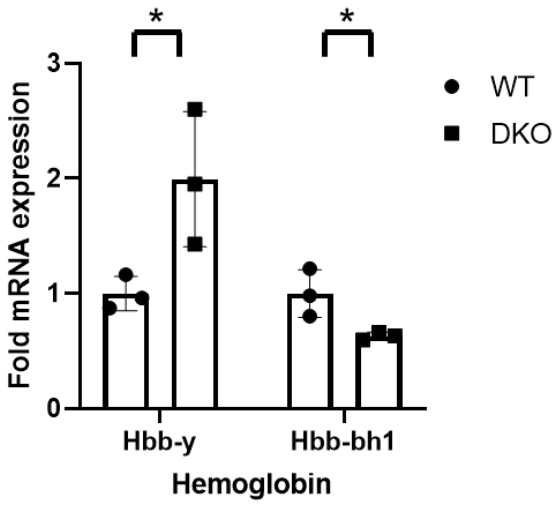

Figure 3-16 Hemoglobin switching is affected in the DKO embryos. Expression of hemoglobin mRNA transcripts in E13.5 livers. Data normalized to Actin represented as fold-change compared to WT, shown as mean ± SD (n = 3 WT and 3 DKO) (*p < 0.05, **p < 0.01, ***p < 0.001)

3.3.7 The differentiation of hematopoietic stem cells is affected by the loss of inositol pyrophosphates

Erythropoiesis is only a part of the maturation and differentiation of hematopoietic stem cells. Hematopoietic stem cells are essential to the development of the circulatory system and immune system. Defects in the hematopoietic stem cells have more effects not only in the maturation of erythroid cells but also influence the differentiation of lymphoid cells and other immune cells. The results of the loss of IP7 on other cell lineages of hematopoietic stem cells cannot be excluded. Therefore, it is necessary to track the differentiation of hematopoietic stem cells in detail. This will help us reveal the functions of inositol pyrophosphates in the differentiation of hematopoietic stem cells.

To further study the role of inositol pyrophosphates in the differentiation and

development of hematopoietic stem cells, the blood of E18.5 embryos was analysed by a hematology analyser. The results show that loss of inositol pyrophosphates in the DKO embryos affects the components of blood cells. In the DKO blood, there were more white blood cells and fewer red blood cells and hemoglobin. This is consistent with the defective maturation of erythroid progenitor cells. In the white blood cells, there were more monocytes and neutrophils but fewer lymphocytes in the DKO blood, while the eosinophils and basophils showed no difference. These robust differences in the blood cells components between WT and DKO embryos indicate the importance of inositol pyrophosphates in the differentiation of hematopoietic stem cells (Figure 3-17).

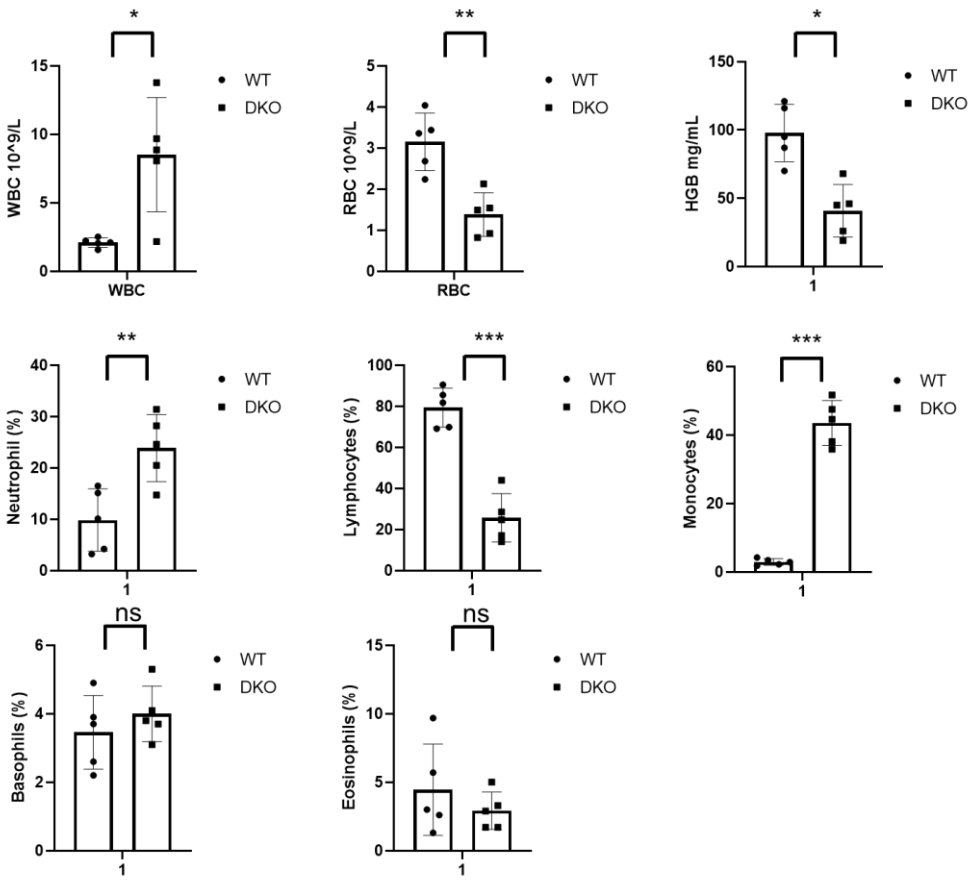

Figure 3-17 Loss of inositol pyrophosphates in the mice affects the components of blood cells. Hematological parameters, white blood cell count, red blood cell count, total hemoglobin and individual cell counts of blood cells were determined at E18.5 with a hematology analyser. WBC white blood cells, RBC red blood cells, HGB hemoglobin. Significant differences in cell counts are indicated with asterisks (n = 5 WT and 5 DKO) (ns no significance, *p < 0.05, **p < 0.01, ***p < 0.001).

We previously revealed the vital role of inositol pyrophosphates in erythropoiesis, which is part of the differentiation of hematopoietic stem cells. To further provide more details about the differentiation of hematopoietic stem cells upon loss of inositol pyrophosphates, surface maker antibodies were analysed by FACS to track the differentiation of hematopoietic stem cells in the late gestational stage. Because hematopoietic stem cells begin to migrate to bone marrow from fetal livers from

E15.5, the fetal livers at E15.5 were analysed.

According to the results of FACS, there are more leukocytes and myeloid cells in the DKO fetal livers (Figure *3-18*), consistent with the greatly increased monocyte count of the DKO blood.

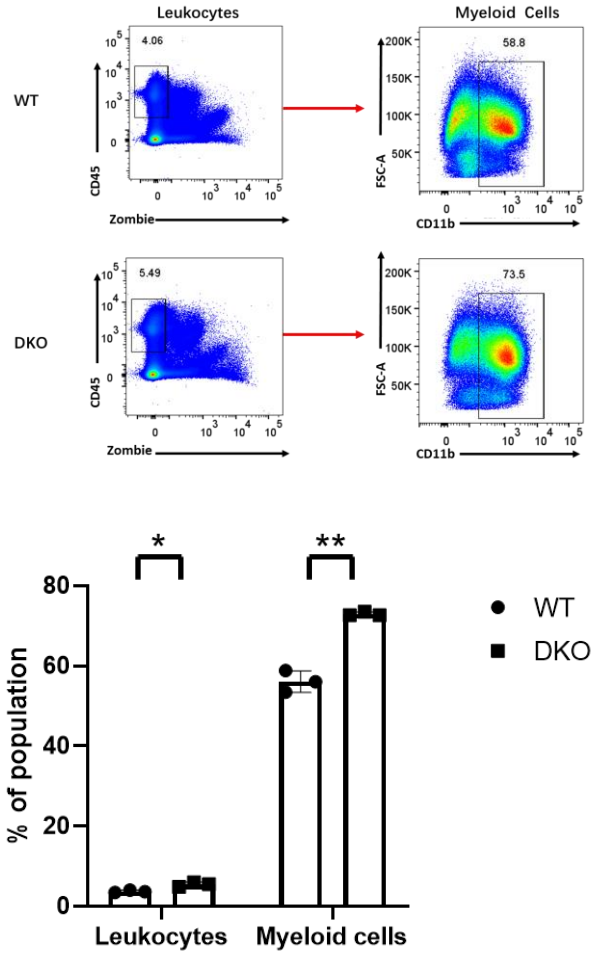

Figure 3-18 There are more leukocytes and myeloid cells in the DKO fetal livers. Cell populations of fetal livers at E15.5 were analysed by FACS (upper panels) with cells gated by Zombie-CD45 as marker of leukocytes, and CD45 and CD11b as markers of myeloid cells. Significant difference between genotypes is indicated with asterisks (lower panel). Data shown as mean ± SD (n = 3 WT and 3 DKO) (*p < 0.05, **p < 0.01, ***p < 0.001). Done with Chang Li.

FACS analysis was also performed with markers for specific lymphocyte populations, including T cells, B cells and natural killer (NK) cells (Figure *3-19*).

The analysis shows that the differentiation of hematopoietic stem cells is myeloid-biased in the DKO, which is consistent with defects in function of hematopoietic stem cells (Bernitz et al., 2016; Elias et al., 2017; Flach et al., 2014; X. Li et al., 2020; Pilzecker et al., 2017; Weiss & Ito, 2015; Young et al., 2016).

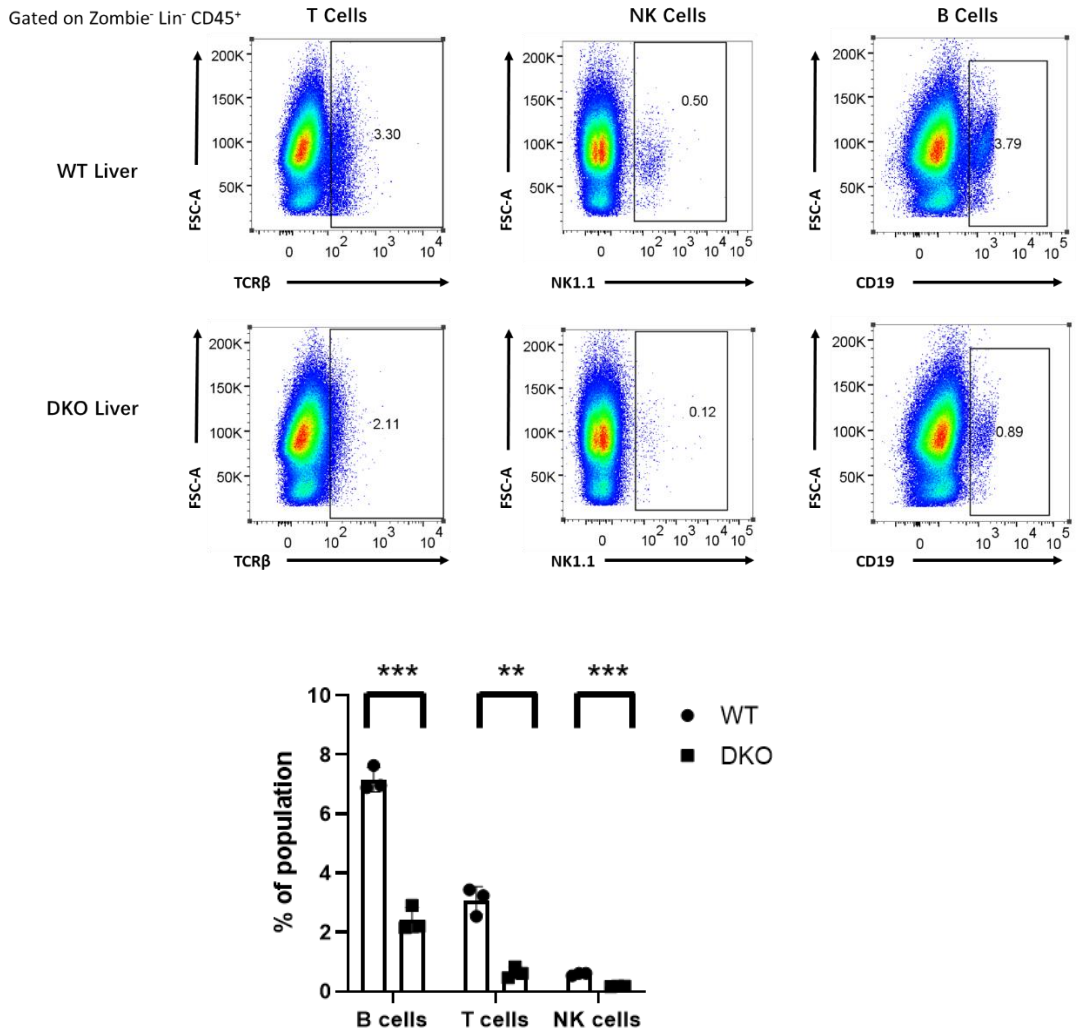

Figure 3-19 There are fewer lymphocytes in the DKO fetal livers. Cell populations of fetal livers at E15.5 were analysed by FACS (upper panels) with cells gated by Zombie- Lin- CD45+. TCRβ, NK1.1 and CD19 are the markers of T cells, NK cells and B cells, respectively. Significant differences between genotypes are indicated with asterisks (lower panel). Data shown as mean ± SD (n = 3 WT and 3 DKO) (*p < 0.05, **p < 0.01, ***p < 0.001). Done with Chang Li.

Further analysis was undertaken by FACS with markers for hematopoietic stem

cells (Figure 3-20) and with markers for common myeloid progenitors and common lymphocytes (Figure 3-21). Loss of inositol pyrophosphates in the DKO was accompanied by significant increase in hematopoietic stem cells (Figure 3-20) and a reduction in common myeloid progenitors (CMP) and common lymphocytes progenitors (CLP) (Figure 3-21). Clearly, DKO has profound effects on the differentiation of hematopoietic stem cells.

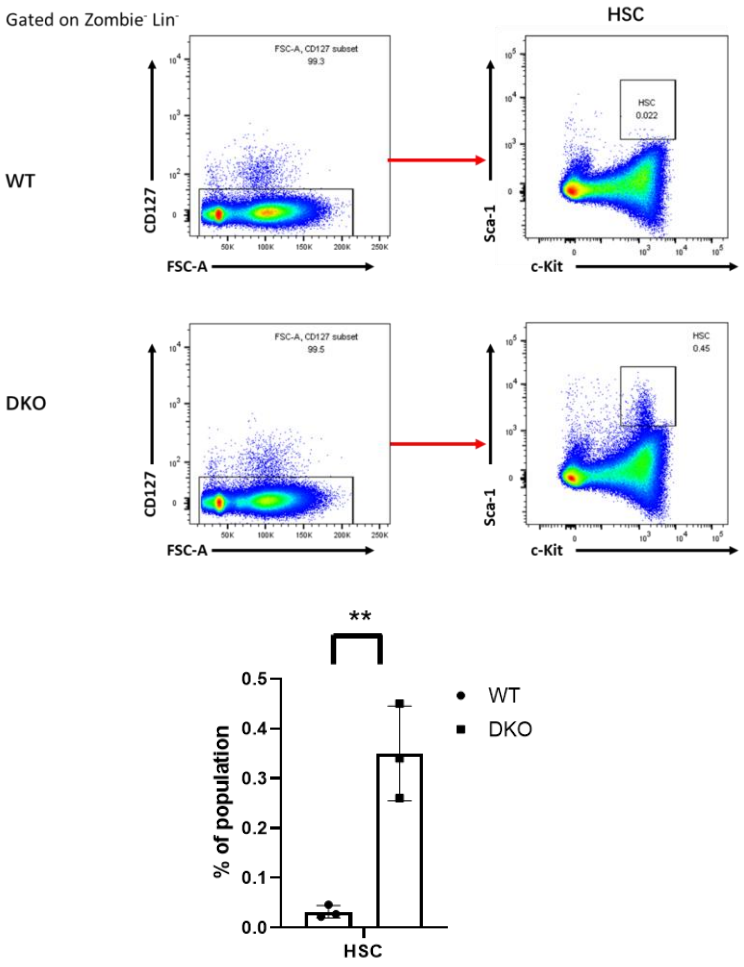

Figure 3-20 There are more hematopoietic stem cells (HSC) in the DKO fetal livers. The hematopoietic stem populations of fetal livers at E15.5 were analysed by FACS (upper panels) with cells gated by Zombie– Lin-. Significant difference between genotypes is indicated with asterisks (lower panel). Data shown as mean ± SD (n = 3 WT and 3 DKO) (*p < 0.05, **p < 0.01, ***p < 0.001). Done with Chang Li.

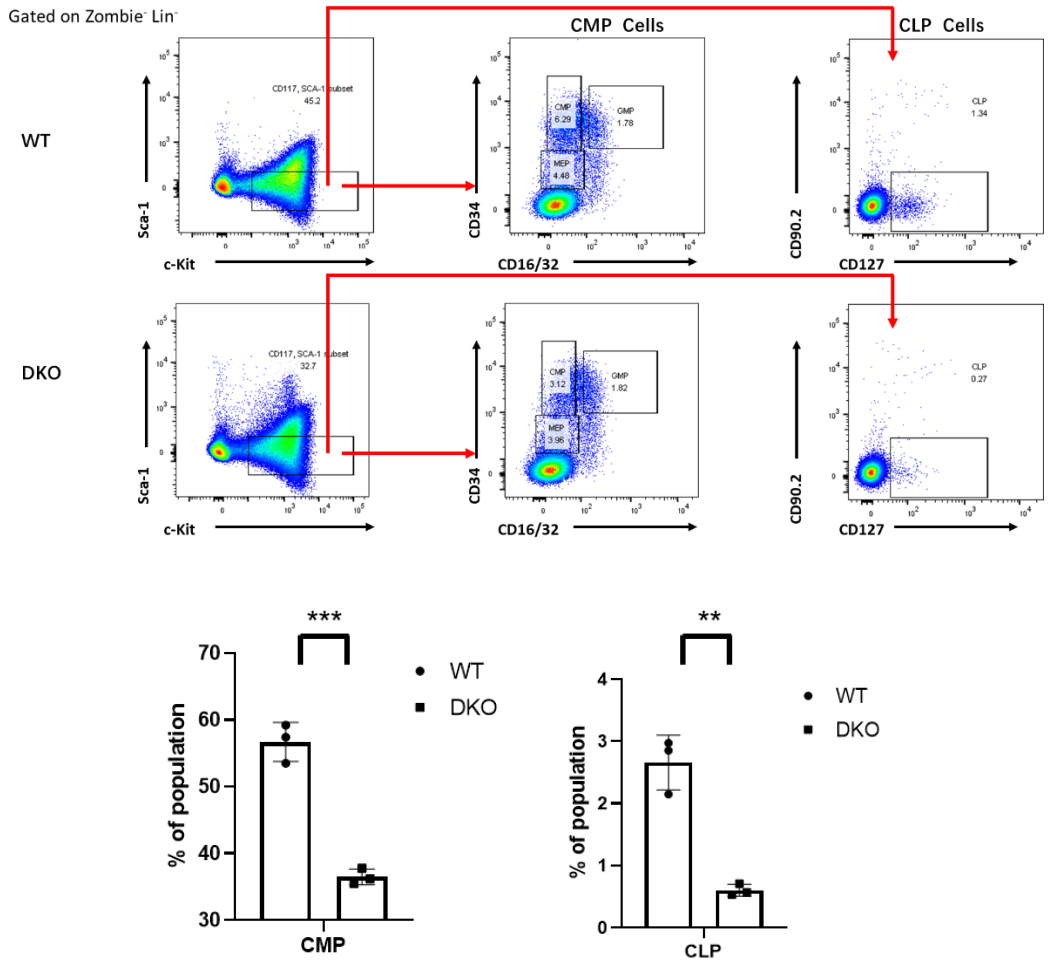

Figure 3-21 There are fewer common myeloid progenitors (CMP) and common lymphocyte progenitors (CLP) in the DKO fetal livers. Cell populations of fetal livers at E15.5 were analysed by FACS (upper panels) with cells gated by Zombie-Lin-. Significant differences in cell types between genotypes are indicated with asterisks (lower panel). Data shown as mean ± SD (n = 3 WT and 3 DKO) (*p < 0.05, **p < 0.01, ***p < 0.001). Done with Chang Li.

Functional defects in the hematopoietic stem cells are known to lead to myeloid-biased differentiation (Flach et al., 2014; Pilzecker et al., 2017; Young et al., 2016). Both the FACS and hematological analysis show that there are more myeloid cells but fewer

lymphocytes in the fetal livers and blood of the DKO (**Figure *3-17***, **Figure *3-18***, **Figure *3-19***, **Figure 3-21**). While there are more myeloid cells in the DKO fetal livers, it is reasonable that there are fewer CMP. However, there should be more CLP in the DKO fetal livers because of compensatory proliferation for the lack of lymphocytes. The presence of reduced CLP in the DKO fetal livers is indicative of defective lymphopoiesis. Furthermore, the larger HSC population in the DKO fetal livers likely arises because of affected differentiation of HSC or compensatory proliferation for the lack of CMP and CLP. Therefore, it seems that inositol pyrophosphates play a vital role in the hematopoietic stem cells, the loss of which leads to myeloid-biased differentiation.

3.4 Discussion

In this chapter, we found that double deletions of IP6K1 and IP6K2 result in complete loss of IP_7, in MEF, at least, and lead to mice lethality. This highlights the importance of IP_7 in the development of mammals. Previous researchers have noted significant roles of IP_7 in the secretion of insulin and male mice reproductive capacity (Bhandari et al., 2008; Malla & Bhandari, 2017). As for the complete depletion of IP_7 in the whole body, the development of mice embryos is affected. From E15.5, the DKO embryos begin to show anaemia with pale colour and smaller size. Even though the DKO embryos do not offer many morphologic

differences with WT embryos at E13.5 and E14.5, the maturation of erythroid progenitors is affected in the DKO fetal livers. In addition, the hemoglobin switching in the hematopoietic stem cells is also affected by the loss of IP_7. The blood analysis shows that there are more white blood cells and monocytes as well as neutrophils in the DKO embryos. Fewer red blood cells and hemoglobin can explain anaemia in the DKO embryos. This evidence shows that complete depletion of IP_7 has pronounced effect on the differentiation of hematopoietic stem cells.

To further reveal how the loss of IP_7 affects the differentiation of hematopoietic stem cells, surface marker antibodies were applied to track the differentiation of hematopoietic stem cells with fetal livers. According to the results of FACS, hematopoietic stem cells in the DKO fetal livers shows myeloid-biased differentiation. There are more leukocytes and myeloid cells in the DKO embryos. In contrast, the lymphocyte lineage cells are fewer in the DKO embryos, including T cells, B cells and NK cells. However, loss of inositol pyrophosphates in the whole body leads to fewer CMP and CLP while there are more hematopoietic stem cells in the DKO group.

It is essential to find the precise time point of DKO mice death because this will provide crucial clues to the direct cause of DKO mice death. In addition, the embryonic lethality of DKO mice indicates the importance of inositol

pyrophosphates in the development of mammals. However, it is unknown what is the direct cause for the DKO mice lethality. Another path to answer this question is to delete IP6K1 and IP6K2 in specific tissues. For example, if deletion of IP_7 in the whole body shows defects in the erythroid progenitors and IP_7 loss restricted solely to the erythroid progenitors shows similar phenotypes with IP_7 loss through the entire body, IP_7 loss from other tissues does not lead to defects, one can conclude that depletion of IP_7 in erythroid progenitors is the direct cause of lethality in mice.

3.5 Chapter conclusions

In this chapter, we found that double deletion of IP6K1 and IP6K2 led to complete depletion of IP_7 in mice and resulted in mice lethality. From E15.5, the DKO embryos began to show evident anaemia, such as pale skin and smaller size because of lacking red blood cells and hemoglobin. In addition, double deletions of IP6K1 and IP6K2 affect the differentiation of hematopoietic stem cells and lead to myeloid-biased differentiation.

Chapter 4 Loss of IP6K1 and IP6K2 affects fetal lung development and leads to mice lethality at birth

4.1 Introduction

According to the results of chapter 3, I have already confirmed double deletions of IP6K1 and IP6K2 led to mice lethality. Therefore, it was necessary to determine the precise timepoints of homozygous mice death as it would provide essential clues for me to reveal the actual cause of homozygous lethality.

During the development of mice embryos, DKO embryos show anaemia from E15.5 and the maturation of erythroid progenitors are affected at E13.5. In addition, I could not get any DKO mice at P21 among over 100 offspring of heterozygous DKO self-crossing. However, when I determined the genotypes of the offspring of self-crossing at P6, no homozygous DKO mice were found. I narrowed down the precise dead timepoint of DKO mice around birth.

The above work helps me narrow down the precise time point of DKO mice lethality from the later gestational stages to the postnatal stage. During this period, defects in the development of blood, heart, and vessels always cause cardiovascular insufficiency, while defects in lungs and skin are the major causes of postnatal lethality (Ward et al., 2012). Defects in the DKO embryos including smaller fetal livers, pale bodies and affected maturation of hematopoietic stem cells show that cardiovascular insufficiency should be an essential factor of DKO mice lethality. However, the precise time point of DKO mice death will provide crucial clues of

DKO mice lethality.

4.2 Chapter aims

The aims of this chapter were to look for the timepoint of homozygous DKO mice death and to reveal the cause of DKO mice lethality.

4.3 Results

4.3.1 Homozygous embryos died at birth due to respiratory failure

As no homozygous knockout mice are viable among over 100 offspring of self-crossing of heterozygous DKO mice, it is reasonable that the homozygous mice die during the gestational period or after birth. In addition, when I compared the DKO embryos with WT embryos, these DKO embryos were still alive at E15.5, E16.5 and even E18.5 (Figure *3-13*).

Therefore, the next step is to check the birth stage. Facing a different environment, newborn infants have to overcome many challenges. During the gestational stage, embryos are protected by the pregnant mice and stay in a comfortable environment where the pregnant mice provide necessary oxygen and nutrients for the embryos. However, from the moment of birth, the infant mice have to breathe by themselves. There also live in a new environment where the temperature and humidity are different from the gestational stages. The newborn mice have to overcome a lot of challenges to their lungs and epithelia, organs for which many cases of gene deletion cause developmental defects manifesting as death at birth.

In reality, the parent mice eat dead or abnormal infants. They sometimes eat the newborn infants when the female mice do not have enough experience of raising infants or the female mice are disturbed during the delivery period. In order to check whether the DKO mice die at birth, I checked the mice cage and determined the genotypes of newborn infants at E19.5, the birth stage of mice. In order not to disturb the delivery times of infants, I collected the newborn mice several hours after birth. I found some dead infant mice with the genotype of IP6K1$^{-/-}$ IP6K2 $^{-/-}$. Compared with WT mice, the dead DKO mice are smaller and paler (Figure *4-1*). The WT mice become reddish because they breathe and absorb oxygen. However, it is not sure whether the differences between WT and DKO mice are so significant at the moment of DKO mice death.

Figure 4-1 The morphology of dead DKO mice and live wild-type as recovered from mice cages several hours after birth.

In fact, the recovery of dead DKO mice just several hours after birth, could arise because DKO mice died either around birth or after birth, because pregnant mice can deliver dead embryos if they are not reabsorbed by the pregnant mice. To answer this question, it is necessary to verify whether the homozygous mice are alive at birth. Therefore, the whole delivery process should be monitored. However, because pregnant mice would eat their infants or stop delivering when they are disturbed during the delivery process, pregnant mice were dissected so that all the newborn mice could be observed at the same time. All the newborn infants including DKO mice were alive and began to breathe after birth. As revealed by video, all the newborn mice can move and opened their mouths. At first, the newborn mice were in dark colour because of hypoxia during the gestational stages. Then WT mice became reddish as they absorbed more oxygen through breathing. However, the cyanotic DKO mice had a lower frequency of breathing and struggle to aspire. The WT or heterozygous DKO mice were more active physically while the DKO mice remained inactive. However, the DKO mice were still alive because they could react and move when their legs were touched. About one hour after birth, the DKO mice stopped breathing, did not open their mouths anymore, nor showed reaction to touch. In general, the DKO mice opened their mouths less frequently, were less active and died within an hour of delivery. In addition, these DKO mice did not turn red as the WT and heterozygous infants did because DKO mice did not

get enough oxygen through breathing (Figure *4-2*). On the other hand, all the WT and heterozygous DKO infants of artificially assisted childbirth survived.

Figure 4-2 DKO mice have difficulty in breathing and die after birth. WT mice are bigger than the DKO mice. WT mice become reddish through breathing while the bodies of DKO mice are in the dark. (n=3 WT and 2 DKO).

4.3.2 Lung development defects in homozygous DKO embryos

The homozygous DKO mice stopped breathing after birth because of respiratory failure. Respiratory failure is a leading cause of the death of newborn infants, especially in premature infants.

In order to further study the cause of the death of DKO mice, the lungs should be inspected closely. The lungs isolated from the WT and DKO newborn mice showed marked differences. The lungs of the DKO infants were smaller and paler. In contrast, the lung WT lungs are bigger. Under microscopy, the distal airways and pulmonary alveoli of WT lungs could be seen while the DKO lungs were still compacted, which means that there is air exchange in the WT lungs but no air exchange in the DKO lungs (Figure *4-3*). When the lungs of WT and DKO put into PBS, the DKO lungs dropped to the bottom while the WT lungs floated above the

liquid because of air exchange in the normal lungs. The lungs isolated from the newborn infants of IP6K1 KO and IP6K2 KO were buoyant like WT (Figure *4-4*). The lungs defects in the DKO mice can explain why the DKO mice breathe slowly and finally stop. Just like the WT and heterozygous infants, the DKO mice open their mouths and struggle to breathe. However, DKO mice cannot breathe successfully because of lung defects and die of respiratory failure.

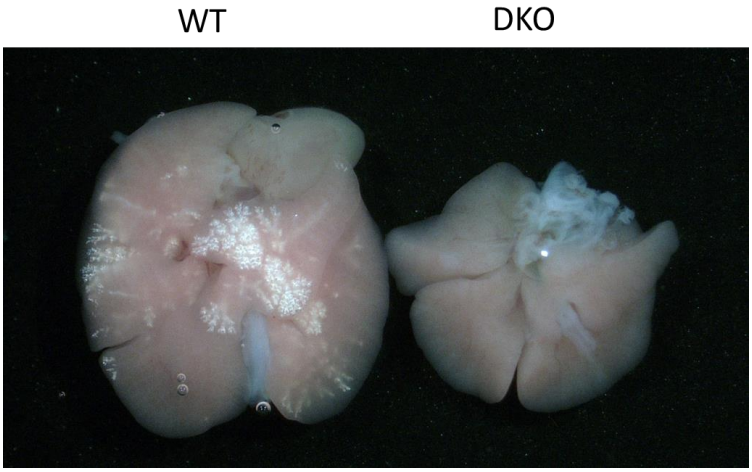

Figure 4-3 Air exchange in the WT lungs but not DKO lungs after birth. In the WT lung, distal airways and pulmonary alveolars are expanding because of air exchange. On the other hand, the DKO lung is more petite and compacted without air exchange.

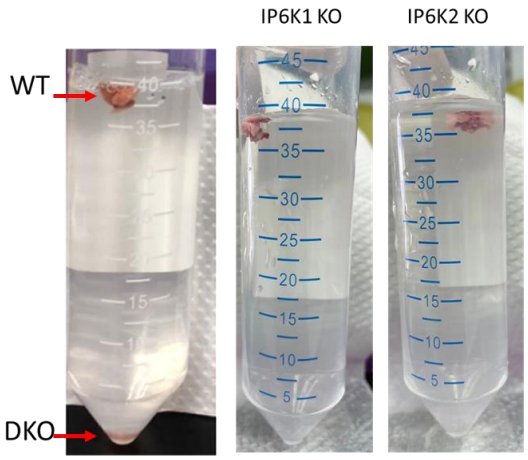

Figure 4-4 The buoyancy of WT, IP6K1 KO and IP6K2 KO lungs. The lungs of WT, IP6K1 KO, IP6K2 KO and DKO were isolated from mice at P0.

To further reveal more details of lung defects in the DKO embryos, lungs of the WT and DKO embryos were studied at E15.5 and E18.5. At E15.5, both of the WT and DKO lungs are in white and the differences between them are not noticeable. At E18.5, the fetal lungs of DKO embryos are smaller than the WT lungs. The DKO lungs are pale while the WT lungs are reddish. In addition, the airways and lung distal alveoli are relatively mature in the WT lungs at E18.5, of which many white airways in the lungs can be seen. On the other hand, the airways and distal alveolars were not apparent in the DKO fetal lungs at E18.5 (Figure 4-5).

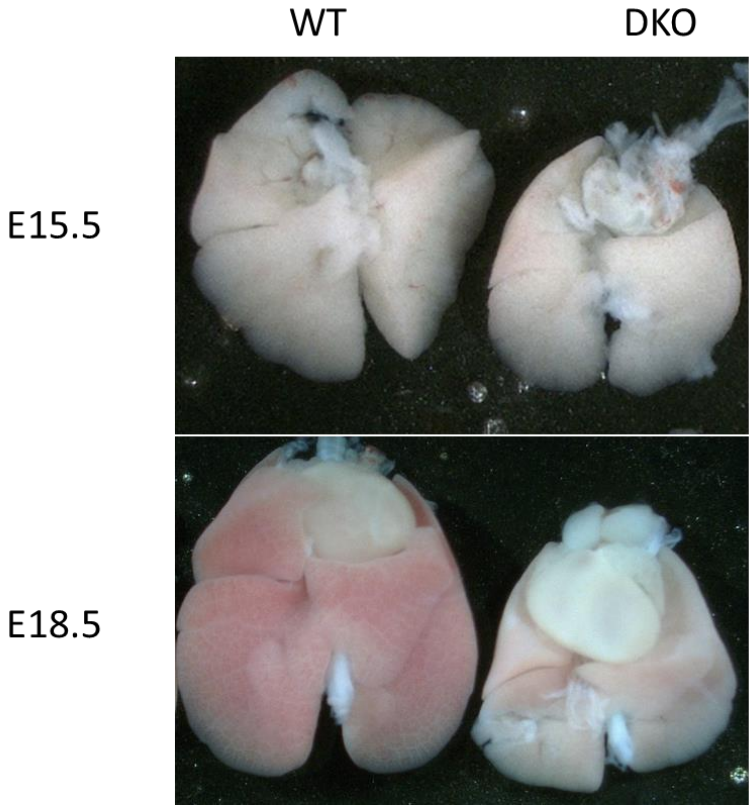

Figure 4-5 Lung defects in the DKO embryos. Lungs were dissected at E15.5 and E18.5. At E15.5, there is no apparent difference between WT and DKO lungs. At E18.5, the DKO lung is pale and small.

To look for more details of developmental defects in the DKO fetal lungs, the lungs of WT and DKO embryos were analysed by Hematoxylin and eosin staining (H&E staining). H&E staining is widely used in medical research to provide more structural details of tissues and cells. The hematoxylin stains the nucleus blue while eosin stains the cytoplasm red. This method can give details on the general layout of cells and show the structure of the tissues. The WT and DKO fetal lungs were analysed by H&E staining at E15.5, E18.5 and P0. At E15.5, the inside layout of WT and DKO lungs were not greatly different. At E18.5, the WT fetal lungs are full of pulmonary alveoli while there are fewer pulmonary alveoli in the DKO fetal lungs. In addition, the WT alveoli are larger and fully extended. However, in the DKO fetal lung, the pulmonary alveoli are smaller and abnormal (Figure 4-6). The well-developed WT fetal lungs have thinner pulmonary walls while the pulmonary walls of DKO fetal lungs are thicker. Without enough pulmonary alveoli in the lung, newborn infants cannot have enough air exchange. In addition, the thicker pulmonary walls of DKO lungs would make the newborn infants more challenging to stretch their lungs. Consistent with this notion, at P0, the pulmonary alveoli of WT lungs are larger with a thin wall because air exchange in the WT lungs expanded the volume of the lungs. On the other hand, the DKO lungs were compacted without any indication of air exchange. The thick wall almost occupied the whole lungs. Therefore, at the late gestational stage, the fetal lungs of DKO embryos had very severe phenotypes. Conveivable, the newborn infants were

tolerant to some extent of hypoxia so that the DKO mice died one hour after birth rather than immediately.

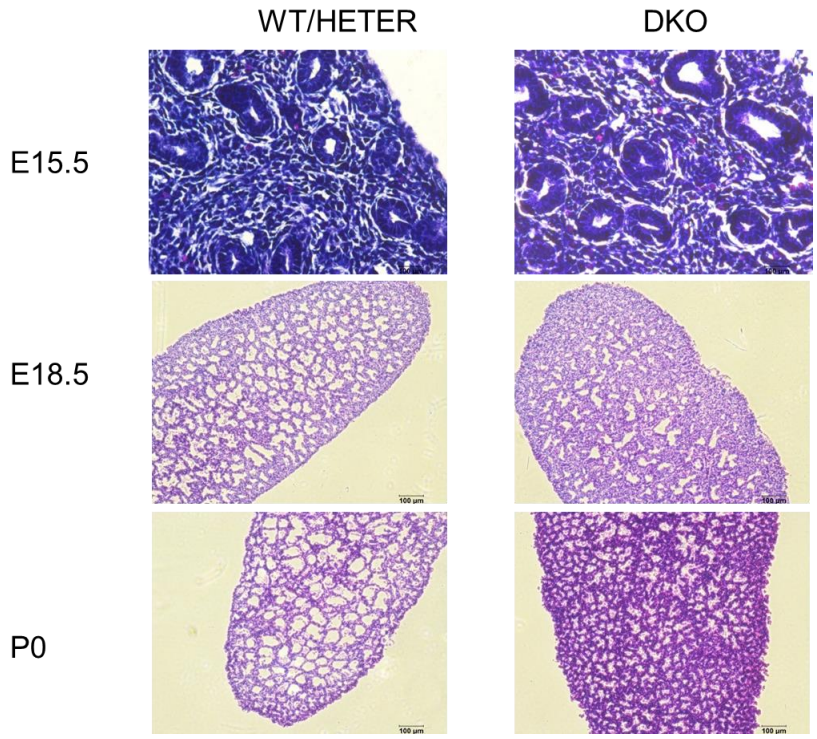

Figure 4-6 H&E staining shows lung defects in the DKO fetal lungs. At E15.5, the inside layout of WT and DKO lungs were not greatly different. At E18.5 and P0, the WT fetal lungs are full of pulmonary alveoli while there are fewer pulmonary alveoli in the DKO fetal lungs. In addition, the WT alveoli are larger and fully extended while the DKO pulmonary alveoli are smaller and abnormal. The alveolar walls in the DKO lungs are thicker than WT alveolar walls. Scale bar=100μm.

4.3.3 The maturation of fetal lungs is delayed in the DKO embryos

Through H&E staining, I found that alveolar development is affected in the DKO fetal lungs. The pulmonary alveoli mainly have two types of cells, alveolar type I (AT1) and alveolar type II (AT2) cells. On the surface of pulmonary alveoli, AT1 cells occupy more than 95%, while AT2 cells consist of about 5%. The physiological function of AT1 cells is air exchange while the AT2 cells secrete

surfactant proteins inducing the maturation of alveoli. To confirm the developmental defects in the DKO fetal lungs, expression of the marker genes of alveolar type I (AT1) and alveolar type II (AT2) were assessed to measure the maturation of pulmonary alveoli. TTF1 and T1a are the marker genes of pulmonary alveolar type I cells. The surfactant proteins SPA, SPB, SPC and SPD are the marker genes of pulmonary alveolar type II cells. At E15.5, the marker genes of AT1 (TTF1 and T1a) are expressed at a lower level in the DKO lungs. In addition, all the maker genes of AT2 cells, SPA, SPB, SPC and SPD are expressed at a lower level in the DKO lungs (Figure *4-7*). This confirms the immaturity of lung pulmonary alveolar cells, including AT1 and AT2 cells in DKO embryos. CC10, the marker gene of Club cells, is reduced significantly in the DKO lungs, which indicates functional defects in the Club cells. The markers genes of fetal lungs show developmental defects in the DKO fetal lungs at the molecular level.

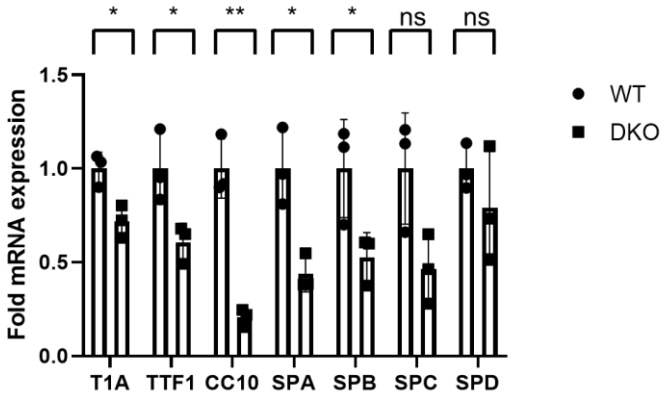

Figure 4-7 The marker genes of AT1(T1A, TTF1), AT2 (SPA, SPB, SPC and SPD) and Club cells (CC10) indicate the immaturity of pulmonary AT1 and AT2 in DKO lungs. Marker gene expression was measured in WT and DKO fetal lungs at E15.5. Data normalized to Actin represented as fold-change compared to WT, shown as mean ± SD (n = 3 WT and 3 DKO) (*p < 0.05, **p < 0.01, ***p < 0.001)

4.3.4 The defects in the epithelial cells of fetal lungs upon loss of IP_7

The marker genes of lung cells reveal defective maturation of pulmonary epithelium in the DKO fetal lungs. To further explore how the DKO fetal lungs are affected by the loss of IP_7, we stained fetal lung tissues with different cell types marker of fetal lungs, including the macrophage and neutrophil cells, AT1 and AT2, club cells, multiciliated cells and smooth muscles cells. According to the staining results, we found that in the DKO fetal lungs there are more neutrophils and macrophages, which are indicated by isolectin B4 and myeloperoxidase separately. These observations indicate that the immune response is activated in the DKO fetal lungs. Previous researches have already revealed that immune response activation in fetal lungs disrupts the morphogenesis of alveolars and distal airways of fetal lungs and finally result in respiratory failure at birth. Activation of NF-kappa B in alveolar macrophages and expression of IL-1 beta has negative effects on the maturation of epithelium cells, especially on the secretion of surfactant proteins from AT2 cells (Blackwell *et al.*, 2011) (Hogmalm *et al.*, 2013).

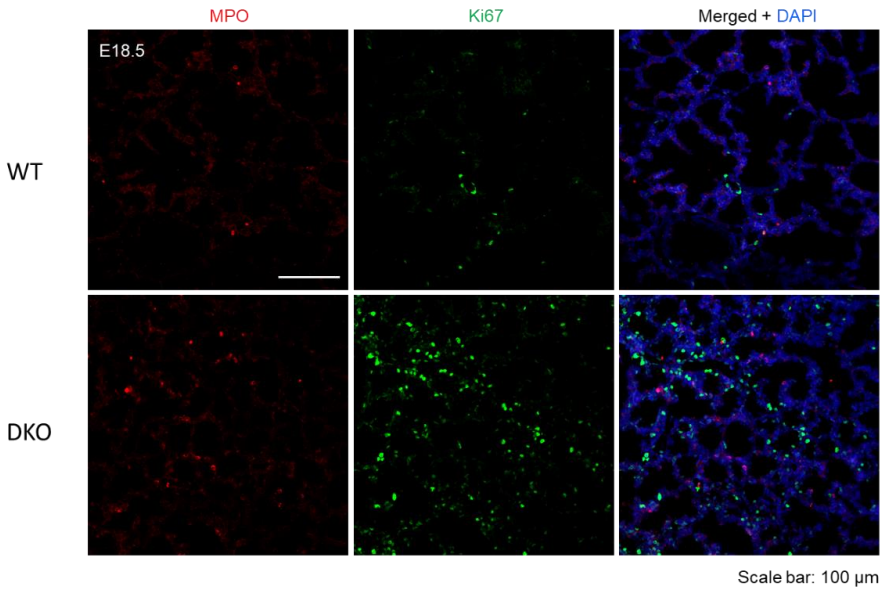

Figure 4-8 There are more neutrophils and more cells in proliferation in the DKO fetal lungs. Confocal fluorescence imaging of sections of E18.5 lung tissues stained with DAPI, myeloperoxidase and Ki67. Scale bar=100 μm. Done by Weitao Cao.

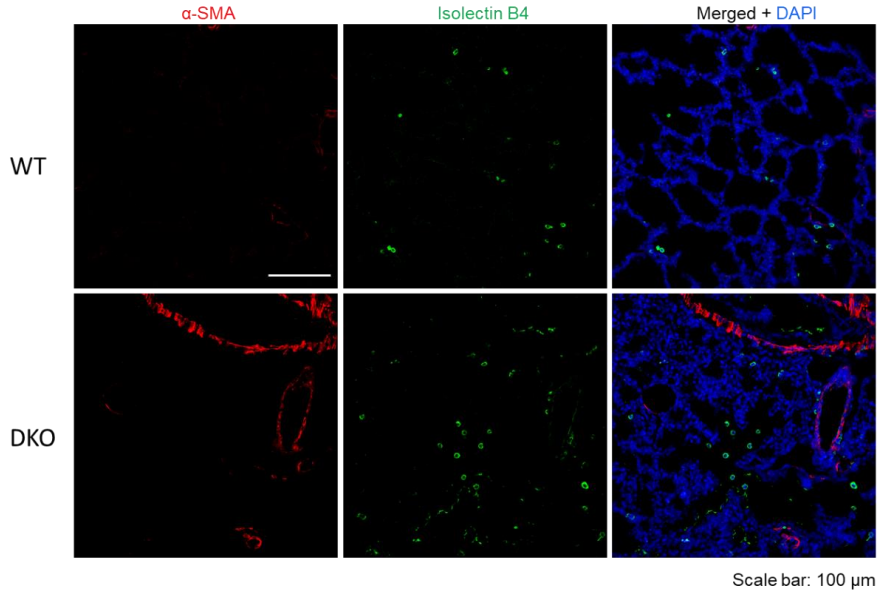

Figure 4-9 There are more macrophages and more myofibroblast in the DKO fetal lungs. Confocal fluorescence imaging of sections of E18.5 lung tissues stained with DAPI, isolectin B4 (macrophage marker) and α-SMA (myofibroblast marker). Scale bar=100 μm. Done by Weitao Cao.

Because the histology of H&E staining also shows that pulmonary alveoli decrease in DKO fetal lungs (Figure 4-6) and the qPCR-measured expression of the marker

genes of AT1 and AT2 are also reduced in the fetal lungs upon loss of IP_7 (Figure 4-7), immunofluorescent staining was conducted to confirm effects of DKO at the protein level (Figure 4-7). The fetal lungs stained with T1A and SPC, the markers of AT1 and AT2 cell, shows the DKO lungs are densely packed tissues (Figure 4-10).

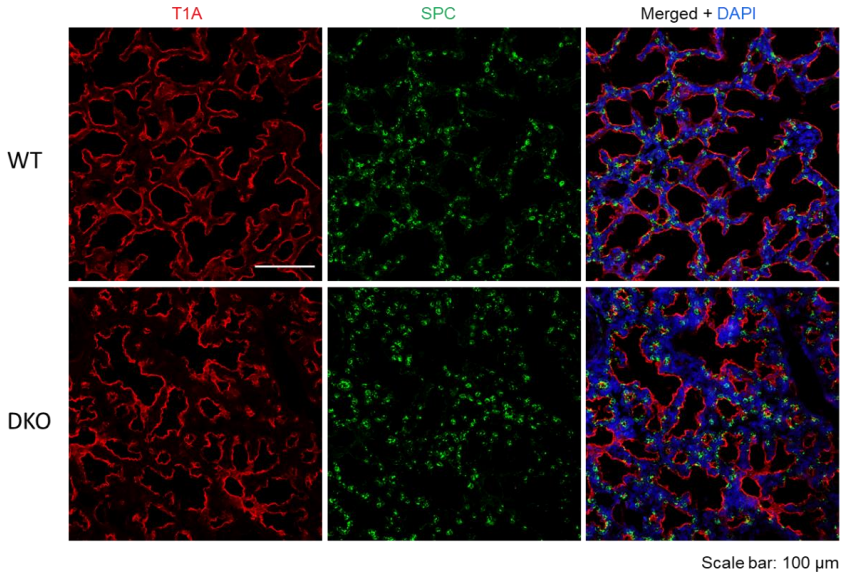

Figure 4-10 Confocal fluorescence imaging of sections of lung tissue stained with DAPI, T1A (marker of AT1 cells) and SPC (marker of AT2 cells). Scale bar=100 µm. Done by Weitao Cao.

Club cell is a secretory cell type that is important for the functional accumulation of pulmonary alveolars and secretion of mucin. The qPCR results with fetal lungs showed that expression of CC10 was lower in the DKO lungs (Figure *4-7*), but the immunofluorescent staining shows no difference in the accumulation of CC10 nor of mucin (MUC5AC) (Figure 4-11).

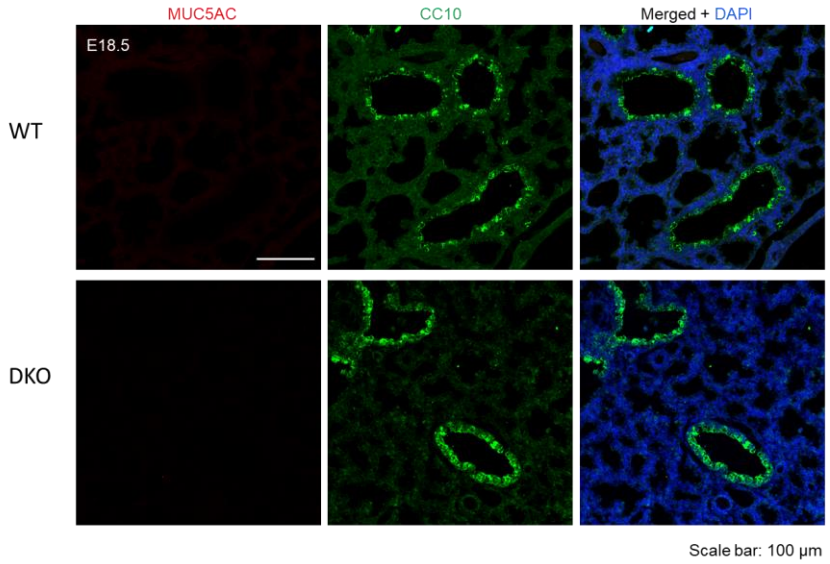

Figure 4-11 DKO fetal lungs show no difference in the differentiation of club cells and secretion of MUC5AC mucin. Confocal fluorescence imaging of sections of lung tissue stained with DAPI, CC10 or MUC5AC markers. Scale bar=100 μm. Done by Weitao Cao.

In addition, to get more details about the differences between the WT and DKO fetal lungs, other lung cells markers were used to stain the fetal lungs. According to these results, acetylated α-Tubulin, a marker of ciliated cells that serve to clear mucus from the airway, exhibited no differences, but we did observe more MUC5B accumulation in the DKO fetal lungs (Figure 4-12). These data indicated that ciliated cells in the DKO lungs have functional defects so that they cannot clear the mucins in the airways.

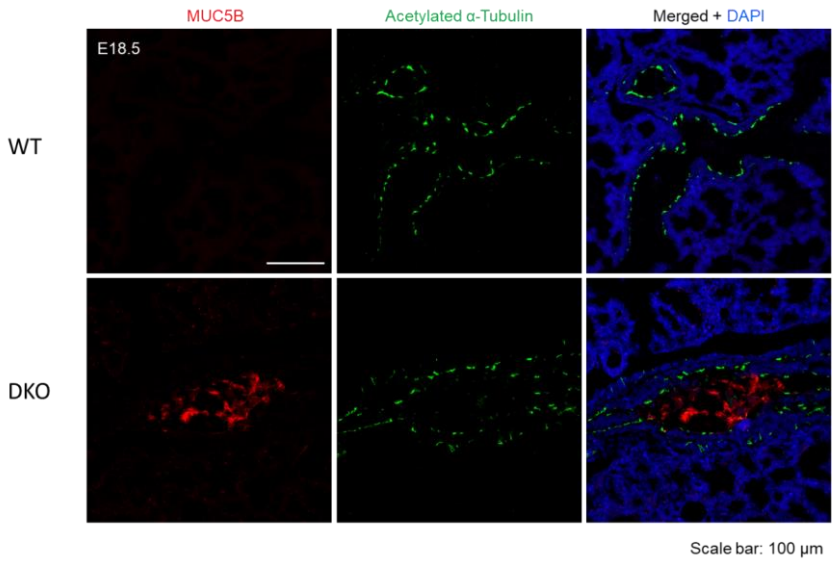

Figure 4-12 DKO fetal lungs have more MUC5B+ mucin accumulation in the airways but unaltered differentiation of ciliated cells. Confocal fluorescence imaging of sections of lung tissue stained with DAPI, acetylated α-Tubulin (marker of ciliated cells) or MUC5B markers. Scale bar=100 μm. Done by Weitao Cao.

Compared with WT lungs, the DKO lungs are smaller. It is reasonable to consider the possibility that the DKO fetal lungs have more apoptosis or cell cycle arrest. To test that possibility that loss of IP_7 leads to cell apoptosis and senescence and a reduction in cell proliferation, lung tissue was subjected to the TUNEL assay Sections of lung tissue of P0 stained with TUNEL assay revealed apoptosis in the DKO lungs, but not all of the cells displayed (Figure 4-13). One would expect there to be fewer cells in proliferation in DKO lungs. However, the fetal lungs of DKO had a stronger signal of Ki67 staining, marker of proliferation, which means that there are more cells in proliferation in the DKO fetal lungs (Figure 4-8).

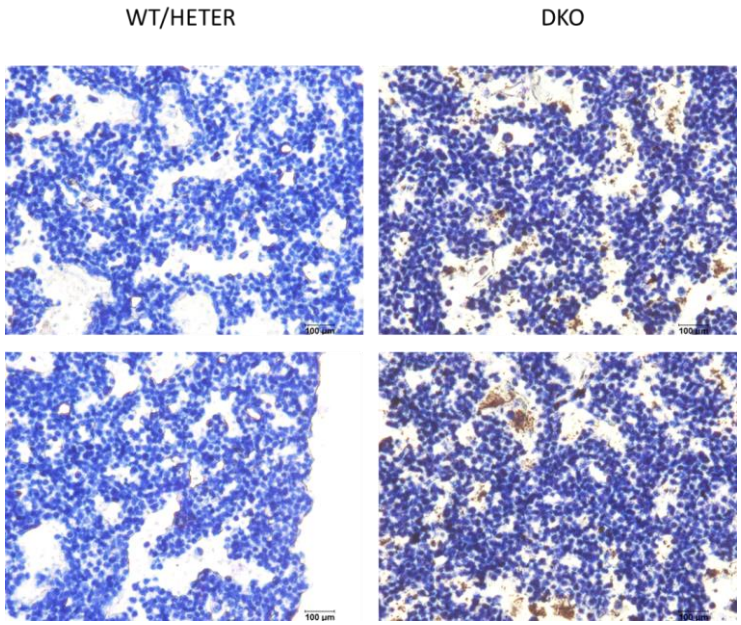

Figure 4-13 There is more apoptosis in the DKO lungs at P0 revealed by the TUNEL assay. These brown dots in the DKO lungs are inside the alveoli. Scale bar is 100 µm.

Recalling that the expression of α-SMA is higher in the DKO lungs than in the WT lungs (Figure 4-9) and that this marker of myofibroblasts is expressed higher in fibrotic lung disease (Peyser et al., 2019), it is possible that the DKO fetal lungs show aspects of fibrotic disease as well as delayed maturation of pulmonary epithelial cells.

In brief summary, the above evidence shows that loss of inositol pyrophosphates has pronounced effects on the maturation and function of cells in the fetal lungs, with additional influence of the DKO cell proliferation, apoptosis and immune infiltration.

4.4 Discussion

In this chapter, I confirmed that mice losing IP6K1 and IP6K2 are lethal and die at

birth because of respiratory failure. This is vital evidence for the importance of IP_7 in the development of mammals. Here, we firstly found that complete depletion of IP_7 affects the development of fetal lungs in mice. Further research showed that the DKO lungs have more macrophages and neutrophils. This evidence showed that the DKO fetal lungs display intensified immune response, which might explain disrupted lung morphogenesis because cytokine secreted from macrophages affected the maturation and differentiation of fetal lungs (Blackwell *et al.*, 2011) (Hogmalm *et al.*, 2013). As for the pulmonary epithelial cells, the development of AT1 and AT2 cells are affected in the DKO fetal lungs upon loss of IP_7. The results of qPCR provided details about the lower expression of cellular markers of AT1, AT2, and club cells in the DKO fetal lungs. In addition, the accumulation of mucin in the airway is a sign of idiopathic pulmonary fibrosis (Hancock *et al.*, 2018). An interesting phenomenon is that while DKO fetal lungs were smaller, they have more cells in proliferation (**Figure *4-8***). An explanation is that loss of IP_7 affects cell differentiation, so these cells are in proliferation. Alternatively, the intensified immune response stimulates cell proliferation. Answering these questions will shed light on the role of IP_7 in mammals.

4.5 Chapter conclusions

Loss of IP_7 led to mice lethality because of respiratory failure. The development of fetal lungs was affected by the loss of IP_7 with delayed maturation of pulmonary alveolar cells, activated immune response and accumulation of mucins. In general,

complete depletion of IP_7 in mice changed lung epithelium morphogenesis a lot and disrupted the functions of alveolar cells.

Chapter 5 RNA sequencing revealed the mechanisms of lung defects in homozygous DKO embryos

5.1 Introduction

There are huge differences between the DKO and WT fetal lungs, including the maturation and differentiation of alveolar epithelium cells, the activated immune response and more cells in proliferation in DKO fetal lungs. From this evidence, we can confirm the importance of inositol pyrophosphates in the development of mice fetal lungs. However, we still know little about the mechanisms of IP_7 action in the development of fetal lungs and why the loss of IP_7 led to activation of immune response and immaturity of alveolar epithelium in fetal lungs. Therefore, I wanted to apply the fetal lungs of DKO and WT at E15.5 to RNA sequencing, to assess gene expression at a whole genomic scale, which could provide important clues to pathways and thereby processes regulated by IP_7 in the development of the fetal lung.

5.2 Chapter aims

The aims of this chapter are to reveal the role of IP_7 in the development of mice fetal lungs. Through gene expression profiling at the genomic scale, I expect to identify pathways and processes in the fetal lungs affected by the loss of IP_7.

5.3 Results

5.3.1 RNA sequencing showed upregulation of immune response genes in the DKO lungs

As I had confirmed that the fetal lungs development was affected by the loss of

inositol pyrophosphate, to further study the differences between DKO and WT fetal lungs, as well as to look for more clues about the functions and mechanisms of inositol pyrophosphate in the fetal lungs, I decided to apply DKO and WT fetal lungs to RNA sequencing.

Fetal lungs of WT and DKO at E15.5 were harvested and used to isolate RNA, three samples of each group. RNA was then sent for RNA sequencing by the NOVA company so as to measure the expression differences in the whole genome-scale. The PC1 value shows that a good consistency between DKO and WT fetal lungs (Figure *5-1*).

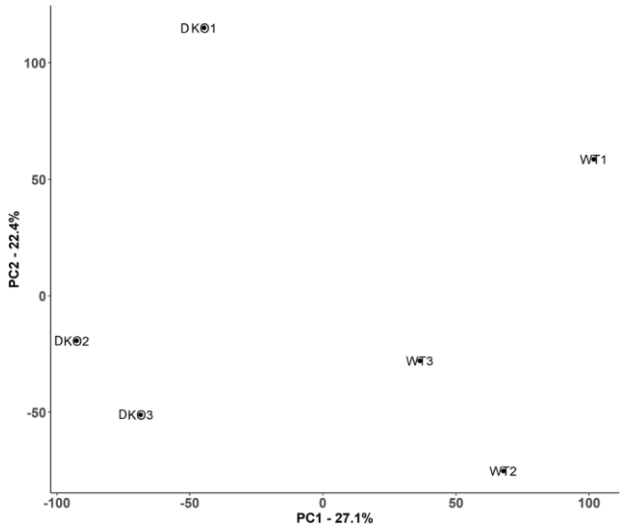

Figure 5-1 PCA analysis. 3 samples of WT and 3 samples of DKO fetal lungs were analysed by RNA sequencing. Analysed by Yi Wen.

According to the RNA sequencing analysis, the genes with more than 20% changes are picked up. There were 492 upregulated genes in the DKO lungs, while there were 92 downregulated in the DKO lungs (Figure *5-2*).

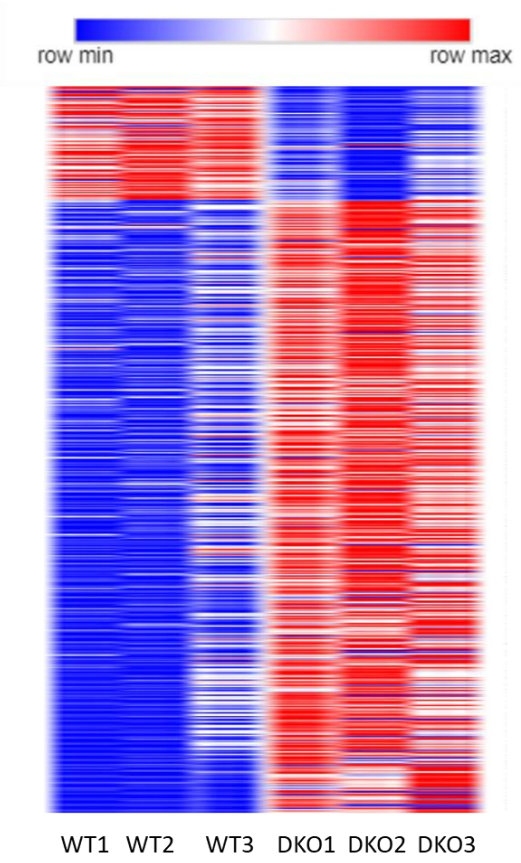

Figure 5-2 RNA sequencing reveals the upregulated and downregulated genes in the DKO fetal lungs. A heatmap of gene expression (upregulation, red; downregulation blue). The log2 fold changes of these genes is more than 0.3 or less than -0.3. Blue indicates down-regulated expression and red indicates up-regulated expression. (n=3 WT and 3 DKO).

Among the 92 downregulated genes, IP6K1 and IP6K2 in the DKO fetal lung were strongly downregulated. This confirms the good quality of this RNA sequencing. In addition, the marker genes of AT1 and AT2 cells were lower in the DKO group, which was already confirmed by qPCR in the above chapter (Figure 4-7).

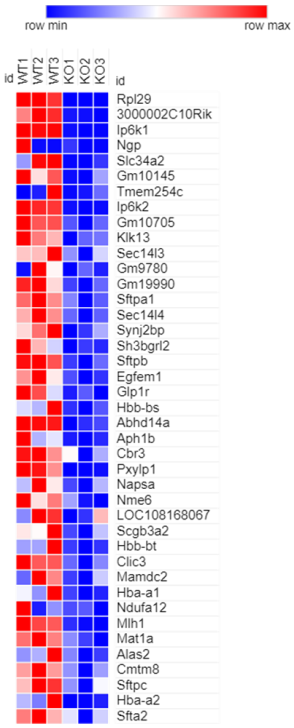

Figure 5-3 A subset of the genes downregulated in the DKO fetal lung. Among these genes, IP6K1 and IP6K2 are the genes deleted by gene editing. Sftpa1, Sftpa2, Sftpb and Sftpc are marker genes of AT2 cells. Hbb-bs, Hbb-bt, Hba-a1 and Hba-a2 encode hemoglobin chains. Blue indicates down-regulated expression and red indicates up-regulated expression. (n=3 WT and 3 DKO).

On the other hand, except for some marker genes of lung and IP6K1 as well as IP6K2 reduced in the DKO group, there were many genes upregulated in the DKO group. Gene ontology analysis points to significant alteration in immune response in the DKO group (Figure 5-4). The most upregulated 20 genes in the list were annotated as immune response genes (Figure 5-5). This is consistent with the accumulation of macrophages and neutrophils in the DKO fetal lungs (Figure 4-8,Figure 4-9).

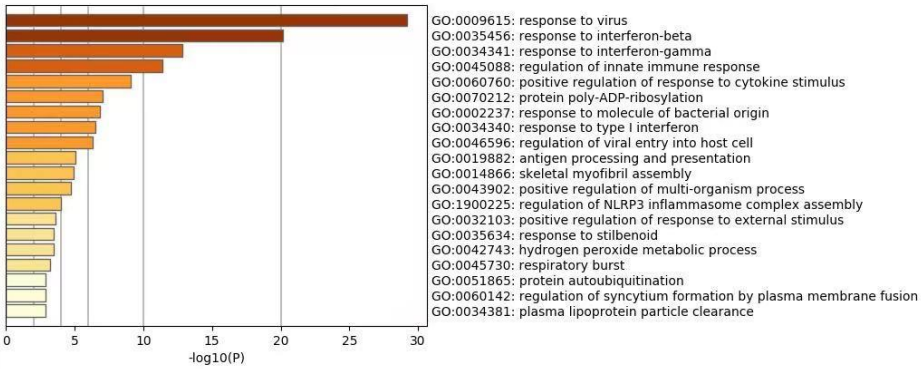

Figure 5-4 The GO analysis of the upregulated genes in the DKO lungs. Most of them link to immune response pathways, including response to virus, response to interferon, innate immune and cytokine stimulus. Done by Sheng Yu.

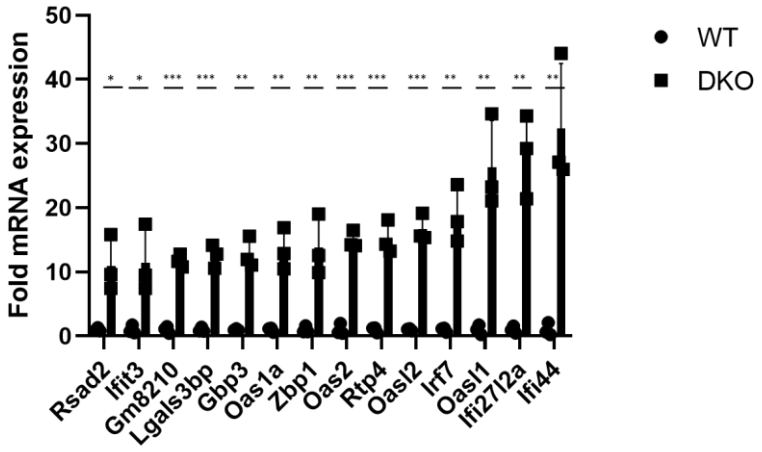

Figure 5-5 The most upregulated genes in DKO lungs are immune response genes. These genes in DKO lungs are upregulated 10-30 folds. Data represented as fold-change compared to WT, shown as mean ± SD (n = 3 WT and 3 DKO) (*p < 0.05, **p < 0.01, ***p < 0.001).

5.3.2 NF-kappa B pathway is activated in the DKO fetal lungs

NF-kappa B is a vital transcriptional factor in the innate immune response. Previous studies demonstrated that activation of the NF-kappa B pathway and IL1 beta overexpression in the fetal lungs led to alveolar morphogenesis defects (Blackwell *et al.*, 2011)(Hogmalm *et al.*, 2013). Phosphorylation of NF-kappa B at

serine 536 is a good indicator of the activation of NF-kappa B. Unphosphorylated NF-kappa B proteins are bound and inactivated by the inhibitor of NF-kappa B (IkB) in the cytoplasm. When the upstream IKK is activated and phosphorylated, the phosphorylated IKK activates IkB through phosphorylation. Phosphorylated IkB release from NF-kappa B and is further ubiquitinated and degraded. Free NF-kappa B is further phosphorylated and translocated into the nucleus where it activates the expression of its downstream genes. We therefore analysed the phosphorylation of NF-kappa B. Interestingly, more NF-kappa B proteins are phosphorylated in the DKO fetal lungs. IKK and IκB are also phosphorylated and activated in the DKO fetal lungs (Figure 5-6).

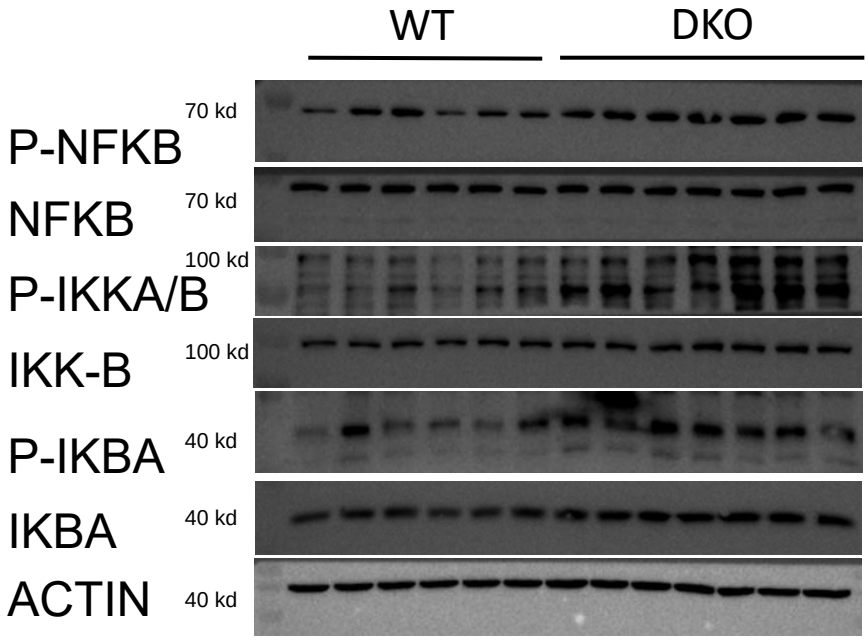

Figure 5-6 Activation of NF-kappa B pathway in the DKO fetal lungs. Western blotting shows enhanced phosphorylation of NF-kapp B, IKKA/B and IKBA normalized to ACTIN, which indicate the activation of NF-kappa B pathway. n=6 WT and 7 DKO.

5.3.3 IRF3 pathway is activated in the DKO fetal lungs

The results above confirmed the activation of NF-kappa B in the DKO fetal lungs. IRF3 is another influential transcriptional faction in the innate immune response. IRF3 is phosphorylated and activated by TBK1. The phosphorylated IRF3 is then translocated into the nucleus where the activated IRF3 also promotes genes expression as a transcriptional factor. It induces the expression of type I IFN and other cytokines. Phosphorylation of IRF3 was confirmed by Western blot. There were more phosphorylated IRF3 in the DKO lungs (Figure 5-7).

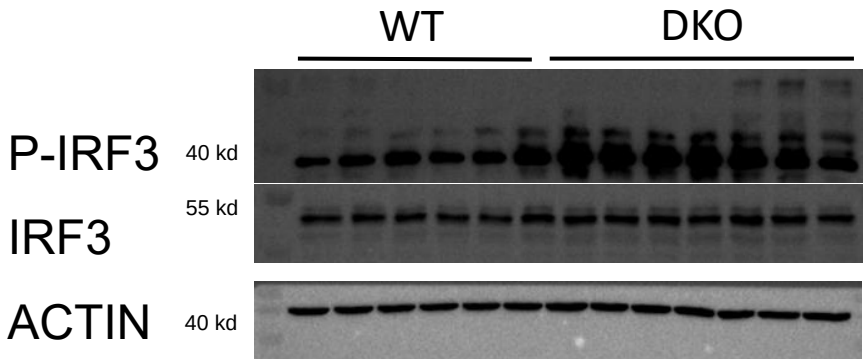

Figure 5-7 The phosphorylation of IRF3 is upregulated in the DKO fetal lungs at E18.5. The accumulation of IRF3 and P-IRF3 is measured with fetal lung at E18.5 by Western Blot normalized to ACTIN. n=6 WT and 7 DKO.

5.3.4 DNA damage is enhanced upon double deletions of IP6K1 and IP6K2

Previous data have showed that immune response activation in the DKO fetal lungs. One of the endogenous factors causing immune response is DNA damage. Consequently, we used the DNA damage marker, phosphorylation of H2AX, to

look for evidence of DNA damage with fetal lungs. Interestingly, the results (Figure 5-8) show H2AX is activated in the lung of DKO embryos, consistent with the observation that IP6K1 deletion increased activation of H2AX when cells were treated with DNA damage inducers (Jadav et al., 2013b). These phenomena reveal the importance of inositol pyrophosphates in DNA damage repair. In my study, the loss of inositol pyrophosphates correlated with intense DNA damage without any inducers. The phenotypes in the DKO embryos are much stronger than in the case of IP6K1 deletion, most likely because double deletions of IP6K1 and IP6K2 lead to complete loss of IP_7 while IP6K1 deletion does not deplete IP_7 completely (Figure 5-8). While there is no precisely defined mechanism to explain the critical role of inositol pyrophosphates in the DNA damage repair pathway, I also detected other marker proteins of DNA damage response, including phosphorylation of KAP1, CHK2 and P53. These proteins and H2AX are substrates of ATM and are phosphorylated by ATM. Their phosphorylation indicates activated DNA damage response in the DKO fetal lungs (Figure *5-8*).

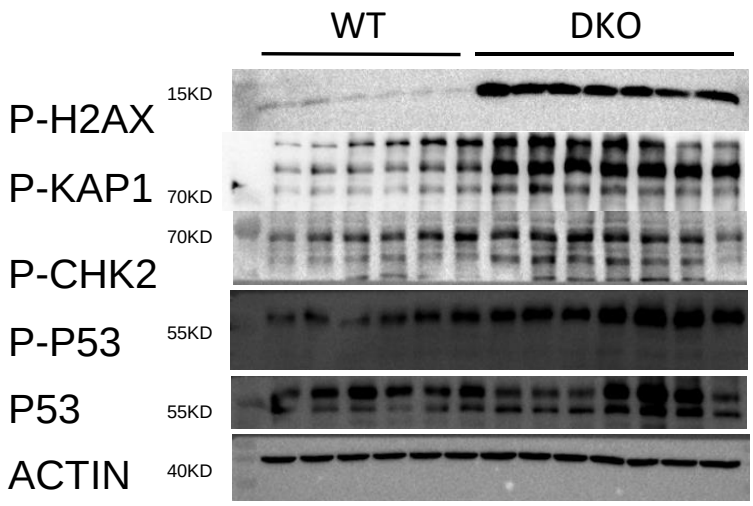

Figure 5-8 DNA damage response is activated in the E18.5 DKO lungs. Western blotting shows increased phosphorylation of H2AX, KAP1, CHK2 and P53 normalized to ACTIN. n=6 WT and 7 DKO.

We further confirmed this phenomenon at the tissue level by immunofluorescent staining with fetal lung tissues. Fetal lungs of E18.5 were stained with the antibody of phosphorylation of H2AX. DKO fetal lungs had a higher level of phosphorylation of H2AX. However, in the DKO fetal lungs, only a few cells showed phosphorylation of H2AX while most lung cells in the fetal lungs did not have DNA damage (Figure *5-9*). Therefore, it was necessary to reveal the cells in the fetal lungs with DNA damages.

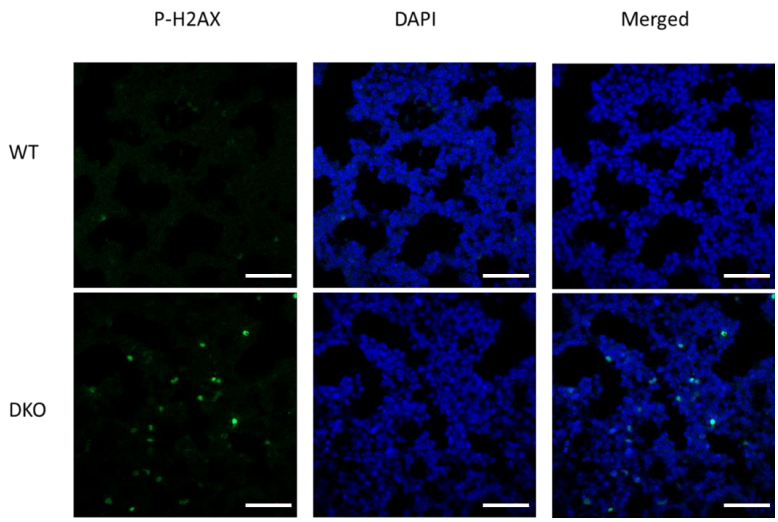

Figure 5-9 There is more DNA damage accumulation in the pulmonary alveoli in the DKO lungs at E18.5. Confocal fluorescence imaging of e phosphorylation of H2AX in tissue slices of fetal lungs at E18.5. The scale bar is 40 μm.

In chapter 4, I used the TUNEL assay to measure apoptosis in the DKO fetal lungs (**Figure *4-10***). In fact, the TUNEL assay is also designed to detect DNA damage. Thus, data from Figure 4-10, also suggested that some cells of DKO fetal pulmonary alveoli have DNA damage.

5.3.5 Search for the cells with DNA damage

According to the results of the P-H2AX staining and TUNEL assay for the fetal lungs tissues, we know that not all the cells show DNA damage. In fact, DNA damage can induce an immune response and immune response can also cause DNA damage (Flannery et al., 2018; Kay et al., 2019). Only part of the cells shows the signal of DNA damage. Therefore, to look for the cell types with DNA damage upon loss of IP_7 is essential to reveal the role of this molecule in the development of mammals. Therefore, I tried to identify the cell types affected through co-

staining the fetal lungs tissues with P-H2AX antibody and cell type marker antibodies.

The fetal lung tissues were stained with a P-H2AX antibody and the marker of macrophages because there is an accumulation of macrophages in the DKO fetal lungs. Isolectin B4, a maker of macrophages, was used to stain the fetal lungs and a P-H2AX antibody was used separately. However, the signal of P-H2AX did not localize to the macrophages (Figure 5-10).

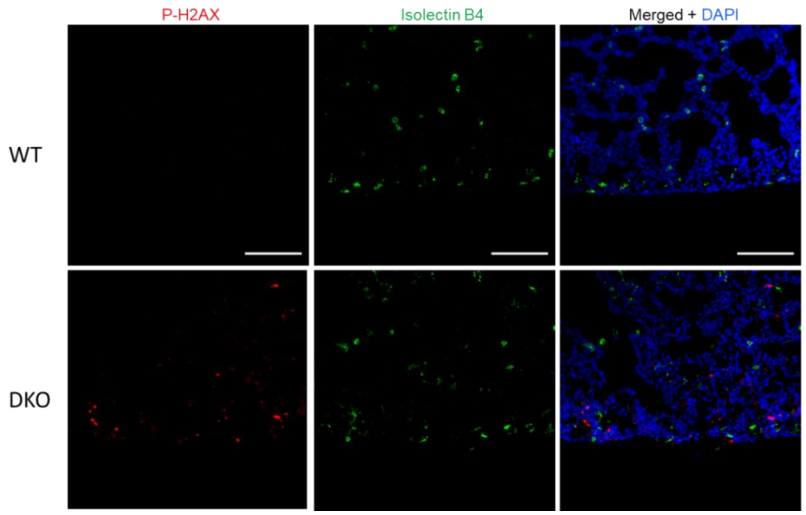

Figure 5-10 No DNA damage in the macrophages. Confocal fluorescent imaging of tissue slices for macrophages (Isolectin B4) or DNA damage (P-H2AX). The scale bar is 100 μm. Done by Weitao Cao.

In addition, to look for whether DNA damage is specific to particular immune cell types of DKO fetal lungs, the fetal lungs were stained side by side with P-H2AX and CD45, a marker of leukocytes. According to Figure 5-11, there were more cells with DNA damage in the DKO fetal lungs. However, the number of leukocytes in the DKO fetal lungs was not obviously larger than that of WT fetal

lungs. The data also show that some immune cells have DNA damage but not all the DNA damage signals colocalize with leukocytes. (Figure *5-11*). In fact, most of the cells with DNA damage are not immune cells.

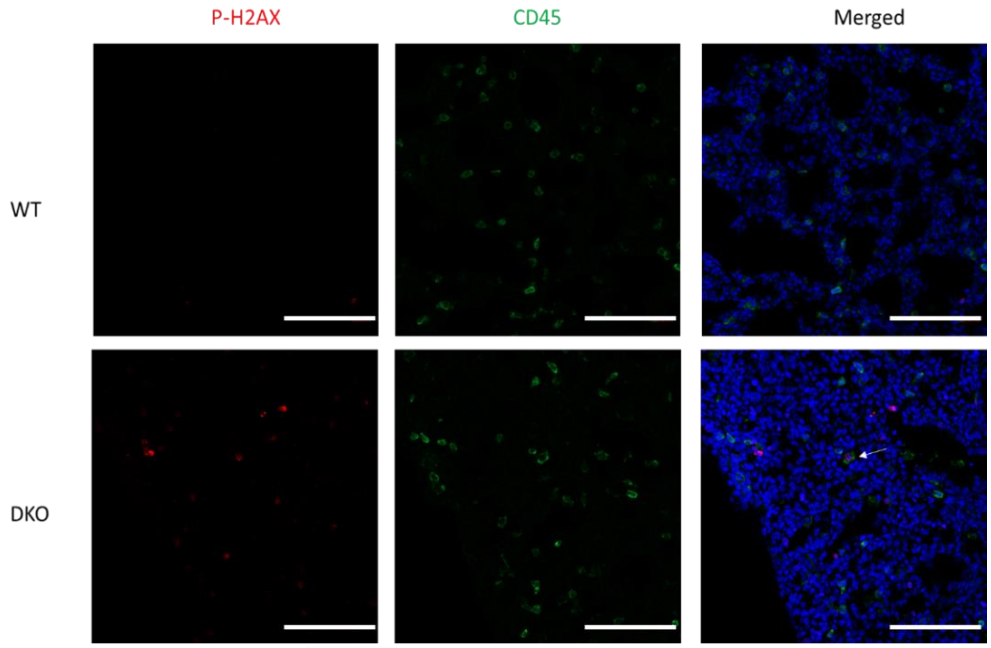

Figure 5-11 Loss of inositol pyrophosphates induces DNA damage in some immune cells. Confocal fluorescent imaging of tissue slices for leucocytes (CD45) or P-H2AX with E18.5 fetal lungs. The scale is 100 µm.

Most of the cells with DNA damage in the DKO fetal lungs do not obviously belong to immune cells and they could therefore be other lung cell types. It will be important for future work on the role of inositol pyrophosphates in fetal lung development to analyse other cell types for DNA damage through co-staining with P-H2AX antibody and cell-specific markers of these cell types.

Endothelial cells are important cells in the lungs. Dysfunction in the endothelial cells affects the maturation of pulmonary epithelium during embryonic

stages(Coulombe et al., 2019). Therefore, it is important to detect whether the endothelial cells are affected in the DKO fetal lungs. Interestingly, the signals of DNA damage are mainly in the endothelial cells, which is marked by CD31 antibody (Figure *5-12*).

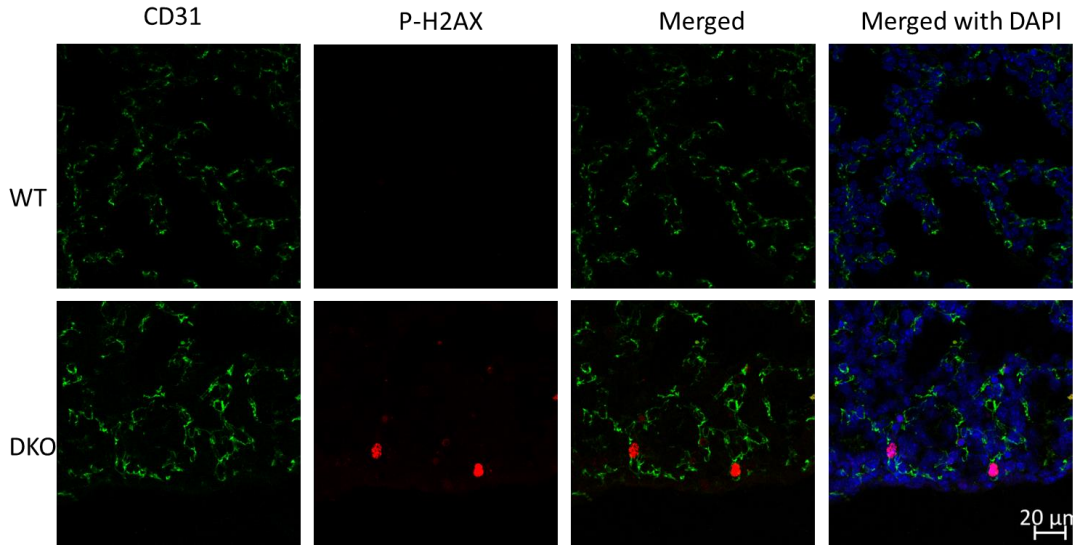

Figure 5-12 DNA damage is mainly localized in the endothelial cells. Confocal fluorescent imaging of tissue slices for endothelial cells (CD31) or P-H2AX with E18.5 fetal lungs. The scale is 20 μm.

5.3.6 Analysis of immune cells in the fetal lungs

There is strong immune activation in the DKO fetal lungs, which is an essential factor of developmental defects in the lungs. Therefore, it is necessary to analyse the immune cells in the DKO fetal lungs, which could provide important clues of the immune activation in the DKO fetal lungs. Therefore, I explored populations of the immune cells in the fetal lungs at E18.5 through the FACS method.

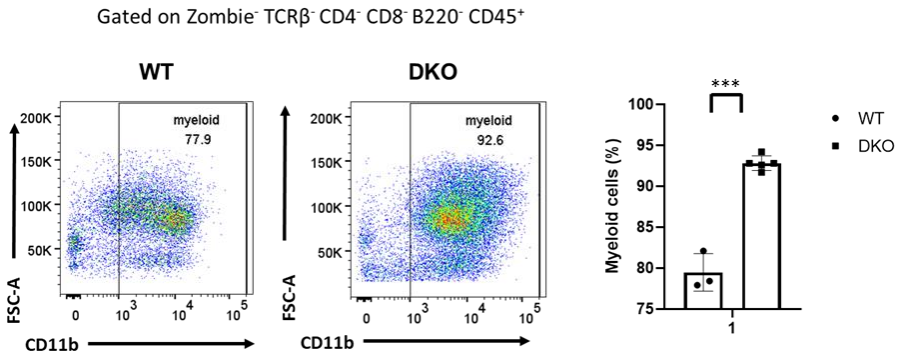

Figure 5-13 There are more myeloid cells in the DKO fetal lungs at E18.5. FACS analysis of fetal lung cell populations. All cells are gated on Zombie$^-$ TCRβ$^-$ CD4$^-$ CD8$^-$ B220$^-$ CD45$^+$, left and middle panels. Significant difference in myeloid populations between WT and DKO are shown (right panel) asterisk. Data shown as mean ± SD (n = 3 WT and 5 DKO) (*p < 0.05, **p < 0.01, ***p < 0.001). Done with Chang Li.

According to the results of FACS, there are more myeloid cells in the DKO fetal lungs (Figure *5-13*). The upregulation of myeloid cells in the DKO fetal lungs can explain innate immune activation. The increase of myeloid cells is consistent with the myeloid-biased differentiation of hematopoietic stem cells. Therefore, the immune activation in the fetal lungs could arise from fetal livers, the site of production of myeloid cells.

The myeloid-biased differentiation of hematopoietic stem cells, revealed in chapter 4, likely leads to lower lymphocytes generation in the DKO fetal livers. There were also fewer B cells detected in the DKO fetal lungs but the accumulation of T cells and NK cells, which are counted by NK1.1 and TCRβ antibodies, showed no noticeable difference (Figure *5-14*).

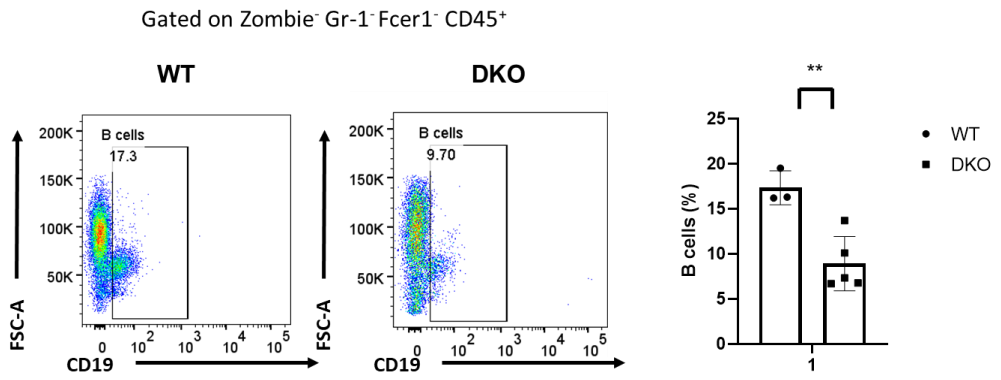

Figure 5-14 There are fewer B cells in the DKO fetal lungs. FACS analysis of fetal lung cell populations. All cells are gates on Zombie⁻ Gr-1⁻ Fcer1⁻ CD45⁺, left and middle panels. Significant difference in B cell populations between WT and DKO are shown (right panel) asterisk. Data shown as mean ± SD (n = 3 WT and 5 DKO) (*p < 0.05, **p < 0.01, ***p < 0.001). Done with Chang Li.

The colocalization of CD45 and P-H2AX, revealed earlier, shows that most of the cells with DNA damage in the DKO fetal lungs are not immune cells. The immune response in the DKO lungs cannot therefore be wholly responsible for lung defects. Most of the cells with DNA damage in the fetal lungs are endothelial cells (Figure *5-12*). Therefore, it is necessary to confirm whether the defective DKO lungs is the result of dysfunctions in the immune cells or endothelial cells or their combined result. This will provide essential clues for the causes of lung defects.

5.4 Discussion

RNA sequencing revealed immune activation in the DKO fetal lungs and Western blotting confirmed the activation of NF-kappa B and IRF3 pathways in the fetal lungs of DKO. Immune activation can be the cause or result of DNA damage. Because of the limitation of antibodies, we were not able to identify the particular

cell types exhibiting DNA damage. Thus, according to current evidence in the DKO fetal lungs, AT1, AT2 and macrophage were not matched with the signals of DNA damage indicated by the P-H2AX antibody. In the near future, it will be promising to combine the use of immunofluorescent staining for P H2AX and marked cell types to provide important clues about the cell type-specific functions of inositol pyrophosphates in the development of fetal lungs.

To summarize, immune activation can be the reason or result of DNA damage. It is not sure whether DNA damage leads to a robust immune response or immune response results in DNA damage in the DKO fetal lungs. Previous studies have revealed that lack of IP_7 affects the efficiency of DNA repair in MEF cells upon DNA damage inducer (Jadav et al., 2013a). However, we show clearly that the loss of inositol pyrophosphates in the mice affects the differentiation of hematopoietic stem cells and leads to myeloid-biased differentiation. In addition, myeloid cells are responsible for innate immune activation. The increase in myeloid cells in the DKO embryos could be the reason for the immune activation in the fetal lungs. Therefore, immune activation in the fetal lungs is from the myeloid-biased differentiation of hematopoietic stem cells but not the DNA damage. However, it is not clear whether DNA damage in the DKO fetal lungs is caused by immune activation or loss of inositol pyrophosphates or their combined results. Immunofluorescent staining shows that only some immune cells have DNA damage and most of the cells with DNA damage in the fetal lungs belong to

endothelial cells. Therefore, it is necessary to validate the importance of inositol pyrophosphates in the endothelial cells and immune cells with specific Cre mice. This will shed light on the mechanism of lung defects in the DKO fetal lungs.

5.5 Chapter conclusions

There is strong immune activation and DNA damage in the DKO fetal lungs. This correlates with an increase in myeloid cells and reductions lymphocytes in the DKO fetal lungs compared to wild-type. Some immune cells and endothelial cells showed DNA damage accumulation.

Chapter 6 Characterization of the mice with tissue-specific IP6K1/2 deletion

6.1 Introduction

There are many apparent phenotypes in the DKO embryos which die of respiratory failure at birth, including in the immune activation in the fetal lungs, developmental defects of fetal lungs, and defective hematopoiesis. However, there is no solid evidence for the cause of DKO mice lethality. For example, as for strong immune activation in the fetal lungs and lung defects, it is not easy to determine the cause and consequence because lungs developmental defects can induce immune activation while immune response also has a negative effect on the development of lungs (Bry, Whitsett and Lappalainen, 2007; Blackwell *et al.*, 2011). In addition, the fetal livers in the DKO embryos are smaller. The DKO embryos are pale with anaemia. Hemoglobin switching and hematopoiesis are also affected in the DKO embryos. Ultimately depletion of IP6K1 and IP6K2 in the whole body induces defects in many tissues and these defects finally result in mice lethality. In order to look for the functions and mechanisms of inositol pyrophosphates and to validate the importance of inositol pyrophosphates in the fetal lungs and hematopoietic stem cells, IP6K1 and IP6K2 should be deleted in specific tissues with different Cre mice. Consequently, VAV Cre mice were used to delete floxed genes in the hematopoietic cells while NKX2.1 Cre mice were used to specifically express Cre recombinase in the developing lungs.

6.2 Chapter aims

In order to classify the functions of inositol pyrophosphate in murine embryonic development and to validate the importance of inositol pyrophosphates in the fetal lungs and hematopoietic cells, IP6K1 and IP6K2 were deleted in specific tissues or cell-types such as hematopoietic cells and pulmonary epithelial cells.

6.3 Results

6.3.1 Delete IP6K1 and IP6K2 in alveolar epithelial cells with NKX2.1 Cre enzyme

The DKO mice die at birth because of respiratory failure and further observations reveal developmental defects in the fetal lungs of DKO embryos. The markers of alveolar epithelial cells, such as alveolar Type 1 and Type 2 cells, are at a lower expression level in the fetal lungs of DKO embryos than in the fetal lungs of wild-type and heterozygous embryos. As loss of IP6K1 and IP6K2 in the whole body lead to severe developmental defects and immune response in the fetal lungs, we examined whether inositol pyrophosphates should play a vital role in the development of fetal lungs or in regulating immune activation in the fetal lungs.

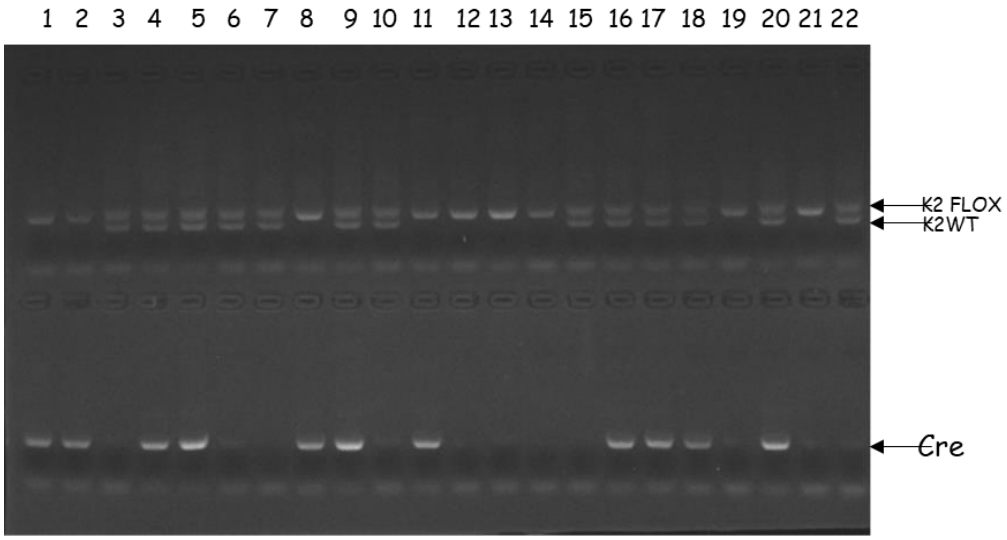

Figure 6-1 Mice of double deletions of IP6K1 and IP6K2 in the lung cells are viable. Genotyping for the offspring of IP6K1 $^{loxp/loxp}$ IP6K2 $^{flox/flox}$ and NKX2.1^{Cre} IP6K1 $^{loxp/WT}$ IP6K2 $^{flox/WT}$ mice. The mice of NO. 1,2,8 and 11 are the homozygous double conditional knockout mice, which have the genotypes of NKX2.1^{Cre} IP6K1 $^{loxp/loxp}$ IP6K2 $^{flox/flox}$. The genotypes are determined at P21.

Genotypes	**NKX2.1^{Cre} IP6K1$^{loxp/WT}$ IP6K2 $^{flox/WT}$**	**NKX2.1^{Cre} IP6K1$^{loxp/loxp}$ IP6K2 $^{flox/flox}$**	**IP6K1$^{loxp/WT}$ IP6K2 $^{flox/WT}$**	**IP6K1$^{loxp/loxp}$ IP6K2 $^{flox/flox}$**
Number	7	4	6	5

Table 6-1 Summary of genotypes of the offspring of IP6K1$^{loxp/loxp}$ IP6K2$^{flox/flox}$ and NKX2.1 ^{Cre} IP6K1$^{loxp/WT}$ IP6K2$^{flox/WT}$ mice. The mice of NKX2.1^{Cre} IP6K1$^{loxp/loxp}$ IP6K2$^{flox/flox}$ are viable and the ratio of these genotypes is not obviously less than the ratio of other genotypes.

We first tried to delete IP6K1 and IP6K2 in embryonic lung epithelium by using NKX2.1 Cre mice, which express Cre enzyme under the control of NKX 2.1 promoter. The NKX2.1 Cre enzyme is expressed explicitly in the epithelium but not in the whole lungs through LacZ staining (Li et al., 2011). It is therefore used to delete target genes in the brain progenitor cells, developing lungs and thyroid

(Xing et al., 2008). However, we found the mice of NKX2.1^{Cre} IP6K1$^{loxp/loxp}$ IP6K2$^{flox/flox}$ to be viable (Figure *6-1*). Even though the loss of inositol pyrophosphates in the whole body leads to severe developmental defects in the fetal lungs, which is the cause of respiratory failure after birth, depletion of inositol pyrophosphates specifically in the pulmonary epithelium with NKX2.1 Cre enzyme does not result in mice lethality (Figure 6-1, Table 6-1). Therefore, these results show that the loss of IP6K1 and IP6K2 in the lung epithelium is not the cause of lung defects in the DKO embryos.

There are distinct developmental phenotypes during the late stages of DKO embryos and the DKO mice are lethal after birth because of respiratory failure. Therefore, I also studied the phenotypes of NKX2.1 Cre cKO mice in embryos. The pregnant mouse was dissected at E18.5 for genotyping by PCR and Western blotting for IP6K1 and IP6K2. There are 9 embryos with 3 homozygous cKO embryos (Figure 6-2). Under the control of NKX2.1 Cre, the mice of NKX2.1^{Cre} IP6K1$^{loxp/loxp}$ IP6K2 $^{flox/flox}$ (NKX2.1 Cre cKO) showed a reduced expression of IP6K1 and IP6K2 but the reduction of IP6K1 and IP6K2 accumulation in the NKX2.1 Cre cKO fetal lungs was not very obvious (Figure 6-3). Li *et al*. found that NKX2.1 Cre enzyme expresses specifically in the epithelium but not in the whole lungs, through LacZ staining (M. Li et al., 2011). Therefore, to further confirm the efficiency of knockout by NKX2.1 Cre recombinase, alveolar epithelial cells should be enriched. In addition, it is known that the NKX2.1 Cre enzyme also

expresses in the thyroid, which can be harvested to confirm the working efficiency of NKX2.1 recombinase (Tiozzo et al., 2012).

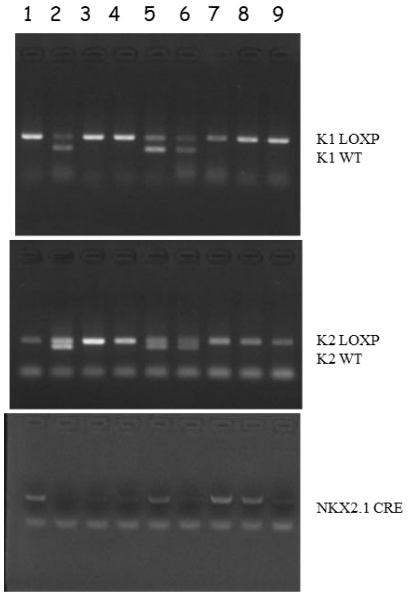

Figure 6-2 Genotyping for the embryos of the offspring of IP6K1 $^{loxp/loxp}$ IP6K2 $^{flox/flox}$ and NKX2.1 ^{Cre} IP6K1 $^{loxp/WT}$ IP6K2 $^{flox/WT}$ mice. Embryos of No. 1, 7 and 8 are NKX2.1^{Cre} IP6K1 $^{loxp/loxp}$ IP6K2 $^{flox/flox}$ embryos. Embryos of No. 3, 4 and 9 are used as the control group. These embryos are dissected at E18.5.

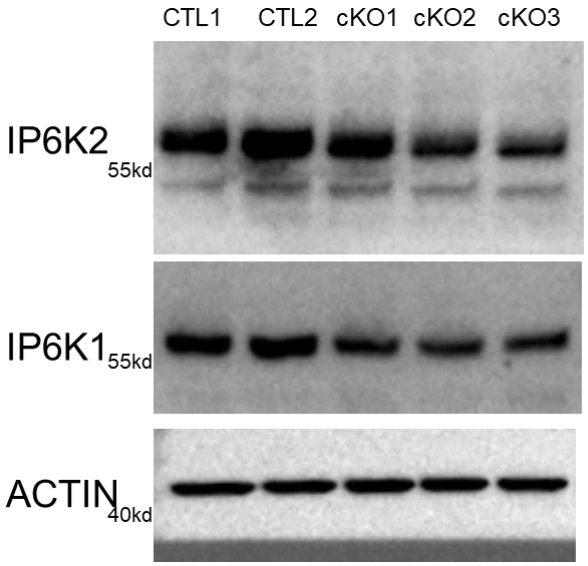

Figure 6-3 IP6K1 and IP6K2 are deleted in the fetal lungs under the control of NKX2.1 Cre recombinase. Protein accumulation was detected in fetal lungs at E18.5 by Western Blot normalized to Actin. n=2 CTL and 3 cKO.

In addition, the loss of inositol pyrophosphates in the lung epithelial cells does not

affect the differentiation and maturation of alveolar epithelial cells (Figure *6-4*) while the differentiation and maturation of pulmonary epithelial cells are affected in the DKO embryos. The marker genes of alveolar Type 1 and Type 2 cells have a lower expression in the fetal lungs upon double deletions of IP6K1 and IP6K2 in the whole body. However, the expression of these markers shows no difference in the fetal lungs between the NKX2.1^{Cre} IP6K1 $^{loxp/loxp}$ IP6K2 $^{flox/flox}$ group and the control group. Therefore, the developmental defects in the pulmonary epithelium of DKO embryos are indirect results of depletion of inositol pyrophosphates in mice.

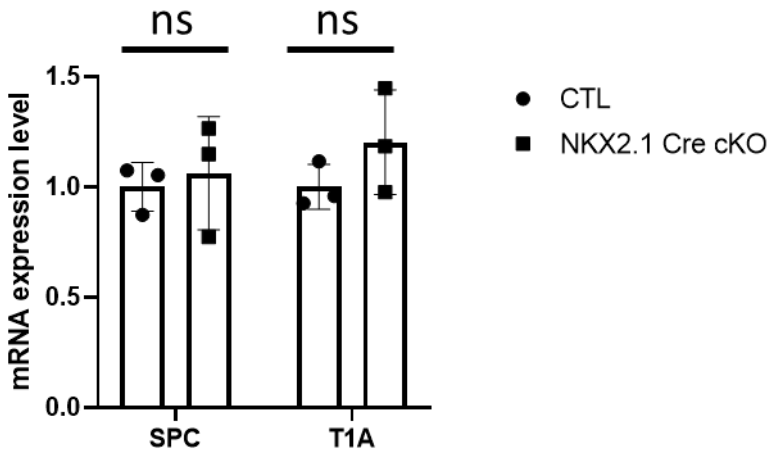

Figure 6-4 Loss of inositol pyrophosphates in the fetal lungs does not lead to affect the differentiation and maturation of alveolar epithelial cells. Gene expression of the SPC marker of alveolar type II cells and T1A marker of alveolar type I cells was assessed by qPCR in fetal lungs at E18.5. Data normalized to Actin represented as fold-change compared to CTL, shown as mean ± SD (n = 3 CTL and 3 NKX2.1 Cre cKO) (ns no significance, *p < 0.05, **p < 0.01, ***p < 0.001)

To further analyse the different phenotypes of conditional, NKX2.1Cre cKO of

IP6K1 and IP6K2, compared to DKO embryos, fetal lungs from the NKX2 Cre cKO embryos were analysed by qPCR for expression of alveolar marker genes. The results showed no difference in expression between NKX2 Cre cKO and control (Figure *6-4*), consistent with lack of defect in fetal lungs or respiratory failure in the conditional KO.

Since there was strong immune activation in the fetal lungs of DKO embryos, chapter 5, I measured the expression of immune cytokines in the fetal lungs upon loss of inositol pyrophosphates by NKX2.1 Cre recombinase. However, again, there was no significant difference in the expression of IL1B in the fetal lungs between the NKX2.1 Cre cKO embryos or the control embryos (Figure *6-5*). Therefore, it is clear that loss of IP6K1 and IP6K2 in the fetal lungs by NKX2.1 Cre enzyme does not affect the development of fetal lungs and induce an immune response, and the immune activation in the DKO fetal lungs most likely arises from myeloid-biased differentiation of hematopoietic stem cell. However, it remains not sure whether the immune activation is the cause or consequence of developmental defects in the DKO fetal lungs.

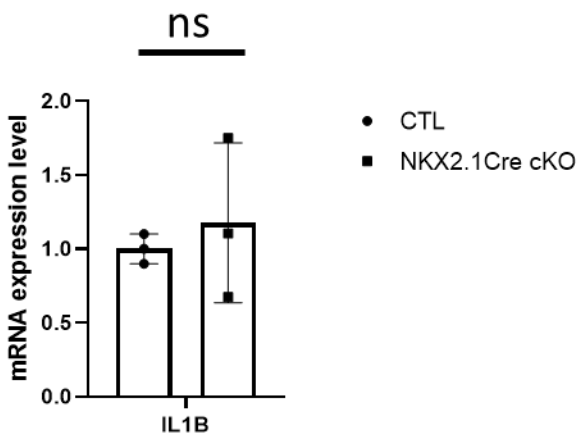

Figure 6-5 Loss of inositol pyrophosphates in the lungs cannot activate the expression of IL1B in the fetal lungs at E18.5. Gene expression of the IL1B was assessed by qPCR in fetal lungs at E18.5. Data normalized to Actin represented as fold-change compared to CTL, shown as mean ± SD (n = 3 CTL and 3 NKX2.1 Cre cKO) (ns no significance, *p < 0.05, **p < 0.01, ***p < 0.001)

In the fetal lungs of DKO embryos, except for immune activation, there is DNA damage upon loss of inositol pyrophosphates. I therefore detected the phosphorylation of H2AX, which is the marker of DNA damage, in the fetal lungs of NKX2.1^{Cre} cKO embryos. However, again, there was no more DNA damage accumulation in the fetal lungs of NKX2.1^{Cre} IP6K1 $^{loxp/loxp}$ IP6K2 $^{flox/flox}$ embryos (Figure *6-6*). Therefore, loss of inositol pyrophosphates in the lung epithelium does not lead to DNA damage, immaturity of alveolar epithelial cells, or immune response.

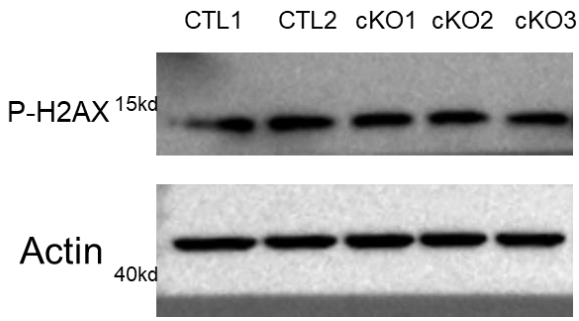

Figure 6-6 Loss of IP6K1 and IP6K2 in fetal lungs does not induce DNA damage in the fetal lungs. Protein extracts were analysed for phosphorylation of H2AX by Western Blotting of fetal lungs of E18.5, normalized to Actin. n=2 CTL and 3 cKO.

6.3.2 The mice losing IP6K1 and IP6K2 in the hematopoietic progenitor cells are viable

During the development of DKO embryos, from E15.5 to P0, the DKO embryos show anaemia, including smaller size, pale skin, delayed maturation of erythroid cells and defective differentiation of hematopoietic stem cells. These phenotypes indicate the importance of inositol pyrophosphates in hematopoiesis which is also crucial to embryonic development. In order to confirm the importance of inositol pyrophosphates in the differentiation and maturation of hematopoietic cells and to determine whether loss of IP6K1 and IP6K2 in the hematopoietic cells is responsible for the immune activation in the fetal lungs and respiratory failure at birth, VAV Cre enzyme was used to excise IP6K1 and IP6K2 in the hematopoietic cells.

VAV Cre mice are always used to delete target genes in the hematopoietic cells and their progenitors. The mice of VAV ^{Cre} IP6K1 $^{loxp/loxp}$ IP6K2 $^{flox/flox}$ were viable as shown by genotyping (Figure *6-7*, Table *6-2*).

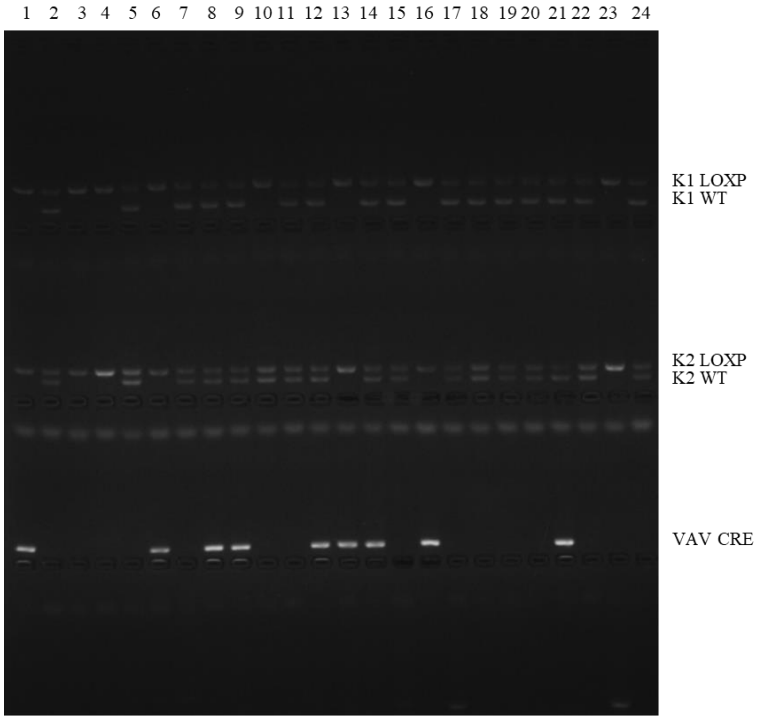

Figure 6-7 The mice of VAV ^{Cre} IP6K1 $^{loxp/loxp}$ IP6K2 $^{flox/flox}$ are viable. Genotyping for the offspring of VAV ^{Cre} IP6K1 $^{WT/loxp}$ IP6K2 $^{WT/flox}$ and IP6K1 $^{loxp/loxp}$ IP6K2 $^{flox/flox}$ mice. Mice of NO. 1, 6, 13, 16 are the mice of VAV ^{Cre} IP6K1 $^{loxp/loxp}$ IP6K2 $^{flox/flox}$. The genotypes are determined at P21.

Genotypes	**VAV ^{Cre} IP6K1 $^{WT/loxp}$ IP6K2 $^{WT/flox}$**	**VAV ^{Cre} IP6K1 $^{loxp/loxp}$ IP6K2 $^{flox/flox}$**	**IP6K1 $^{WT/loxp}$ IP6K2 $^{WT/flox}$**	**IP6K1 $^{loxp/loxp}$ IP6K2 $^{flox/flox}$**
Number	5	4	12	3

Table 6-2 **Summary of the offspring of VAV ^{Cre} IP6K1 $^{WT/loxp}$ IP6K2 $^{WT/flox}$ and IP6K1 $^{loxp/loxp}$ IP6K2 $^{flox/flox}$ mice.** The complete Loss of IP6K1 and IP6K2 in hematopoietic cells does not result in mice lethality. Mice of VAV Cre IP6K1 $^{loxp/loxp}$ IP6K2 $^{flox/flox}$ are viable.

The genotyping indicates that loss of IP_7 in the hematopoietic cells is also not entirely responsible for the respiratory failure at the birth of DKO embryos. This, perhaps, questions the efficiency of knockout by VAV Cre recombinase. Consequently, we measure the the expression of IP6K1 and IP6K2 in fetal livers by qPCR. IP6K1 and IP6K2 were markedly reduced, but not completely, in the fetal livers of VAV^{Cre} cKO

embryos (Figure *6-8*). The fetal liver is the primary site for the maturation and amplification of hematopoietic cells in the late stages of embryonic development, but nevertheless there is heterogeneity in this tissue that might explain cell-specific reductions in expression. We conclude that Cre recombinase in the VAV Cre IP6K1 $^{loxp/loxp}$ IP6K2 $^{flox/flox}$ embryos cannot delete all the IP6K1 and IP6K2 in the fetal liver.

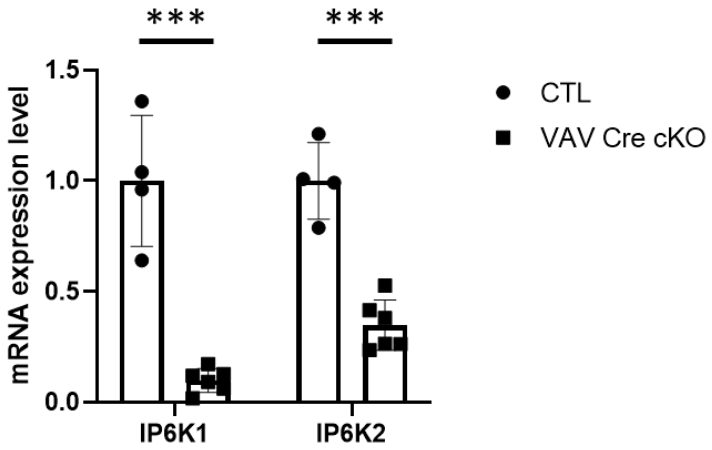

Figure 6-8 IP6K1 and IP6K2 are deleted in the hematopoietic stem cells of VAV Cre cKO embryos via VAV Cre recombinase. The expression of IP6K1 and IP6K2 was measured in fetal livers at E15.5 by qPCR. Data normalized to Actin represented as fold-change compared to CTL, shown as mean ± SD (n = 4 CTL and 6 VAV Cre cKO) (*p < 0.05, **p < 0.01, ***p < 0.001).

To further confirm the loss of IP6K1 and IP6K2 in the hematopoietic cells of VAV ^{Cre} cKO embryos, the accumulation of IP6K1 and IP6K2 proteins were additionally measured by Western Blot. According to the results, IP6K1 and IP6K2 are deleted effectively by the VAV Cre enzyme in the hematopoietic stem cells (Figure *6-9*).

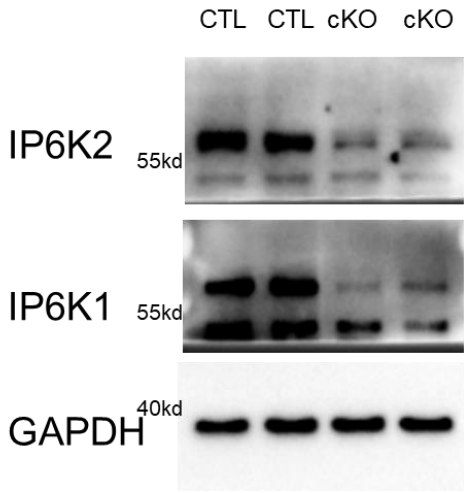

Figure 6-9 IP6K1 and IP6K2 are deleted in the hematopoietic stem cells of VAV Cre cKO embryos via the VAV Cre enzyme. The accumulation of IP6K1 and IP6K2 is measured with fetal livers at E15.5 by Western Blot normalized to GAPDH. n = 2 CTL and 2 VAV Cre cKO.

6.3.3 Loss of IP6K1 and IP6K2 in hematopoietic cells leads to immune activation in fetal lungs

Even though double deletions of IP6K1 and IP6K2 in the hematopoietic cells do not lead to mice lethality, it is necessary to check whether loss of inositol pyrophosphates affect the lungs development and immune activation. In the DKO embryos, phenotypes in the fetal lungs and fetal livers are very obvious. There is a smaller size of fetal livers and fetal lungs in the DKO embryos. The maturation and differentiation of alveolar epithelial cells in the fetal lungs and the hematopoietic stem cells in the fetal livers are affected by the ultimate depletion of IP6K1 and IP6K2 in the whole body. However, loss of IP6K1 and IP6K2 in the lung epithelium by NKX2.1 Cre enzyme does not lead to immune activation and immaturity of alveolar epithelial cells. I therefore checked whether loss of inositol pyrophosphates in hematopoietic cells is responsible for some phenotypes of DKO embryos, aided by the viability and lack of male sterility of the VAV Cre cKO mice

(Figure *6-10*).

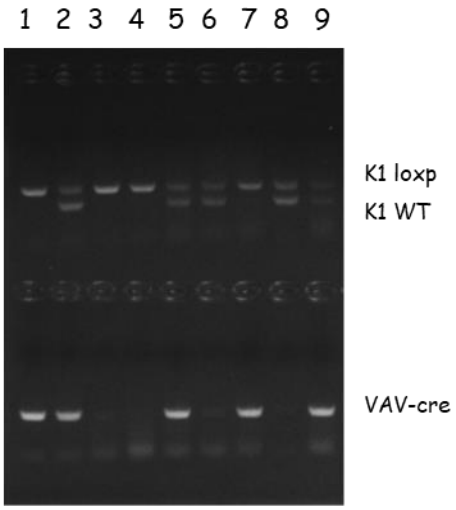

Figure 6-10 PCR screening of genotypes of VAV Cre mice. NO. 1 and 7 embryos are homozygous knockout embryos in hematopoietic cells. NO 3 and 4 embryos are used as the control group. Embryos were produced from IP6K1 $^{loxp/loxp}$ IP6K2 $^{flox/flox}$ and VAV ^{Cre} IP6K1 $^{loxp/wt}$ IP6K2 $^{flox/wt}$ and harvested at E15.5.

The results of the qPCR show that IL1B expression was elevated 3-fold in the fetal lungs of VAV Cre IP6K1 $^{loxp/loxp}$ IP6K2 $^{flox/flox}$ embryos when compared with control fetal lungs (Figure 6-11). The magnitude of this change of IL1B expression is comparable to that that in the DKO lungs at E15.5 (Figure 6-16), suggesting that loss of IP7 in the hematopoietic cells has effects on the immune activation in the fetal lungs.

Overexpression of IL1B leads to fetal airway defects (Hogmalm *et al.*, 2014, Stouch *et al.*, 2016) and our RNA sequencing reveals considerable upregulation of immune cytokines in the DKO fetal lungs. The immune activation in the DKO fetal lungs is considered to be the most critical factor affecting the maturation of pulmonary alveoli and finally results in lung defects and respiratory failure after

birth. However, robust immune response in the fetal lungs induced by deleting IP6K1 and IP6K2 in the hematopoietic cells with VAV Cre recombinase does not lead to developmental defects in fetal lungs and mice lethality at birth.

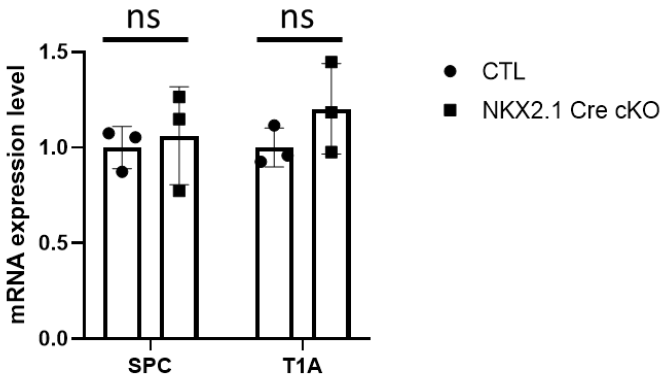

Figure 6-11 Loss of IP6K1 and IP6K2 in the hematopoietic cells does not affect the maturation of AT1 and AT2 cells. The expression of SPC and T1A was measured by qPCR in the fetal lungs at E15.5. Data normalized to Actin represented as fold-change compared to CTL, shown as mean ± SD (n = 3 CTL and 3 VAV Cre cKO).

Analysis of the marker genes of AT1 and AT2 cells show no difference between the VAV^{Cre} cKO and wild-type fetal lungs (Figure *6-11*). Therefore, loss of inositol pyrophosphates in the hematopoietic cells, which induces immune activation in the fetal lungs, does not affect the maturation and differentiation of alveolar epithelial cells, which could perhaps explain whether these mice are viable.

To further confirm that immune activation in the fetal lungs is caused by the loss of inositol pyrophosphates in the hematopoietic cells, I measured the expression of other immune cytokines in fetal lungs of VAV ^{Cre} cKO embryos. Therefore, several immune cytokines in the upregulated list of RNA sequencing of DKO fetal lungs

(Figure 5-2, 5-3), including GBP3, IFI44 and IRF7, were chosen for analysis by qPCR. These cytokines were highly increased in the fetal lungs of VAV Cre cKO embryos, with over 10 - and even 30- fold changes (Figure 6-12).

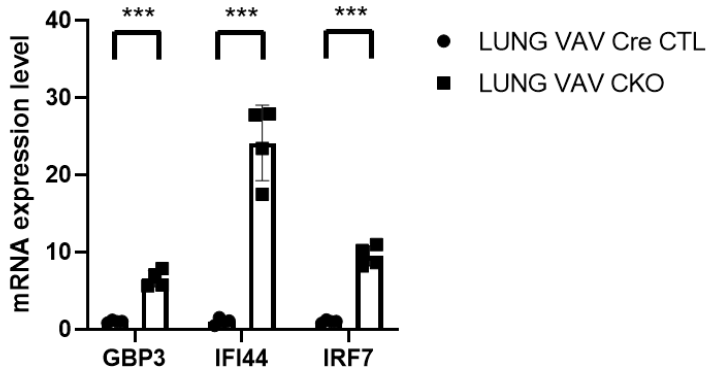

Figure 6-12 Immune activation in the fetal lungs of VAV Cre cKO embryos. The expression of immune cytokines (GBP3, IFI44 and IRF7) was measured with fetal lungs at E15.5 by qPCR. Data normalized to Actin represented as fold-change compared to CTL, shown as mean ± SD (n =4 CTL and 4 VAV Cre cKO) (*p < 0.05, **p < 0.01, ***p < 0.001).

Knockout of IP6K1 and IP6K2 in the hematopoietic cells induces immune activation of fetal lungs, which is consistent with the immune response in the DKO fetal lungs. In order to compare the expression level of these immune cytokines between DKO fetal lungs and VAV ^{Cre} cKO fetal lungs, I also measured the expression of these immune cytokines with qPCR even though RNA sequencing with DKO fetal lungs has already confirmed a high increase of these immune cytokines in the fetal lungs of DKO embryos. Increased expression of the immune cytokines was further confirmed in the fetal lungs of DKO embryos by qPCR. The fold changes of these immune cytokines, GBP3, IFI44 and IRF7, in the DKO fetal lungs are similar to the fold changes in the VAV Cre cKO fetal lungs (Figure 6-13).

Both fetal lungs of VAV Cre cKO and DKO embryos have about 10-fold increase in GBP3, 30-fold in IFI44 and about 15-fold in IRF7. Therefore, the loss of inositol pyrophosphates in the hematopoietic cells is fully responsible for the immune activation in the DKO fetal lungs. According to our previous hypothesis about the lethality of DKO mice, the immune activation in the fetal lungs affects the development of fetal lungs and finally results in respiratory failure at birth. However, the mice losing inositol pyrophosphates in the hematopoietic cells are viable. Therefore, immune activation in the fetal lungs is not entirely responsible for the developmental defects of fetal lungs in the DKO embryos.

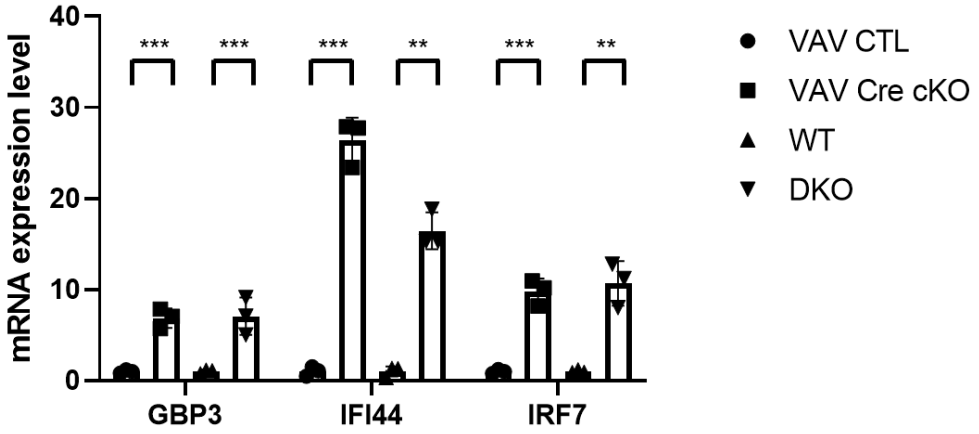

Figure 6-13 The expression of immune cytokines (including GBP3, IFI44 and IRF7) are upregulated in the fetal lungs of DKO and VAV Cre cKO. The expression of immune cytokines was measured by qPCR with fetal lungs at E15.5. Data normalized to Actin represented as fold-change compared to CTL, shown as mean ± SD (n =3 VAV CTL, 3 VAV Cre cKO, 3 WT and 3 DKO) (*p < 0.05, **p < 0.01, ***p < 0.001).

As the immune response in the fetal lungs is induced by the loss of inositol pyrophosphates in the hematopoietic cells, I addressed whether there is an immune response in the fetal livers, the main site for maturation and expansion of hematopoietic stem cells at late gestational stages. Interestingly, the immune cytokines were also highly expressed in the VAV ^{Cre} cKO fetal livers.

In the VAV ^{Cre} cKO embryos, we expect IP6K1 and IP6K2 to be explicitly deleted in the hematopoietic cells. Therefore, the hematopoietic cells should be the original site of immune activation in the VAV ^{Cre} cKO embryos while the immune response in the fetal lungs is translocated from the fetal livers. To further confirm this hypothesis, other immune cytokines are compared in the fetal lungs and in the fetal livers of VAV Cre cKO embryos. Interestingly, the increase of immune cytokines observed in fetal livers is again higher than in the fetal lungs, including GBP3, IFI44 and IRF7 (Figure 6-15). According to these data in the VAV Cre cKO embryos, we can speculate that provide compelling evidence that fetal livers are the original site of immune activation, which is then translocated to fetal lungs. The immune cytokines were also more strongly elevated in the fetal livers when compared to the fetal lungs of DKO embryos (Figure *6-16*). As an important cytokine known to affect the lung development, the 9-fold elevation of IL1B in fetal liver and 3-fold elevation in fetal lung is consistent, as is the 7-fold increase in fetal livers (compared to 3-fold increase in fetal lungs) of the VAV Cre cKO embryos (Figure *6-14*).

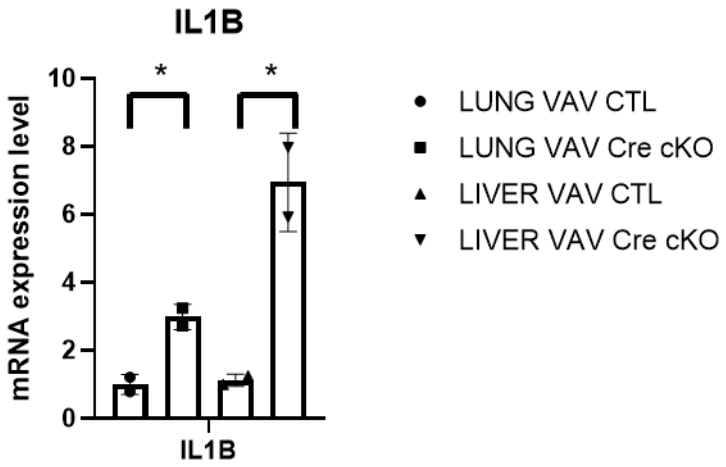

Figure 6-14 The expression of immune cytokines is highly expressed in the fetal lungs and fetal livers in VAV Cre cKO recombinase. The expression of immune cytokines was measured by qPCR at E15.5. Data normalized to Actin represented as fold-change compared to CTL, shown as mean ± SD (n =2 for each group) (*p < 0.05, **p < 0.01, ***p < 0.001).

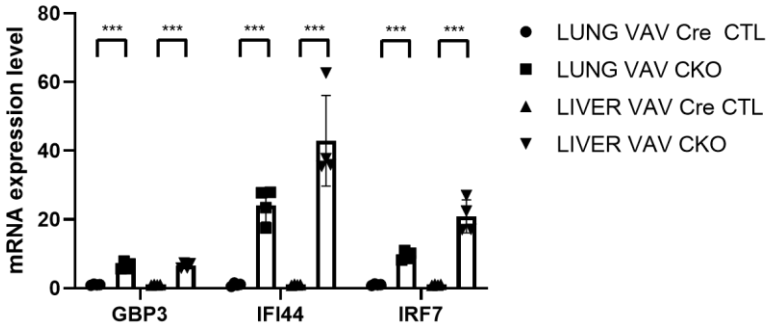

Figure 6-15 Immune cytokines increase in the fetal lungs and fetal livers of VAV Cre cKO embryos. Cytokines (GBP3, IFI44, IRF3) were measured by qPCR. Data normalized to Actin represented as fold-change compared to CTL, shown as mean ± SD (n = 3 for each group) (*p < 0.05, **p < 0.01, ***p < 0.001)

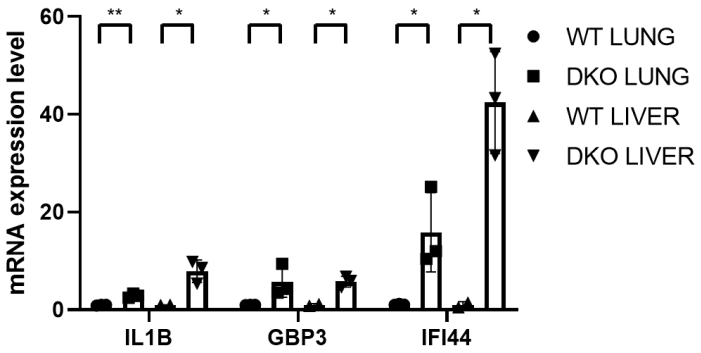

Figure 6-16 Loss of IP6K1 and IP6K2 in the whole body induces immune activation in the fetal lungs and in the fetal livers. The expression of immune cytokines was measured with fetal lungs and fetal livers from E15.5 embryos by qPCR. Data normalized to Actin represented as fold-change compared to WT, shown as mean ± SD (n = 3 for each group) (*p < 0.05, **p < 0.01, ***p < 0.001).

Through comparing the immune activation in the DKO embryos and VAV Cre cKO embryos, it can be concluded that the immune response is induced by the loss of inositol pyrophosphates in the hematopoietic cells. The fetal livers are the original sites of immune cytokines. However, the VAV Cre cKO mice are viable even though their fetal lungs also have increased immune cytokines.

The expression of markers genes of alveolar type 1 and type 2 cells showed no differences between the VAV ^{Cre} cKO fetal lungs and the control fetal lungs (Figure 6-11). This indicates that the immune activation in the fetal lungs caused by loss of inositol pyrophosphates in the hematopoietic cells does not affect the maturation and differentiation of pulmonary epithelial cells. To test this further, phosphorylation of H2AX was assessed in lungs of the conditional VAV ^{Cre} cKO by Western Blotting.

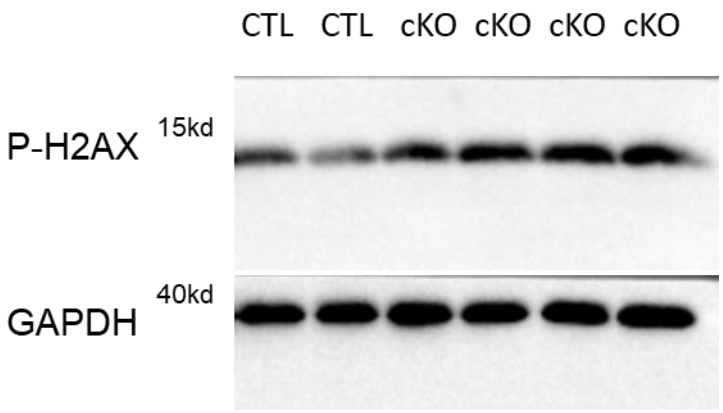

Figure 6-17 Loss of IP6K1 and IP6K2 in the hematopoietic cells by VAV Cre enzyme also induce DNA damage in the fetal lungs. Phosphorylation of H2AX indicates DNA damage. This is detected by Western Blot and normalized to GAPDH with E18.5 fetal lungs. n=2 CTL and 4 cKO.

While the data of DKO embryos show that loss of IP6K1 and IP6K2 in the whole body leads to intense DNA damage in the fetal lungs (chapter 5), loss of IP6K1 and IP6K2 in the hematopoietic cells by the VAV Cre enzyme also enhances DNA damage in the fetal lungs. There is more DNA damage in the VAV Cre cKO fetal lungs than in control fetal lungs (Figure *6-17*). However, the intensity of DNA damage in the VAV Cre cKO fetal lungs is weaker than in the DKO fetal lungs (Figure *5-8*). This supports the hypothesis that DNA damage in the fetal lungs is induced by immune activation, while the lungs cells in the DKO embryos have a low capacity for DNA damage repair. One can speculate that even though double deletions of IP6K1 and IP6K2 in the hematopoietic cells induces immune activation and DNA damage in the fetal lungs, this immune response does not affect the differentiation and maturation of alveolar epithelial cells in the fetal lungs because the DNA damage repair is not compromised in all the lung cells of VAV^{Cre} cKO embryos.

The immune activation in the fetal lungs is caused by defected differentiation of hematopoietic stem cells upon loss of inositol pyrophosphates. However, the immune activation in the fetal lungs does not affect the development of fetal lungs. In addition, loss of inositol pyrophosphates in the lung epithelium by NKX2.1 Cre recombinase has no effect on the development of fetal lungs. We therefore propose that the lung defects in the DKO embryos are induced by other cell types of lungs but not lung epithelial cells, or the combined results of the loss of inositol pyrophosphates in the fetal lungs and immune activation. In fact, immune activation is a kind of stress of DNA damage while loss of inositol pyrophosphates affects DNA damage repair (Rathan S. Jadav *et al.*, 2013; Kay *et al.*, 2019). To validate this hypothesis, the VAV Cre cKO mice were crossed with NKX2.1 Cre cKO mice in order to deplete inositol pyrophosphates in both the hematopoietic system (via VAV Cre) and lung epithelium (via NKX2.1 Cre). The mice of VAV ^{Cre} -NKX ^{Cre} cKO are viable (Figure *6-18*). This shows that inositol pyrophosphates do not play a vital role in the lung epithelium. The delayed maturation of AT1 and AT2 cells is caused indirectly by functional defects of other cells in the lungs upon loss of inositol pyrophosphates. Therefore, it remains essential to look for the cells with DNA damage in the DKO fetal lungs.

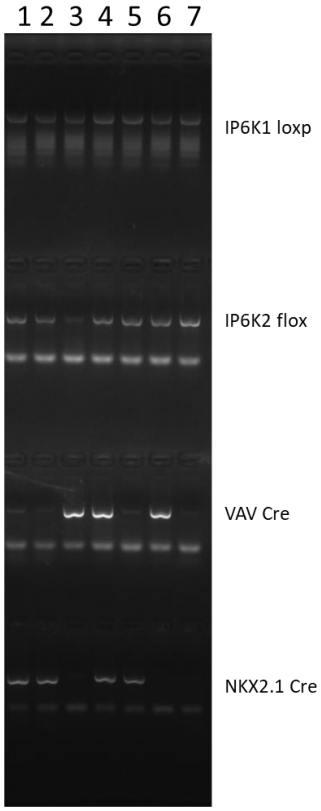

Figure 6-18 The mice of VAV Cre -NKX Cre cKO are viable. The genotypes of the offspring of NKX2.1 Cre cKO and VAV Cre cKO mice were determined at P21. NO.4 is a mouse with NKX2.1 Cre and VAV Cre enzyme.

6.3.4 Loss of IP6K1 and IP6K2 in the hematopoietic cells affects the differentiation and maturation of erythroid cells

In chapter 3, it was shown that hemoglobin expression in the DKO embryos is affected upon loss of inositol pyrophosphates in the whole body. Hbb-y globin takes the place of Hbb-bh1 globin during the maturation of erythroid lineage cells (Sankaran et al., 2010b). In the DKO embryos, more Hbb-y globin and less Hbb-bh1 globin at E15.5 indicates that hemoglobin switching is affected. I therefore detected the expression of hemoglobin in the VAV ^{Cre} cKO fetal livers through qPCR in order to determine whether the defects of hemoglobin switching in the DKO embryos are initially caused by loss of IP_7 in the hematopoietic cells. The

expression of HBB-y, Zeta globin, HBB-bh1 and HBB-b1/b2 hemoglobins was lower in the VAV ^{Cre} cKO embryos than in the controls (Figure *6-19*). Therefore, no matter whether depletion of inositol pyrophosphates is achieved globally or specifically in hematopoietic cells, the expression of hemoglobin is affected. This reveals the significance of inositol pyrophosphates in the differentiation of hematopoietic stem cells and erythropoiesis.

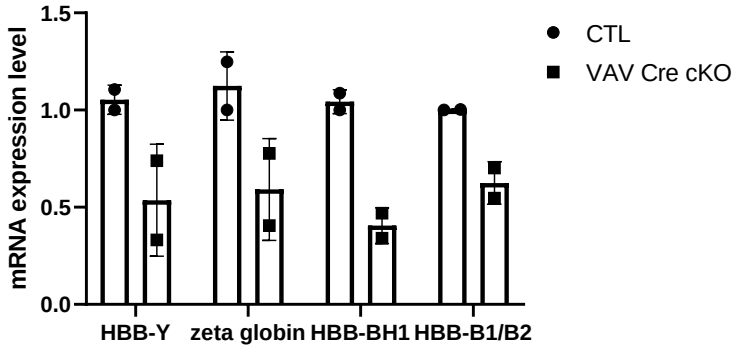

Figure 6-19 There is lower hemoglobin expression in the fetal livers upon loss of IP6K1 and IP6K2 in the hematopoietic cells. The expression of hemoglobin was measured by qPCR with fetal livers at E13.5. (n=2 CTL and 2 VAV Cre cKO).

Not only does the loss of IP6K1 and IP6K2 in the whole body affect switching of hemoglobin, it also affects the maturation and differentiation of erythroid progenitor cells. To test this further the maturation and differentiation of erythroid progenitors was tested in the VAV Cre cKO embryos. Here, antibodies to Ter119 and CD71 were used to track the maturation of erythroid progenitor cells, because, during the maturation of erythroid progenitor cells, the expression of Ter119 increases (Jayapal et al., 2015) while the expression of CD71 increases and then

decreases. Fetal livers of VAV Cre cKO embryos and the control group at E15.5 were stained with Ter119 and CD71 antibodies and are analysed by flow cytometry. According to the signals of Ter119 and CD71, erythroid progenitor cells can be classified into 5 groups, from S0 to S4, indicating the increasing maturity of erythroid progenitor cells.

However, the signal of Ter119 and CD71 did not show the functions of inositol pyrophosphates in the maturation of erythroid progenitors in these sub-groups. No noticeable trend was observed in the data (Figure *6-20*). Because it has been reported that development of erythroid cells is accompanied by an increase in the expression of Ter119 (Jayapal et al., 2015), I also measured the expression of Ter119 alone, with reference to DAPI. According to the signal of Ter119, there is delayed maturation in the erythropoiesis, indicated by reduction in expression of Ter119, upon loss of inositol pyrophosphates in the hematopoietic cells (Figure *6-21*).

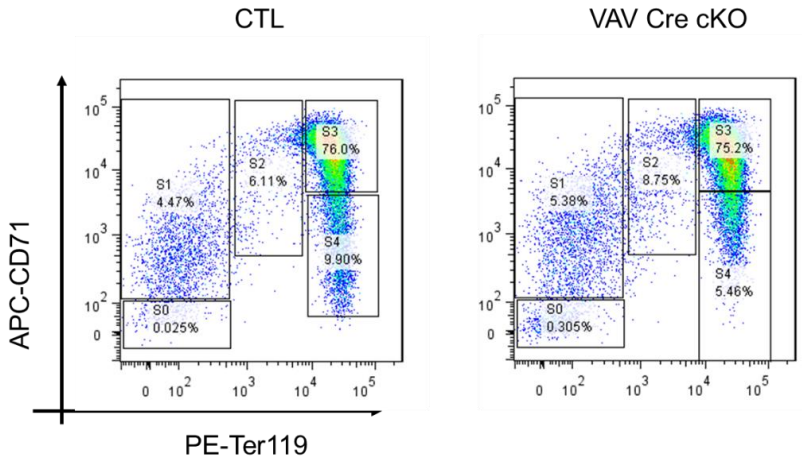

Figure 6-20 Maturation of erythroid progenitors upon loss of inositol pyrophosphates in the hematopoietic cells by VAV Cre recombinase. Cell populations were assessed by FACs with antibody to Ter119 and CD71. n=3 CTL and 3 VAV Cre cKO.

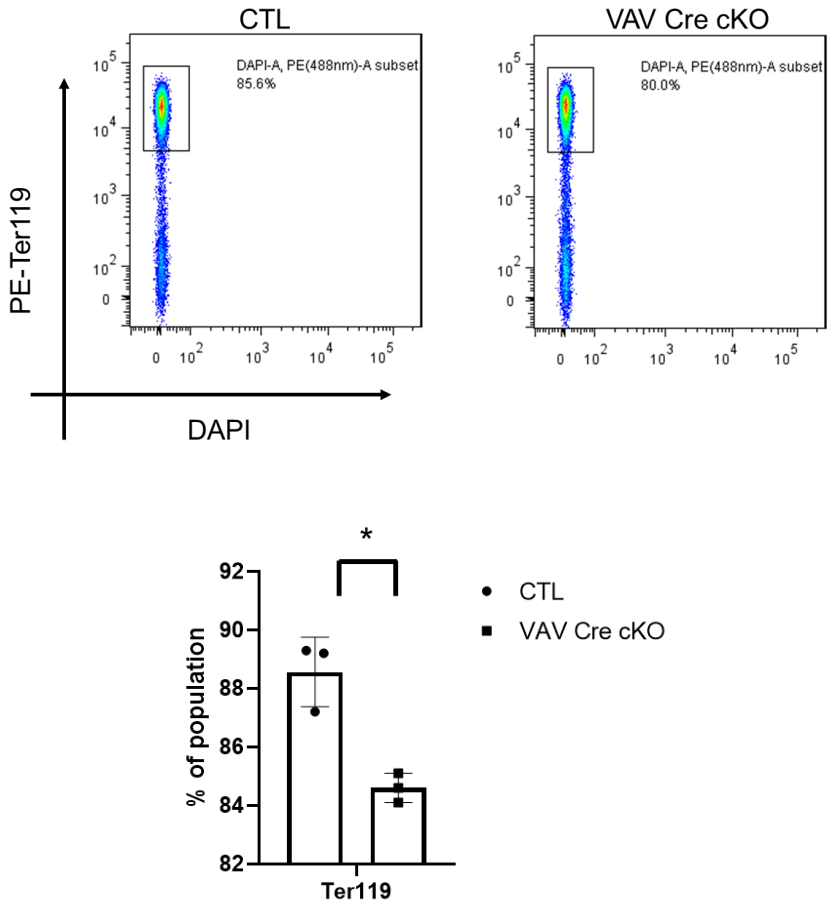

Figure 6-21 The expression of Ter119 reveals delayed differentiation and maturation of erythroid progenitor cells in VAV Cre cKO embryos. Cell populations were assessed by FACS analysis with antibody to Ter119 and DAPI staining (upper panel) and changes in population in VAV Cre cKO relative to control are shown (lower panel). Data represented as fold-change compared to CTL, shown as mean ± SD (n = 3 CTL and 3 VAV Cre cKO) (*p < 0.05, **p < 0.01, ***p < 0.001).

To further reveal the functions of inositol pyrophosphates in the differentiation of hematopoietic stem cells, the peripheral blood of E18.5 embryos were analysed with a hematology analyser. Interestingly, there were more monocytes and fewer lymphocytes in the VAV Cre cKO mice (Figure *6-22*). This, again, is consistent with the similar blood components of DKO embryos, which shows myeloid-biased

differentiation (Figure *3-17*).

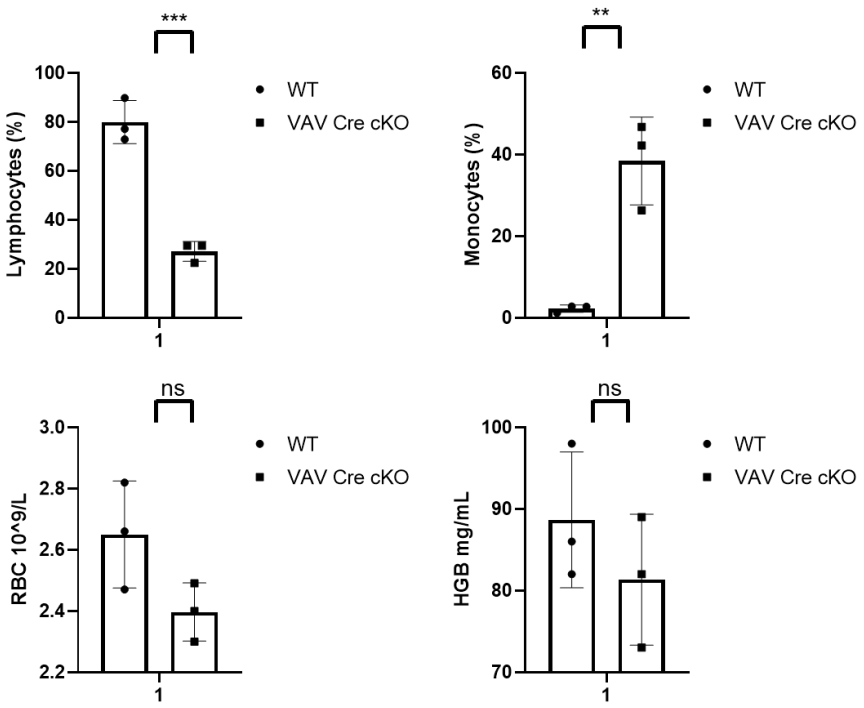

Figure 6-22 Loss of inositol pyrophosphates in the hematopoietic cells affects the blood components. Whole blood of E18.5 embryos was analysed with a blood analyser. Significant differences in lymphocyte and monocyte counts are indicated with asterisks. (n=3 WT and 3 VAV Cre cKO) (*p < 0.05, **p < 0.01, ***p < 0.001).

However, the red blood cell count and hemoglobin content showed no difference in the VAV Cre cKO mice (Figure *6-21*). This result is inconsistent with less hemoglobin expression and defective erythropoiesis observed (*Figure 6-19*).

In brief summary, our data have revealed that there is an activated immune response in the fetal lungs and fetal livers of VAV Cre cKO embryos. Loss of inositol pyrophosphates in the hematopoietic also affected the maturation of erythrocytes and blood components in the mature mice. This evidence indicates the vital role of inositol pyrophosphates in the differentiation of hematopoietic stem cells.

6.4 Discussion

The purpose of experiments described in this chapter is to validate the functions of inositol pyrophosphates in the development of fetal lungs and the hematopoietic system. Although the lung defects are the final results of DKO mice lethality at birth, conditional KO of inositol pyrophosphate synthesis in the developing lungs with NKX2.1 Cre enzymes yields mice that are viable. NKX2.1 Cre cKO mice do not show any effects on the development of lungs. Therefore, the developmental defects in the DKO fetal lungs could be an indirect consequence. However, DNA damage or apoptosis was only observed in a proportion of cell types in the DKO fetal lungs. Again, more detailed analysis of lung cell types will shed light on the functions of inositol pyrophosphates in the development of fetal lungs.

Except for apparent phenotypes in the DKO fetal lungs, the fetal livers also show apparent phenotypes in the DKO embryos. Fetal livers, the essential sites for the amplification and maturation of hematopoietic stem cells, are smaller in the DKO embryos. In addition, immune cells responsible for the immune response in the fetal lungs and fetal livers are mainly from the differentiation of hematopoietic stem cells in fetal livers. Therefore, VAV Cre recombinase was used to validate the functions of inositol pyrophosphates in the hematopoietic system. Upon the loss of inositol pyrophosphates in the hematopoietic cells, VAV Cre cKO mice were viable. There was also no noticeable difference in the size of the embryos or fetal livers.

However, the embryos of VAV Cre cKO show immune activation in the fetal livers and fetal lungs at E15.5. We previously proposed that the developmental defects of DKO fetal lungs are because of immune activation. However, immune activation caused by the loss of inositol pyrophosphates in the hematopoietic system does not lead to developmental defects in the fetal lungs.

Therefore, it is confirmed that inositol pyrophosphates play an essential role in the differentiation of hematopoietic stem cells. However, immune response in the fetal livers and fetal lungs is not entirely responsible for DKO mice lethality at birth. The developmental defects of fetal lungs could be a combined result, such as defects in the lungs and hematopoietic system simultaneously. Immune activation caused by loss of inositol pyrophosphates in the hematopoietic systems is a challenge for the cells in the fetal lungs. In addition, the loss of of inositol pyrophosphates caused cellular defects in t DNA damage repair (Jadav et al., 2013a). Therefore, it seems that the cells that are sensitive to immune cytokines and which have a lower capacity of DNA damage repair in the DKO fetal lungs have functional defects and finally lead to delayed maturation of pulmonary alveoli and lung defects. However, inositol pyrophosphates are not essential to the lung epithelium because the loss of inositol pyrophosphates in the lung epithelium and hematopoietic system simultaneously does not lead to mice lethality at birth. To reveal the cause of lung defect upon loss of inositol pyrophosphates in the whole body, it is necessary, again, to identify the cell population with DNA damage in the

DKO fetal lungs.

6.5 Chapter conclusion

Both NKX2.1 Cre cKO and VAV Cre cKO mice are viable. Loss of inositol pyrophosphate in fetal lungs does not affect the maturation of pulmonary epithelial cells or leads to immune activation in the fetal lungs while there is a robust immune response and developmental defects in the fetal lungs of DKO embryos. Therefore, the developmental defects in the fetal lungs of DKO embryos are not from the loss of inositol pyrophosphates in the lung epithelium. Loss of inositol pyrophosphates in the hematopoietic cells affects the differentiation and maturation of hematopoietic stem cells and is the cause of immune activation in the fetal livers and fetal lungs. However, immune activation in the fetal lungs caused by the defects in the hematopoietic system does not induce any developmental defects in fetal lungs, including the maturation of pulmonary epithelial cells. In conclusion, inositol pyrophosphates are required for hematopoietic development.

Chapter 7 Final discussion and thesis conclusions

7.1 Final discussion

In this study, I studied the functions and mechanisms of inositol pyrophosphate in mammalian development through deleting IP6K1 and IP6K2 in mice. As IP6K1 and IP6K2 are on the same chromosome, previous studies have never deleted these two genes at the same time in these mice though these two genes have been deleted in HCT116 cell lines with CRISPR-Cas9 technology with complete depletion of IP_7 (M. S. Wilson et al., 2019). On the basis of IP6K1 conditional knockout mice, I developed double conditional knockout mice of IP6K1 and IP6K2. IP_7 is wholly lost in the DKO MEF cells. Because IP6K3 is expressed in limited tissues, such as the brain and tissues, double deletions of IP6K1 and IP6K2 should lead to complete loss of IP_7 in many tissues. Therefore, the double deletions mice of IP6K1 and IP6K2 are good models to study the functions and mechanisms of IP_7 in the cellular pathways and mammalian development.

Double deletions of IP6K1 and IP6K2 lead to mice die at birth because of respiratory failure. This is because of developmental defects in the DKO fetal lungs. After delivery from the pregnant mice, the newborn DKO mice cannot breathe properly with their compacted and immature lungs. H&E staining shows that the fetal lungs of DKO embryos lack of pulmonary alveoli which are important sites for air exchange. Further research shows that immune response is activated in the DKO fetal lungs, especially the accumulation of macrophages and neutrophils in

the DKO fetal lungs. Previous studies have also revealed that activation of the immune response affects the morphogenesis of distal airways in fetal lungs (Blackwell *et al.*, 2011). The overexpression of immune cytokines like IL-1beta is also responsible for the development and maturation of distal airways (Hogmalm *et al.*, 2013). Upon double deletions of IP6K1 and IP6K2, RNA sequencing reveals that assorted immune cytokines are highly expressed in the fetal lungs. The detection of the activation of NF-kappa B and IRF3 pathways as critical pathways of the innate immune response is an important observation, here. The results of Western Blot showed that activation of NF-kappa B and IRF3 pathways in the DKO fetal lungs, in which the phosphorylation of NF-kappa B and IRF3 are accumulated in the DKO fetal lungs.

However, immune activation in the fetal lungs cannot fully be responsible for lung defects because the loss of inositol pyrophosphates in hematopoietic cells induces an intense immune response in the fetal lungs but does not lead to any lung defects. In fact, inositol pyrophosphates are essential to the differentiation of hematopoietic stem cells. In the DKO embryos, the hematopoietic stem cells have a myeloid-biased differentiation with more myeloid cells but fewer lymphocytes. More myeloid cells in the DKO embryos induce an innate immune response. In addition, there are also more myeloid cells but fewer lymphocytes in the DKO fetal lungs. This can explain immune activation in the DKO fetal lungs.

Loss of inositol pyrophosphates in the hematopoietic cells by VAV Cre

recombinase induces an immune response in the fetal livers and the fetal lungs. In addition, there is more DNA damage in the VAV Cre cKO fetal lungs but the DNA damage in the VAV Cre cKO fetal lungs is weaker than in the DKO fetal lungs. This reveals that immune activation in the fetal lungs is from the hematopoietic system, while DNA damage in the fetal lungs is a combined result of immune activation and DNA damage repair defects in the fetal lungs.

Even though the DKO fetal lungs and the VAV Cre cKO face the same challenges from immune cytokines, the lung cells in the VAV Cre cKO embryos do not lack inositol pyrophosphates while the lung cells in the DKO embryos lack inositol pyrophosphates which are essential to DNA damage repair (Jadav et al., 2013a). Except for H2AX, other substrates of ATM, including KAP1, CHK2 and P53, are highly phosphorylated in the DKO fetal lungs. This means that intense DNA damage in the fetal lungs. Previous research has found that deletion of IP6K1 affects the DNA damage repair upon DNA damage inducers. The DNA damage response defects can be rescued by overexpressing IP6K1 but not kinase-dead IP6K1 (Jadav et al., 2013a). This is an example that dosage-dependent decrease of IP_7 reduce the effectiveness of DNA damage repair (Jadav et al., 2013b). In this case, complete depletion of IP_7 results in DNA damage accumulation without any artificial DNA damage inducers because immune cytokines are DNA damage stress for fetal lungs.

Lung cells in the VAV Cre cKO embryos still have the capacity of DNA damage

repair, while lung cells in the DKO embryos have defects in DNA damage repair because of lacking inositol pyrophosphates. Therefore, there is intense DNA damage in the DKO fetal lungs while the fetal lungs of VAV Cre cKO embryos also have DNA damage accumulation. In fact, not all the lung cells in the DKO embryos have DNA damage accumulation. In fact, most of pulmonary cells with DNA damage in the DKO fetal lungs are immune cells and endothelial cells. This will provide crucial clues for us about the cause of lung defects because the cells with DNA damage in the DKO fetal lungs should be more dependent on inositol pyrophosphates in DNA damage repair.

Loss of inositol pyrophosphates in the developing lung with NKX2.1 Cre enzyme does not lead to any defects in the fetal lungs, including the maturation of pulmonary alveoli or DNA damage. This indicates that loss of inositol pyrophosphates in the lung epithelium is not the primary cause of DNA damage in the fetal lungs. In addition, the mice of $NKX2.1^{Cre}$ - VAV^{Cre} cKO are viable. This means loss of inositol pyrophosphates in the hematopoietic system and lung epithelium does not lead to mice lethality. Therefore, to elucidate the cause of lung defects of DKO embryos, it is necessary to test the functions of inositol pyrophosphates in other cells of lungs, especially the endothelial cells.

According to the evidence in the DKO and VAV Cre cKO embryos, it is confirmed that inositol pyrophosphates play a vital role in the differentiation of hematopoietic stem cells. However, we have no idea about how the loss of inositol pyrophosphates

leads to functional defects in the hematopoietic stem cells. There is also more DNA damage in the fetal livers of VAV Cre cKO embryos. However, the DNA damage in the VAV Cre cKO fetal livers is not as intense as in the DKO fetal livers. Our data indicate DNA damage in the fetal lungs is a combined result of DNA damage stress and defects in DNA damage repair. DNA damage is not the cause and may be a result of immune activation in the fetal lungs. In the hematopoietic stem cells, the myeloid-biased differentiation of hematopoietic stem cells is the cause of innate immune activation. However, it is not clear what the cause of the myeloid-biased differentiation in the hematopoietic stem cells. DNA damage in the hematopoietic stem cells will lead to myeloid bias differentiation (Elias et al., 2017; Flach et al., 2014; Pilzecker et al., 2017; Weiss & Ito, 2015). Therefore, it remains of project to study the functions and mechanisms of inositol pyrophosphates in hematopoietic stem cells.

In the DKO fetal lungs, DNA damage is obvious at E18.5 while at E15.5, there is no apparent DNA damage accumulation in the DKO fetal lungs. Previous study reveals the important role of IP_7 in DNA damage repair upon DNA damage inducers(Jadav et al., 2013b). In the DKO fetal lungs, severe DNA damage accumulation in the E18.5 but not E15.5 fetal lungs. Therefore, DNA damage in the DKO fetal lungs is an accumulating result. In fact, the pulmonary defects are apparent at E18.5 but not at E15.5. This indicates DNA damage is an important factor of defective development of mice lungs. DNA damage accumulation in the

VAV Cre cKO fetal lungs reveals that immune activation is an important factor of DNA damage.

According to the above results, the lung defects in the DKO embryos should be a combine result of dysfunctions in several types of lung cells. Loss of inositol pyrophosphates should affect the DNA damage repair in all cell types. However, without DNA damage inducers, the DNA damage should be accumulated in the sensitive cells firstly, such as immune cells and endothelial cells. Here, I propose a possible mechanism of developmental defects in the DKO fetal lungs. Loss of inositol pyrophosphates in the hematopoietic cells leads to immune activation, which is the inducer of DNA damage. Based on our data, endothelial cells are so sensitive to immune activation and more DNA damage accumulating in the endothelial cells. The dysfunction of endothelial cells will result delayed maturation of endothelial cells and defective development of pulmonary alveoli. The lung defect is the cause of respiratory failure at birth (Figure *7-1*).

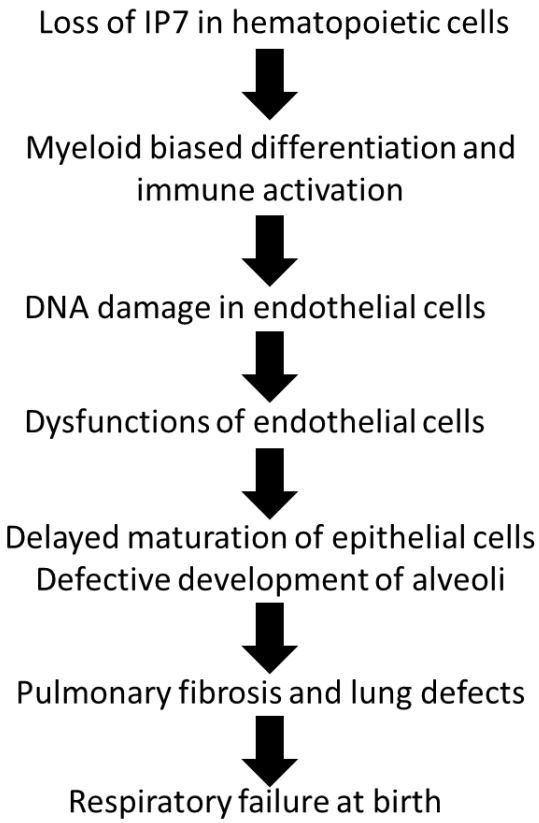

Figure 7-1 The possible mechanism of respiratory failure at birth in DKO mice. Loss of inositol pyrophosphates leads to immune activation, which is the inducer of DNA damage. Endothelial cells are so sensitive to immune activation and more DNA damage accumulating in the endothelial cells. The dysfunction of endothelial cells will result delayed maturation of endothelial cells and defective development of pulmonary alveoli. The lung defect is the cause of respiratory failure at birth.

IP_7 is an inhibitor of AKT. IP_7 decrease leads to activation of AKT (Chakraborty et al., 2010). Activation of AKT will activate its downstream pathway, including the NF-kappa B pathway (Kane *et al.*, 1999; Romashkova and Makarov, 1999; Sizemore, Leung and Stark, 1999). Therefore, it is reasonable that loss of IP_7 activates the phosphorylation of AKT which then activate the NF-kappa pathway. In addition, the AKT pathway is also crucial to hematopoiesis while dysregulation of AKT affects the functions of hematopoietic stem cells (Juntilla et al., 2010; Wu et al., 2021).

7.2 Future work

In this project, mice of double deletions of IP6K1 and IP6K2 are lethal because of respiratory failure at birth. Lung defects in the DKO embryos, such as immune activation, DNA damage, delayed maturation of pulmonary epithelial cells, are caused by loss of inositol pyrophosphates in the whole body. However, it is still unknown the mechanisms of lung defects upon loss of inositol pyrophosphates. Therefore, an important avenue of future work is to reveal the cause and mechanism of lung defects in the DKO embryos. To find out the cells affected in the fetal lungs upon loss of inositol pyrophosphates in the whole body is the priority. This will shed light on the functions of inositol pyrophosphates in the development of the lungs. There are four major cell types in the lungs, including endothelial cells, epithelial cells, immune cells and mesenchymal cells. Up to now, the loss of inositol pyrophosphates in the lung epithelial cells and immune cells does not lead to lung defects. In the future, it is also necessary to check the functions of inositol pyrophosphates in the lung mesenchymal and endothelial cells with specific Cre mice, such as TBX4 Cre and Tie2 Cre mice. It is also promising to validate the combined results of deleting IP6K1 and IP6K2 in different pulmonary cells at the same time.

In addition, loss of inositol pyrophosphates also leads to myeloid-biased differentiation of hematopoietic stem cells. To elucidate how the loss of inositol pyrophosphates in the hematopoietic stem cells affect the functions and

differentiation of hematopoietic stem cells will help us understand the mechanism of inositol pyrophosphates in the cellular pathways. It is also essential to track the differentiation of hematopoietic stem cells upon loss of inositol pyrophosphates in the hematopoietic system by the VAV Cre enzyme.

Our working hypothesis of the lethality of DKO mice encapsulates the combined results of immune activation and DNA damage response defects in the fetal lungs. STING is an essential mediator of the innate immune response that can be activated by DNA damage via either the cGAS or ATM pathway (Flannery et al., 2018). Inhibition of STING in the DKO embryos could therefore reduce immune activation in the DKO embryos. It will be informative to check whether loss of STING in the DKO embryos can rescue the mice lethality or lungs defects or differentiation defects of hematopoietic stem cells.

Chapter 8 Reference

Azevedo, C., Burton, A., Ruiz-Mateos, E., Marsh, M., & Saiardi, A. (2009). Inositol pyrophosphate mediated pyrophosphorylation of AP3B1 regulates HIV-1 Gag release. *Proceedings of the National Academy of Sciences of the United States of America*, *106*(50), 21161–21166. https://doi.org/10.1073/pnas.0909176106

Balany, J., & Bhandari, V. (2015). *Understanding the impact of infection , inflammation , and Their Persistence in the Pathogenesis of Bronchopulmonary Dysplasia*. *2*(December), 1–10. https://doi.org/10.3389/fmed.2015.00090

Barkauskas, C. E., Chung, M. I., Fioret, B., Gao, X., Katsura, H., & Hogan, B. L. M. (2017). Lung organoids: Current uses and future promise. *Development (Cambridge)*, *144*(6), 986–997. https://doi.org/10.1242/dev.140103

Bernitz, J. M., Kim, H. S., MacArthur, B., Sieburg, H., & Moore, K. (2016). Hematopoietic Stem Cells Count and Remember Self-Renewal Divisions. *Cell*, *167*(5), 1296-1309.e10. https://doi.org/10.1016/j.cell.2016.10.022

Berridge, M. J., & Irvine, R. F. (1984). Inositol trisphosphate, a novel second messenger in cellular signal transduction. *Nature*, *312*(5992), 315–321. https://doi.org/10.1038/312315a0

Bhandari, R., Juluri, K. R., Resnick, A. C., & Snyder, S. H. (2007). *Gene deletion of inositol hexakisphosphate kinase 1 reveals inositol pyrophosphate regulation of insulin secretion , growth , and spermiogenesis*. 2–6.

Bhandari, R., Juluri, K. R., Resnick, A. C., & Snyder, S. H. (2008). Gene deletion of

inositol hexakisphosphate kinase 1 reveals inositol pyrophosphate regulation of insulin secretion, growth, and spermiogenesis. *Proceedings of the National Academy of Sciences of the United States of America*, *105*(7), 2349–2353. https://doi.org/10.1073/pnas.0712227105

Bhandari, R., Saiardi, A., Ahmadibeni, Y., Snowman, A. M., Adam, R. C., Kristiansen, T. Z., Molina, H., Pandey, A., Werner, J. K., Juluri, K. R., Ku, Y., Prestwich, G. D., Parang, K., & Snyder, S. H. (2007). Protein pyrophosphorylation by inositol pyrophosphates is a posttranslational event. *Proceedings of the National Academy of Sciences of the United States of America*, *104*(39), 15305–15310. https://doi.org/10.1073/pnas.0707338104

Blackwell, T. S., Hipps, A. N., Han, W., Barham, W. J., Michael, C., Yull, F. E., & Prince, L. S. (2020). *NF- κ B Signaling in Fetal Lung Macrophages Disrupts Airway Morphogenesis*. https://doi.org/10.4049/jimmunol.1101495

Bosanac, I., Michikawa, T., Mikoshiba, K., & Ikura, M. (2004). Structural insights into the regulatory mechanism of IP 3 receptor. *Biochimica et Biophysica Acta - Molecular Cell Research*, *1742*(1–3), 89–102. https://doi.org/10.1016/j.bbamcr.2004.09.016

Bry, K., Whitsett, J. A., & Lappalainen, U. (2007). *IL-1 □ Disrupts Postnatal Lung Morphogenesis in the Mouse*. *36*, 32–42. https://doi.org/10.1165/rcmb.2006-0116OC

Chakraborty, A. (2017). *The inositol pyrophosphate pathway in health*. *9*.

https://doi.org/10.1111/brv.12392

Chakraborty, A., Koldobskiy, M. A., Bello, N. T., Maxwell, M., Potter, J. J., Juluri, K. R., Maag, D., Kim, S., Huang, A. S., Dailey, M. J., Saleh, M., Snowman, A. M., Moran, T. H., Mezey, E., & Snyder, S. H. (2010). Inositol Pyrophosphates Inhibit Akt Signaling , Thereby Regulating Insulin Sensitivity and Weight Gain. *Cell*, *143*(6), 897–910. https://doi.org/10.1016/j.cell.2010.11.032

Chin, A. C., Gao, Z., Riley, A. M., Furkert, D., Wittwer, C., Dutta, A., Rojas, T., Semenza, E. R., Felder, R. A., Pluznick, J. L., Jessen, H. J., Fiedler, D., Potter, B. V. L., Snyder, S. H., & Fu, C. (2020). The inositol pyrophosphate 5-InsP7drives sodium-potassium pump degradation by relieving an autoinhibitory domain of PI3K p85α. *Science Advances*, *6*(44), 1–14. https://doi.org/10.1126/sciadv.abb8542

Coulombe, P., Paliouras, G. N., Clayton, A., Hussainkhel, A., Fuller, M., Jovanovic, V., Dauphinee, S., Umlandt, P., Xiang, P., Kyle, A. H., Minchinton, A. I., Humphries, R. K., Hoodless, P. A., Parker, J. D. K., Wright, J. L., & Karsan, A. (2019). Endothelial Sash1 Is Required for Lung Maturation through Nitric Oxide Signaling. *Cell Reports*, *27*(6), 1769-1780.e4. https://doi.org/10.1016/j.celrep.2019.04.039

Cridland, C., & Gillaspy, G. (2020). Inositol pyrophosphate pathways and mechanisms: What can we learn from plants? *Molecules*, *25*(12). https://doi.org/10.3390/molecules25122789

Dharampuriya, P. R., Scapin, G., Wong, C., John Wagner, K., Cillis, J. L., & Shah, D. I. (2017). Tracking the origin, development, and differentiation of hematopoietic stem cells. *Current Opinion in Cell Biology*, *49*, 108–115. https://doi.org/10.1016/j.ceb.2018.01.002

Dick, R. A., Mallery, D. L., Vogt, V. M., & James, L. C. (2018). IP6 regulation of HIV capsid assembly, stability, and uncoating. *Viruses*, *10*(11), 1–11. https://doi.org/10.3390/v10110640

Dong, J., Ma, G., Sui, L., Wei, M., Satheesh, V., Zhang, R., Ge, S., Li, J., Zhang, T. E., Wittwer, C., Jessen, H. J., Zhang, H., An, G. Y., Chao, D. Y., Liu, D., & Lei, M. (2019). Inositol Pyrophosphate InsP8 Acts as an Intracellular Phosphate Signal in Arabidopsis. *Molecular Plant*, *12*(11), 1463–1473. https://doi.org/10.1016/j.molp.2019.08.002

Dzierzak, E., & Philipsen, S. (2013). *Erythropoiesis : Development and Differentiation*. 1–16.

Elias, H. K., Bryder, D., & Park, C. Y. (2017). Molecular mechanisms underlying lineage bias in aging hematopoiesis. *Seminars in Hematology*, *54*(1), 4–11. https://doi.org/10.1053/j.seminhematol.2016.11.002

Flach, J., Bakker, S. T., Mohrin, M., Conroy, P. C., Pietras, E. M., Reynaud, D., Alvarez, S., Diolaiti, M. E., Ugarte, F., Forsberg, E. C., Le Beau, M. M., Stohr, B. A., Méndez, J., Morrison, C. G., & Passegué, E. (2014). Replication stress is a potent driver of functional decline in ageing haematopoietic stem cells. *Nature*,

512(7513), 198–202. https://doi.org/10.1038/nature13619

Flannery, M., Dunphy, G., Almine, J. F., Nevels, M. M., Bowie, A. G., Flannery, M., Almine, J. F., Connolly, D. J., Paulus, C., & Jønsson, K. L. (2018). *Non-canonical Activation of the DNA Sensing Adaptor STING by ATM and IFI16 Mediates NF- k B Signaling after Nuclear DNA Damage Article Non-canonical Activation of the DNA Sensing Adaptor STING by ATM and IFI16 Mediates NF-k B Signaling after Nuclear DNA* . 745–760. https://doi.org/10.1016/j.molcel.2018.07.034

Furkert, D., Hostachy, S., Nadler-Holly, M., & Fiedler, D. (2020). Triplexed Affinity Reagents to Sample the Mammalian Inositol Pyrophosphate Interactome. *Cell Chemical Biology*, *27*(8), 1097-1108.e4. https://doi.org/10.1016/j.chembiol.2020.07.017

Giglia-mari, G., Zotter, A., & Vermeulen, W. (2011). *DNA Damage Response*. 1–19.

Grinenko, T., Eugster, A., Thielecke, L., Ramasz, B., Krüger, A., Dietz, S., Glauche, I., Gerbaulet, A., Von Bonin, M., Basak, O., Clevers, H., Chavakis, T., & Wielockx, B. (2018). Hematopoietic stem cells can differentiate into restricted myeloid progenitors before cell division in mice. *Nature Communications*, *9*(1), 1–10. https://doi.org/10.1038/s41467-018-04188-7

Hancock, L. A., Hennessy, C. E., Solomon, G. M., Dobrinskikh, E., Estrella, A., Hara, N., Hill, D. B., Kissner, W. J., Markovetz, M. R., Villalon, D. E. G., Voss, M. E., Tearney, G. J., Carroll, K. S., Shi, Y., Schwarz, M. I., Thelin, W. R., Rowe, S.

M., Yang, I. V, Evans, C. M., & Schwartz, D. A. (n.d.). Muc5b overexpression causes mucociliary dysfunction and enhances lung fibrosis in mice. *Nature Communications*, *2018*, 1–10. https://doi.org/10.1038/s41467-018-07768-9

Hattangadi, S. M., Wong, P., Zhang, L., Flygare, J., & Lodish, H. F. (2011). *Review article From stem cell to red cell : regulation of erythropoiesis at multiple levels by multiple proteins , RNAs , and chromatin modifications*. *118*(24), 6258–6268. https://doi.org/10.1182/blood-2011-07-356006.

Herriges, M., & Morrisey, E. E. (2014). Lung development: Orchestrating the generation and regeneration of a complex organ. *Development (Cambridge)*, *141*(3), 502–513. https://doi.org/10.1242/dev.098186

Hogmalm, A., Bry, M., Strandvik, B., & Bry, K. (2020). *IL-1 □ expression in the distal lung epithelium disrupts lung morphogenesis and epithelial cell differentiation in fetal mice*. *Cmv*. https://doi.org/10.1152/ajplung.00154.2013

Jadav, R. S., Chanduri, M. V. L., Sengupta, S., & Bhandari, R. (2013a). Inositol pyrophosphate synthesis by inositol hexakisphosphate kinase 1 is required for homologous recombination repair. *Journal of Biological Chemistry*, *288*(5), 3312–3321. https://doi.org/10.1074/jbc.M112.396556

Jadav, R. S., Chanduri, M. V. L., Sengupta, S., & Bhandari, R. (2013b). *Inositol Pyrophosphate Synthesis by Inositol Hexakisphosphate Kinase 1 Is Required for Homologous Recombination Repair *. *288*(5), 3312–3321. https://doi.org/10.1074/jbc.M112.396556

Jafari, M., Ghadami, E., Dadkhah, T., & Akhavan-Niaki, H. (2019). PI3k/AKT signaling pathway: Erythropoiesis and beyond. *Journal of Cellular Physiology*, *234*(3), 2373–2385. https://doi.org/10.1002/jcp.27262

Jayapal, S. R., Wang, C. Q., Bisteau, X., Caldez, M. J., Lim, S., Tergaonkar, V., Osato, M., & Kaldis, P. (2015). Hematopoiesis specific loss of Cdk2 and Cdk4 results in increased erythrocyte size and delayed platelet recovery following stress. *Haematologica*, *100*(4), 431–438. https://doi.org/10.3324/haematol.2014.106468

Jobe, A. H. (2016). *Mechanisms of Lung Injury and Bronchopulmonary Dysplasia*. 1076–1078.

Juntilla, M. M., Patil, V. D., Calamito, M., Joshi, R. P., Birnbaum, M. J., & Koretzky, G. A. (2010). *AKT1 and AKT2 maintain hematopoietic stem cell function by regulating reactive oxygen species*. *115*(20), 4030–4038. https://doi.org/10.1182/blood-2009-09-241000.The

Kalikkot, R., Cuevas, M., & Shivanna, B. (2017). *Bronchopulmonary dysplasia : A review of pathogenesis and pathophysiology*. *132*(August), 170–177. https://doi.org/10.1016/j.rmed.2017.10.014

Kane, L. P., Shapiro, V. S., Stokoe, D., & Weiss, A. (n.d.). *Induction of NF- κ B by the Akt / PKB kinase*. *28*, 601–605.

Kay, J., Thadhani, E., Samson, L., & Engelward, B. (2019). *In fl ammation-induced DNA damage , mutations and cancer ☆ , ☆☆*. *83*(June).

https://doi.org/10.1016/j.dnarep.2019.102673

Kingsley, P. D., Malik, J., Emerson, R. L., Bushnell, T. P., McGrath, K. E., Bloedorn, L. A., Bulger, M., & Palis, J. (2006). “Maturational” globin switching in primary primitive erythroid cells. *Blood*, *107*(4), 1665–1672. https://doi.org/10.1182/blood-2005-08-3097

Koulnis, M., Pop, R., Porpiglia, E., Shearstone, J. R., Hidalgo, D., & Socolovsky, M. (2011). *Identification and Analysis of Mouse Erythroid Progenitors using the CD71 / TER119 Flow-cytometric Assay*. *22363547*, 1–7. https://doi.org/10.3791/2809

Kröber, T., Bartsch, S. M., & Fiedler, D. (2021). Advances in Biological Regulation Pharmacological tools to investigate inositol polyphosphate kinases – Enzymes of increasing therapeutic relevance. *Advances in Biological Regulation*, *October*, 100836. https://doi.org/10.1016/j.jbior.2021.100836

Lee-Six, H., & Kent, D. G. (2020). Tracking hematopoietic stem cells and their progeny using whole-genome sequencing. *Experimental Hematology*, *83*, 12–24. https://doi.org/10.1016/j.exphem.2020.01.004

Lee, T., Lee, J., Won, J., Yang, Y., Park, S. J., Lee, S., Pavlovic, I., Kong, B., Jho, Y. S., Jessen, H. J., Shin, Y., Kim, S. H., Yoon, T., Lee, T., Lee, J., Won, J., Yang, Y., Ju, S., Lee, S., & Pavlovic, I. (2017). *Inositol pyrophosphates inhibit synaptotagmin- dependent exocytosis*. *114*(33), 1–7. https://doi.org/10.1073/pnas.1712781114

Li, M., Krishnaveni, M. S., Li, C., Zhou, B., Xing, Y., Banfalvi, A., Li, A., Lombardi, V., Akbari, O., Borok, Z., & Minoo, P. (2011). *Epithelium-specific deletion of TGF- β receptor type II protects mice from bleomycin-induced pulmonary fibrosis*. *121*(1), 277–287. https://doi.org/10.1172/JCI42090.that

Li, X., Zeng, X., Xu, Y., Wang, B., Zhao, Y., Lai, X., Qian, P., & Huang, H. (2020). Mechanisms and rejuvenation strategies for aged hematopoietic stem cells. *Journal of Hematology and Oncology*, *13*(1). https://doi.org/10.1186/s13045-020-00864-8

Liu, T., Zhang, L., Joo, D., & Sun, S. (2017). *NF- κ B signaling in in fl ammation*. *April*. https://doi.org/10.1038/sigtrans.2017.23

Losito, O., Szijgyarto, Z., Resnick, A. C., & Saiardi, A. (2009). Inositol pyrophosphates and their unique metabolic complexity: Analysis by gel electrophoresis. *PLoS ONE*, *4*(5), 2–10. https://doi.org/10.1371/journal.pone.0005580

Malla, A. B., & Bhandari, R. (2017). IP6K1 is essential for chromatoid body formation and temporal regulation of Tnp2 and Prm2 expression in mouse spermatids. *Journal of Cell Science*, *130*(17), 2854–2866. https://doi.org/10.1242/jcs.204966

Mayle, A., Luo, M., Jeong, M., & Goodell, M. A. (2013). Flow cytometry analysis of murine hematopoietic stem cells. *Cytometry Part A*, *83 A*(1), 27–37. https://doi.org/10.1002/cyto.a.22093

Mazo, I. B., Massberg, S., & von Andrian, U. H. (2011). Hematopoietic stem and progenitor cell trafficking. *Trends in Immunology*, *32*(10), 493–503. https://doi.org/10.1016/j.it.2011.06.011

Metzger, R. J., Klein, O. D., Martin, G. R., & Krasnow, M. A. (2008). The branching programme of mouse lung development. *Nature*, *453*(7196), 745–750. https://doi.org/10.1038/nature07005

Michell, R. H., Kirk, C. J., Jones, L. M., Downes, C. P., & Creba, J. A. (1981). The stimulation of inositol lipid metabolism that accompanies calcium mobilization in stimulated cells: defined characteristics and unanswered questions. *Philosophical Transactions of the Royal Society of London. Series B, Biological Sciences*, *296*(1080), 123–138. https://doi.org/10.1098/rstb.1981.0177

Monserrate, J. P., & York, J. D. (2010). Inositol phosphate synthesis and the nuclear processes they affect. *Current Opinion in Cell Biology*, *22*(3), 365–373. https://doi.org/10.1016/j.ceb.2010.03.006

Mouse Immune Cell Marker Guide. (2021). 2021.

Nagpal, L., Kornberg, M. D., Albacarys, L. K., & Snyder, S. H. (2021). Inositol hexakisphosphate kinase-2 determines cellular energy dynamics by regulating creatine kinase-B. *Proceedings of the National Academy of Sciences of the United States of America*, *118*(6). https://doi.org/10.1073/pnas.2020695118

Palis, J. (2014). *Primitive and definitive erythropoiesis in mammals*. *5*(January), 1–9. https://doi.org/10.3389/fphys.2014.00003

Papaioannou, V. E., & Behringer, R. R. (2012). Early embryonic lethality in genetically engineered mice: Diagnosis and phenotypic analysis. *Veterinary Pathology*, *49*(1), 64–70. https://doi.org/10.1177/0300985810395725

Park, S. J., Lee, S., Park, E., & Kim, S. (2017). *Animal Cells and Systems Inositol pyrophosphates as multifaceted metabolites in the regulation of mammalian signaling networks Inositol pyrophosphates as multifaceted metabolites in the regulation of mammalian signaling networks*. https://doi.org/10.1080/19768354.2017.1408684

Peng, C., Ouyang, Y., Lu, N., & Li, N. (2020). *The NF- κ B Signaling Pathway , the Microbiota , and Gastrointestinal Tumorigenesis : Recent Advances*. *11*(June), 1–13. https://doi.org/10.3389/fimmu.2020.01387

Peyser, R., Macdonnell, S., Gao, Y., Cheng, L., Kim, Y., Kaplan, T., Ruan, Q., Wei, Y., Ni, M., Adler, C., Zhang, W., Devalaraja-narashimha, K., Grindley, J., Halasz, G., & Morton, L. (2019). *De fi ning the Activated Fibroblast Population in Lung Fibrosis Using Single-Cell Sequencing*. *61*(1), 74–85. https://doi.org/10.1165/rcmb.2018-0313OC

Pilzecker, B., Buoninfante, O. A., Van Den Berk, P., Lancini, C., Song, J. Y., Citterio, E., & Jacobs, H. (2017). DNA damage tolerance in hematopoietic stem and progenitor cells in mice. *Proceedings of the National Academy of Sciences of the United States of America*, *114*(33), E6875–E6883. https://doi.org/10.1073/pnas.1706508114

Rao, F., Cha, J., Xu, J., Xu, R., Vandiver, M. S., Tyagi, R., Tokhunts, R., Koldobskiy, M. A., Fu, C., Barrow, R., Wu, M., Fiedler, D., & Barrow, J. C. (2014). Article Inositol Pyrophosphates Mediate the DNA-PK / ATM-p53 Cell Death Pathway by Regulating CK2 Phosphorylation of Tti1 / Tel2. *Molecular Cell*, *54*(1), 119–132. https://doi.org/10.1016/j.molcel.2014.02.020

Romashkova, J. A., & Makarov, S. S. (1999). *NF- k B is a target of AKT in anti-apoptotic PDGF signalling*. *401*(September), 2–6.

Saiardi, A., Bhandari, R., & Resnick, A. C. (2004). *Phosphorylation of Proteins by Inositol Pyrophosphates*. *December*, 2101–2106.

Saiardi, A., Sciambi, C., Mccaffery, J. M., Wendland, B., & Snyder, S. H. (n.d.). *Inositol pyrophosphates regulate endocytic trafficking*. Retrieved April 6, 2021, from www.pnas.org.

Sankaran, V. G., & Orkin, S. H. (2013). The switch from fetal to adult hemoglobin. *Cold Spring Harbor Perspectives in Medicine*, *3*(1). https://doi.org/10.1101/cshperspect.a011643

Sankaran, V. G., Xu, J., & Orkin, S. H. (2010a). Advances in the understanding of haemoglobin switching: Review. *British Journal of Haematology*, *149*(2), 181–194. https://doi.org/10.1111/j.1365-2141.2010.08105.x

Sankaran, V. G., Xu, J., & Orkin, S. H. (2010b). *Advances in the understanding of haemoglobin switching*. *March*, 181–194. https://doi.org/10.1111/j.1365-2141.2010.08105.x

Scherer, P. C., Ding, Y., Liu, Z., Xu, J., Mao, H., Barrow, J. C., Wei, N., Zheng, N., Snyder, S. H., & Rao, F. (2016). Inositol hexakisphosphate (IP6) generated by IP5K mediates cullin-COP9 signalosome interactions and CRL function. *Proceedings of the National Academy of Sciences of the United States of America*, *113*(13), 3503–3508. https://doi.org/10.1073/pnas.1525580113

Shahzad, T., Radajewski, S., Chao, C., Bellusci, S., & Ehrhardt, H. (2016). Pathogenesis of bronchopulmonary dysplasia : when inflammation meets organ development. *Molecular and Cellular Pediatrics*. https://doi.org/10.1186/s40348-016-0051-9

Sizemore, N., Leung, S., & Stark, G. R. (1999). *Activation of Phosphatidylinositol 3-Kinase in Response to Interleukin-1 Leads to Phosphorylation and Activation of the NF-□ B p65 / RelA Subunit*. *19*(7), 4798–4805.

Stouch, A. N., Mccoy, A. M., Greer, R. M., Lakhdari, O., Yull, F. E., Blackwell, T. S., Hoffman, M., Prince, L. S., Stouch, A. N., Mccoy, A. M., Greer, R. M., Lakhdari, O., Yull, F. E., Blackwell, T. S., Hoffman, H. M., & Prince, L. S. (2020). *IL-1 β and Inflammasome Activity Link Inflammation to Abnormal Fetal Airway Development*. https://doi.org/10.4049/jimmunol.1500906

Sulli, G., & Micco, R. Di. (2012). Crosstalk between chromatin state and DNA damage response in cellular senescence and cancer. *Nature Reviews Cancer*, *12*(10), 709–720. https://doi.org/10.1038/nrc3344

Tiozzo, C., Danopoulos, S., Lavarreda-pearce, M., Baptista, S., Varimezova, R.,

Alam, D. Al, Warburton, D., Virender, R., Langhe, S. De, Cristofano, A. Di, Bellusci, S., & Minoo, P. (2012). *Embryonic epithelial Pten deletion through Nkx2 . 1-cre leads to thyroid tumorigenesis in a strain-dependent manner*. 111–122. https://doi.org/10.1530/ERC-10-0327

Turan, S., Galla, M., Ernst, E., Qiao, J., Voelkel, C., Schiedlmeier, B., Zehe, C., & Bode, J. (2011). Recombinase-mediated cassette exchange (RMCE): Traditional concepts and current challenges. *Journal of Molecular Biology*, *407*(2), 193–221. https://doi.org/10.1016/j.jmb.2011.01.004

Turgeon, B., Meloche, S., & Recherche, I. De. (2021). *Interpreting Neonatal Lethal Phenotypes in Mouse Mutants : Insights Into Gene Function and Human Diseases*. 1–26. https://doi.org/10.1152/physrev.00040.2007.

Ward, J. M., Elmore, S. A., & Foley, J. F. (2012). Pathology methods for the evaluation of embryonic and perinatal developmental defects and lethality in genetically engineered mice. *Veterinary Pathology*, *49*(1), 71–84. https://doi.org/10.1177/0300985811429811

Weiss, C. N., & Ito, K. (2015). DNA damage: A sensible mediator of the differentiation decision in hematopoietic stem cells and in leukemia. *International Journal of Molecular Sciences*, *16*(3), 6183–6201. https://doi.org/10.3390/ijms16036183

Wilber, A., Nienhuis, A. W., & Persons, D. A. (2011). *Review article Transcriptional regulation of fetal to adult hemoglobin switching : new therapeutic*

opportunities. *117*(15), 3945–3953. https://doi.org/10.1182/blood-2010-11-316893.The

Wilson, M. S. C., Bulley, S. J., Pisani, F., Irvine, R. F., & Saiardi, A. (2015). A novel method for the purification of inositol phosphates from biological samples reveals that no phytate is present in human plasma or urine. *Open Biology*, *5*(3). https://doi.org/10.1098/rsob.150014

Wilson, M. S., Jessen, H. J., & Saiardi, A. (2019). The inositol hexakisphosphate kinases IP6K1 and -2 regulate human cellular phosphate homeostasis, including XPR1-mediated phosphate export. *Journal of Biological Chemistry*, *294*(30), 11597–11608. https://doi.org/10.1074/jbc.RA119.007848

Wilson, M., & Saiardi, A. (2018). Inositol Phosphates Purification Using Titanium Dioxide Beads. *Bio-Protocol*, *8*(15), 1–8. https://doi.org/10.21769/bioprotoc.2959

Wu, F., Chen, Z., Liu, J., & Hou, Y. (2021). Akt − mTOR network at the interface of hematopoietic stem cell homeostasis. *Experimental Hematology*, 1–9. https://doi.org/10.1016/j.exphem.2021.08.009

Xu, Y., Li, H., Bajrami, B., Kwak, H., Cao, S., Liu, P., Zhou, J., & Zhou, Y. (2013). *Cigarette smoke (CS) and nicotine delay neutrophil spontaneous death via suppressing production of diphosphoinositol pentakisphosphate*. https://doi.org/10.1073/pnas.1302906110/-/DCSupplemental.www.pnas.org/cgi/doi/10.1073/pnas.1302906110

Yi, Z., Cohen-Barak, O., Hagiwara, N., Kingsley, P. D., Fuchs, D. A., Erickson, D. T., Epner, E. M., Palis, J., & Brilliant, M. H. (2006). Sox6 directly silences epsilon globin expression in definitive erythropoiesis. *PLoS Genetics*, *2*(2), 129–139. https://doi.org/10.1371/journal.pgen.0020014

Young, K., Borikar, S., Bell, R., Kuffler, L., Philip, V., & Trowbridge, J. J. (2016). Progressive alterations in multipotent hematopoietic progenitors underlie lymphoid cell loss in aging. *Journal of Experimental Medicine*, *213*(11), 2259–2267. https://doi.org/10.1084/jem.20160168

Zhang, X., Li, N., Zhang, J., Zhang, Y., Yang, X., Luo, Y., Zhang, B., Xu, Z., Zhu, Z., Yang, X., Yan, Y., Lin, B., Wang, S., Chen, D., Ye, C., Ding, Y., Lou, M., Wu, Q., Hou, Z., … Rao, F. (2021). 5-IP7 is a GPCR messenger mediating neural control of synaptotagmin-dependent insulin exocytosis and glucose homeostasis. *Nature Metabolism*, *3*(10), 1400–1414. https://doi.org/10.1038/s42255-021-00468-7

Zhou, D., Liu, K., Sun, C. W., Pawlik, K. M., & Townes, T. M. (2010). KLF1 regulates BCL11A expression and γ- to β-globin gene switching. *Nature Genetics*, *42*(9), 742–744. https://doi.org/10.1038/ng.637